Eur. Phys. J. C (2025) 85:1437
https://doi.org/10.1140/epjc/s10052-025-14957-6

THE EUROPEAN PHYSICAL JOURNAL C

Regular Article - Experimental Physics

Search for squarks and gluinos in pp collisions at $\sqrt{s} = 13$ TeV and 13.6 TeV in events with τ-leptons, jets and missing transverse momentum using the ATLAS detector

ATLAS Collaboration[⋆]

CERN, 1211 Geneva 23, Switzerland

Received: 2 July 2025 / Accepted: 17 October 2025

Abstract A search for R-parity-conserving supersymmetry in events with large missing transverse momentum, jets and at least one hadronically decaying τ-lepton is presented. Both gluino and squark pair production are considered, with the cascade decay of each gluino or squark producing either a τ-slepton or a τ-sneutrino. Three channels are examined, requiring either exactly one hadronically decaying τ-lepton and no other leptons, exactly one hadronically decaying τ-lepton and at least one other lepton, or two or more hadronically decaying τ-leptons. Analyses in the three channels are optimised independently and combined statistically. Two separate analysis strategies, either a cut-and-count or machine-learning approach, are used. The search uses 140 fb^{-1} and 51.8 fb^{-1} of pp collision data recorded by the ATLAS detector at the Large Hadron Collider during 2015–2018 at $\sqrt{s} = 13$ TeV and 2022–2023 at $\sqrt{s} = 13.6$ TeV, respectively. Gluino masses below 2.25 TeV and squark masses up to 1.7 TeV are excluded

Contents

P. Dervan, J. Khubua, U. Mallik and I.P.J. Shipsey: Deceased.

⋆ e-mail: atlas.publications@cern.ch

1 Introduction

The Standard Model (SM) of particle physics is a powerful and experimentally well-validated theory. The SM describes excitations and interactions of quantum fields, representing elementary particles, and can be used to give extremely precise predictions of the results of elastic and inelastic particle collisions. The latest triumph of the SM is its prediction of the Higgs boson and the discovery in 2012 of a compatible particle by the ATLAS [1] and CMS [2] experiments in the proton–proton (pp) collisions produced by CERN's Large Hadron Collider (LHC) [3]. Although the precision of the SM and its impact on particle physics is hard to underestimate, it is fundamentally an incomplete, effective theory. The usual list of limitations of the SM includes its inability to explain the large difference between the electroweak scale and the Planck scale of the gravitational interactions (known as the "hierarchy problem"), the associated fine-tuning of the Higgs potential, and its lack of viable dark matter candidates (whose existence is corroborated by multiple astronomical observations [4–6]).

When trying to describe the symmetries of special relativity and the internal gauge symmetries of quantum fields by a common mechanism in an attempt to extend the SM, it can be shown that the only way they can be combined into a common symmetry Lie group is as a direct product [7], meaning that no interaction between them is possible. One of the only ways to overcome this restriction is through the introduction of graded Lie superalgebras [8], which gives rise to supersymmetry (SUSY) [9–14], an extension of the SM which postulates the existence of an additional (super)symmetry between bosons and fermions. A direct consequence of SUSY is that every known SM particle has at least one superpartner with the same quantum numbers, but a spin that differs by one

Published online: 18 December 2025

half, resulting in a plethora of new particles. This "fascinating mathematical structure" [15] leads to additional loop corrections to the Higgs boson mass which perfectly cancel out with those from the SM [16–19], thus solving the hierarchy problem.

To accommodate experimental observations, especially the stability of the proton, a conserved quantum number $R = (-1)^{3(B-L)+2s}$ [20] is often postulated, where B and L are the baryon and total lepton numbers, and s is the spin of the particle. Phenomenologically, this implies that SUSY particles are pair-produced at collider experiments, and that the lightest supersymmetric particle (LSP) is stable and can be a viable dark matter candidate [21,22]. If supersymmetry was preserved, the superpartners would have the same mass as the SM particles, but this has not been observed. Therefore, supersymmetry must be broken, and this introduces a wide range of possible SUSY mass spectra [23]. A common feature of SUSY models is the mixing of binos, winos and higgsinos (the superpartners of the electroweak gauge bosons and the Higgs boson, respectively). Their mass eigenstates are known as charginos ($\tilde{\chi}^{\pm}_{1,2}$) and neutralinos ($\tilde{\chi}^{0}_{1,2,3,4}$), where the subscript denotes their ordering in increasing mass. Third-generation squarks and sleptons are more likely to have lower masses than their first- and second-generation counterparts and be next-to-lightest supersymmetric particle (NLSP) candidates [24–26], and are of special interest for experimental searches because they provide distinct signatures. The third-generation sneutrino is another option for the NLSP [27–34] that can produce similar signatures. The ATLAS Collaboration has an extensive programme of searches for SUSY-inspired signatures [35,36].

2 Analysis targets

This paper describes a search for pair production of gluinos or first- or second-generation left-handed squarks (superpartners of gluons and quarks, respectively), with τ-sleptons ($\tilde{\tau}$) and τ-sneutrinos ($\tilde{\nu}_\tau$) as co-NLSPs, targeting final states with τ-leptons, jets, and missing transverse momentum. Gluinos are allowed to decay into an off-shell squark and a quark, a common decay mode in the minimal supersymmetric model (MSSM). Squarks are assumed to be left-handed and from the first or second generation, and to decay via the second-lightest neutralino $\tilde{\chi}^0_2$ or the lightest chargino $\tilde{\chi}^{\pm}_1$, as these are the common decay modes for the left-handed squarks. Both the $\tilde{\chi}^{\pm}_1$ and $\tilde{\chi}^0_2$ are assumed to couple to $\tilde{\tau}$ and $\tilde{\nu}_\tau$ in association with a SM τ-lepton or ν_τ, with the branching ratios set to 0.5. The $\tilde{\tau}$ and $\tilde{\nu}_\tau$ decay into the LSP $\tilde{\chi}^0_1$ and a SM τ-lepton or ν_τ. Such cascade chains arise naturally in the MSSM when the $\tilde{\tau}$ or $\tilde{\nu}_\tau$ are light. The simplified SUSY models [25,26,37] considered in this paper are shown in Fig. 1. According to the pMSSM scan [38], these final states are uniquely sensitive to a subset of SUSY models. The ATLAS Collaboration previously searched for such signals using data gathered during 2015–2016 [39,40], excluding gluino masses below 2 TeV and LSP masses below 1 TeV, and CMS considered similar signatures with data gathered during 2011 [41], excluding gluino masses below 1.15 TeV. The present search uses 140 fb^{-1} and 51.8 fb^{-1} of pp collision data recorded by the ATLAS detector [42] during 2015–2018 at centre-of-mass energies of $\sqrt{s} = 13$ TeV and 2022–2023 at $\sqrt{s} = 13.6$ TeV.

The kinematic properties of the final-state particles depend heavily on the masses of SUSY particles in the decay chains. The simplified models are parameterised in terms of the gluino or squark mass $m(\tilde{g}/\tilde{q})$ and the LSP mass $m(\tilde{\chi}^0_1)$. The other SUSY particles in the decay chain, namely $\tilde{\chi}^0_2$ and $\tilde{\chi}^{\pm}_1$, and $\tilde{\tau}$ and $\tilde{\nu}_\tau$, are considered to be pairwise mass-degenerate. Their masses are determined from the two free parameters of the model as:

$$m(\tilde{\chi}^{\pm}_1) = m(\tilde{\chi}^0_2) = \frac{1}{2}\left[m(\tilde{g}/\tilde{q}) + m(\tilde{\chi}^0_1)\right],$$
$$m(\tilde{\tau}) = m(\tilde{\nu}_\tau) = \frac{1}{2}\left[m(\tilde{\chi}^{\pm}_1) + m(\tilde{\chi}^0_1)\right]. \quad (1)$$

This parameterisation follows the conventions used in ATLAS searches for gluinos and squarks with cascade decays [43,44] used to simplify the model parameter phase space. The sensitivity of the analysis does not depend strongly on the assumptions of Eq. (1) as long as the mass differences between SUSY particles $\Delta m(\tilde{g}/\tilde{q}, \tilde{\chi}^{\pm}_1/\tilde{\chi}^0_2)$ and $\Delta m(\tilde{\chi}^{\pm}_1/\tilde{\chi}^0_2, \tilde{\chi}^0_1)$ are larger than a few GeV. The $\tilde{\chi}^0_1$ is set to be bino-like, while the $\tilde{\chi}^0_2$ and $\tilde{\chi}^{\pm}_1$ are wino-like, to facilitate the decays considered. The coupling to all other SUSY particles is set to 0. The narrow-width approximation is utilised for all decays. The simplified models considered are primarily inspired by the MSSM, but other SUSY models such as the NUHM [45,46], mSUGRA [47], or GMSB [48] can also produce similar final states.

These simplified models result in a range of τ-lepton-rich signatures. The search is split into three orthogonal channels, which are combined in a simultaneous fit, and which contain events with:

- exactly one hadronically decaying τ-lepton and no electron or muon (1TAU0LEP);
- exactly one hadronically decaying τ-lepton and at least one electron or muon (1TAU1LEP);
- at least two hadronically decaying τ-leptons (2TAU).

The additional kinematic information in the 1TAU1LEP and 2TAU channels is used to separate signal from background more efficiently. In principle, a 0TAU1LEP channel would also be sensitive to the considered signal models, but the higher branching ratio and competitive reconstruction and identification efficiency for hadronically decaying τ-leptons make

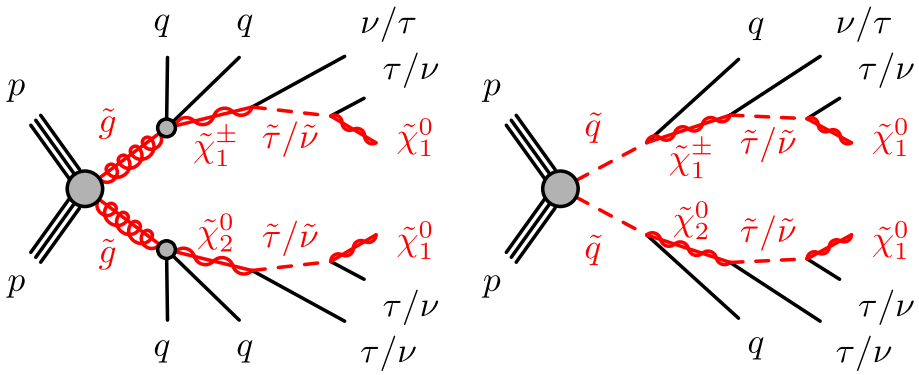

Fig. 1 Diagrams showing the production and decay of **a** a gluino pair and **b** a squark pair. In the gluino case, the two-step decay via an off-shell squark $\tilde{g} \to \tilde{q}^* q \to qq\tilde{\chi}_2^0/\tilde{\chi}_1^\pm$ is symbolised by a four-body vertex

1TAU0LEP a more promising channel. The 0TAU1LEP channel would also overlap heavily with the dedicated searches for SUSY with exactly one electron or muon in the final state [49], while 1TAU0LEP is complementary to it.

The analysis uses two independent approaches. In the first one, machine learning (ML) classifiers are used to split the whole available phase space into various analysis regions. This is the most inclusive way to analyse the data because it uses every event (with a minor exception discussed below), and no additional kinematic requirement is applied. The second is based on the more traditional cut-and-count approach used in previous search iterations [39,40]. The event selection is tailored to target different signal topologies and suppress the main SM backgrounds. The use of kinematic variables makes the interpretation simpler than in the ML approach. The combination of improved analysis techniques, a larger data sample, and enhanced calibration and identification algorithms for jets and b-jets, light leptons (electrons and muons, denoted by ℓ), and τ-leptons, significantly improves the sensitivity of the search to new physics.

The paper is structured as follows. In Sect. 3, a brief description of the ATLAS detector is given. Section 4 offers an overview of the Monte Carlo (MC) samples used by the analysis. Section 5 describes the reconstruction, identification, and calibration procedures for final-state objects. The machine-learning and cut-and-count approaches are presented in Sect. 6. Section 7 discusses the data-driven estimations of events with jets misidentified as τ-leptons (fake taus), common to both approaches. The statistical procedures and systematic uncertainties affecting the analysis are gathered in Sect. 8. Finally, the results are presented in Sect. 9.

3 ATLAS detector

The ATLAS experiment [42,50] is a multipurpose cylindrical particle detector at the LHC with nearly 4π coverage in solid angle.[1] Located at the heart of the ATLAS detector, the inner tracking detector begins 33 mm from the beam axis and is surrounded by a thin superconducting solenoid providing a 2 T axial magnetic field. It consists of a silicon pixel detector (starting with the "insertable B-layer" [51,52] added before Run 2), a silicon microstrip tracker, and a transition radiation tracker, and covers the pseudorapidity range $|\eta| < 2.5$. Beyond the solenoid, lead/liquid-argon (LAr) sampling calorimeters measure the energy and position of electromagnetic showers with high granularity. In the central region $|\eta| < 1.7$ the steel/scintillator-tile calorimeter provides hadronic energy measurements. In the endcap and forward regions, LAr calorimeters with copper or tungsten absorbers are used for both electromagnetic and hadronic shower measurements up to $|\eta| = 4.9$. The outermost layer of the ATLAS detector is the muon spectrometer. It consists of separate trigger and high-precision tracking chambers, operating in a magnetic field generated by three large air-core toroidal superconducting magnets with eight coils each.

A two-level trigger system is used to select and record events of interest. The level-1 trigger is implemented in custom hardware. It uses information from the calorimeters and the muon spectrometer to accept events at a rate below 100 kHz. This is followed by the high-level trigger, which is fully software-based [53,54]. It is used to reduce the average accepted event rate to 1.25 kHz in Run 2 and 3 kHz in Run 3.

An extensive software suite [55] is used in data simulation, in the reconstruction and analysis of real and simulated data, in detector operations, and in the trigger and data acquisition systems of the experiment.

[1] ATLAS uses a right-handed coordinate system with its origin at the nominal interaction point (IP) in the centre of the detector and the z-axis along the beam pipe. The x-axis points from the IP to the centre of the LHC ring, and the y-axis points upwards. Cylindrical coordinates (r, ϕ) are used in the transverse plane, ϕ being the azimuthal angle around the z-axis. The pseudorapidity is defined in terms of the polar angle θ as $\eta = -\ln\tan(\theta/2)$. Angular distance is measured in units of $\Delta R \equiv \sqrt{(\Delta\eta)^2 + (\Delta\phi)^2}$.

4 Data and simulated event samples

The analysis is performed on two data samples collected with the ATLAS detector during proton–proton collisions at $\sqrt{s} = 13$ TeV and $\sqrt{s} = 13.6$ TeV with a bunch-crossing separation of 25 ns. The 13 TeV data sample corresponds to an integrated luminosity of 140 fb^{-1} collected during 2015–2018 (Run 2 of the LHC). The 13.6 TeV data sample was recorded during 2022–2023 (early Run 3) and corresponds to 51.8 fb^{-1}. The luminosity is measured mainly by the LUCID-2 detector [56], which records Cherenkov light produced in the quartz windows of photomultipliers located close to the beampipe. A set of data quality requirements is applied to the data to ensure that the LHC beam conditions were stable and the ATLAS detector was fully functional [57]. The quoted integrated luminosity is computed after the rejection of luminosity blocks failing these requirements.

All events used by the analysis are required to pass a missing transverse momentum ($E_{\mathrm{T}}^{\mathrm{miss}}$) trigger [53,54,58] requirement. During data-taking, the selection thresholds increased gradually from 70 to 115 GeV, and the computation algorithms were modified, e.g. by including information on charged-particle tracks [54]. These triggers are able to select signal events with an efficiency of 80–90% for most of the models considered, and around 40% for the most compressed scenarios (i.e. the $\Delta m(\tilde{g}/\tilde{q}, \tilde{\chi}_1^0) \lessapprox 100$ GeV region). The analysis also relies on single-lepton [59,60] and single-jet [61] triggers in some low-$E_{\mathrm{T}}^{\mathrm{miss}}$ regions used for auxiliary measurements to estimate how many jets are misidentified as τ-leptons (further described in Sect. 7).

The analysis makes use of MC simulations to model the SM backgrounds and SUSY signals. The event generators and the cross-section computation accuracies are summarised in Table 1. The ATLAS simulation framework [62,63] was used to produce all MC samples. Its detailed simulation of the detector response based on GEANT4 [64] ensures that the same reconstruction and identification algorithms can be applied to data and MC events. The effect of multiple interactions in the same and neighbouring bunch crossings (pileup) was modelled by overlaying each simulated hard-scattering event with inelastic pp collision events. The pileup model combines collision events from EPOS 2.0.1.4 [65], using the LHC tune, and PYTHIA 8 [66], using the A3 tune [67] and the NNPDF2.3LO set of parton distribution functions (PDFs) [68].

The two main SM background categories consist of events with jets misidentified as τ-leptons (fake taus, modelled inclusively for all production processes with a data-driven approach described in Sect. 7), and $t\bar{t}$ and single-top-quark events, collectively referred to as "Top". The $W(\tau\nu)$+jets event contribution is significant in the 1TAU0LEP channel, while diboson and $Z(\tau\tau)$+jets events become more relevant in the 1TAU1LEP and 2TAU channels. Events from all other SM processes (W+jets and Z+jets without τ-leptons, and various $t\bar{t}V$ and Higgs boson production processes) are grouped into the "Other" category.

Independent SUSY signal event samples were simulated for different simplified models. The range of gluino (squark) masses considered is 0.5–2.6 (0.4–2.0) TeV, and the corresponding range of $\tilde{\chi}_1^0$ masses is 0.1–1.7 (0.1–1.3) TeV, with a granularity of 200 GeV for $m(\tilde{g}/\tilde{q})$ and 100 GeV for $m(\tilde{\chi}_1^0)$ (with additional mass points in the compressed region). The matrix element (ME) calculation is performed at tree level and includes the emission of up to two additional partons. The ME–parton-shower matching uses the CKKW-L prescription [69,70], with the merging scale set to one quarter of the mass of pair-produced particles. Signal cross-sections are calculated to approximate next-to-next-to-leading order in the strong coupling constant, adding the resummation of soft gluon emission at next-to-next-to-leading-logarithm accuracy (giving "approximate NNLO+NNLL" accuracy) [71–79]. The nominal cross-section and its uncertainty are derived using the PDF4LHC21_40_PDFAS PDF set, following the recommendations of Ref. [80].

5 Event reconstruction and kinematic variables

The reconstruction algorithms and selection criteria described in this section are harmonised across Run 2 and Run 3. If an event contains several objects of the same type, they are ordered in decreasing transverse momentum, p_{T}.

Primary vertices are reconstructed from inner-detector tracks with $p_{\mathrm{T}} > 500$ MeV [126,127]. The primary vertex with the largest sum of squared track p_{T} is chosen as the hard-scatter vertex, and serves as the origin for all the objects described below except for τ-leptons, where a dedicated algorithm is used [128].

Jets are reconstructed from particle-flow objects [129] using the anti-k_t algorithm [130,131] with a radius parameter of $R = 0.4$. Jets undergo a sequence of calibrations which include components derived both from simulation and in situ measurements to correct for the difference between data and MC simulations [132]. Only jets with $p_{\mathrm{T}} > 20$ GeV and $|\eta| < 2.8$ are considered, this avoids objects whose energy is split between endcap and forward calorimeters. A neural-network-based jet vertex tagger (NNJVT) [133] using the default ("FixedEffPt") working point is applied to jets with $p_{\mathrm{T}} < 60$ GeV and $|\eta| < 2.5$ to suppress those from pileup. Jets originating from the hadronisation of b-quarks are tagged with the DL1dv01 tagger [134–136]. It uses a fixed 85%-efficiency working point corresponding to a selection that correctly identifies 85% of the b-jets with $|\eta| < 2.5$, as determined in a sample of simulated $t\bar{t}$ events, and is applied only to jets in that $|\eta|$ range. The b-tagging efficiencies in simu-

Table 1 Summary of the generators used to simulate the signal and background processes. The "dedicated" tune is the set of tuned parton-shower parameters developed by the SHERPA authors. The symbol "V" stands for a vector boson

Physics process	$\sqrt{s}$ [TeV]	Generator	Parton shower	Accuracy	Tune	PDF (generator)	PDF (shower)
$Z(\ell\ell)$+jets	13	SHERPA 2.2.11 [81]	SHERPA 2.2.11 [82]	NNLO [83]	Dedicated	NNPDF3.0NNLO [84,85]	NNPDF3.0NNLO
	13.6	SHERPA 2.2.14	SHERPA 2.2.14	NNLO	Dedicated	NNPDF3.0NNLO	NNPDF3.0NNLO
$Z(\tau\tau)$+jets	13/13.6	SHERPA 2.2.14	SHERPA 2.2.14	NNLO	Dedicated	NNPDF3.0NNLO	NNPDF3.0NNLO
$W(\ell\nu)$+jets	13	SHERPA 2.2.11	SHERPA 2.2.11	NNLO	Dedicated	NNPDF3.0NNLO	NNPDF3.0NNLO
	13.6	SHERPA 2.2.14	SHERPA 2.2.14	NNLO	Dedicated	NNPDF3.0NNLO	NNPDF3.0NNLO
VV, VVV	13	SHERPA 2.2.1, 2.2.2, 2.2.14	SHERPA 2.2.1, 2.2.2, 2.2.14	NLO [86–89]	Dedicated	NNPDF3.0NNLO	NNPDF3.0NNLO
	13.6	SHERPA 2.2.14	SHERPA 2.2.14	NLO	Dedicated	NNPDF3.0NNLO	NNPDF3.0NNLO
$t\bar{t}$	13/13.6	POWHEG BOX v2 [90–93]	PYTHIA 8 [94]	NNLO+NNLL [95–101]	A14 [102]	NNPDF3.0NLO	NNPDF2.3LO [68]
Single-top:							
Wt	13/13.6	POWHEG BOX v2	PYTHIA 8	NLO+NNLL [103,104]	A14	NNPDF3.0NLO	NNPDF2.3LO
s- and t-channels	13/13.6	POWHEG BOX v2	PYTHIA 8	NLO [105,106]	A14	NNPDF3.0NLO	NNPDF2.3LO
$t\bar{t}+V$	13/13.6	MADGRAPH5_AMC@NLO 2.3.3 [107]	PYTHIA 8	NLO [108]	A14	NNPDF3.0NLO	NNPDF2.3LO
$t\bar{t}+H$	13/13.6	POWHEG BOX v2 [109]	PYTHIA 8	NLO [107]	A14	NNPDF3.0NLO	NNPDF2.3LO
$VH(\tau\tau)$	13/13.6	POWHEG BOX v2 [93,110,111]	PYTHIA 8	NNLO + NLO [112–118]	AZNLO [119]	NNPDF3.0NLO	NNPDF2.3LO
$ggH(\tau\tau)$	13	POWHEG BOX v2	PYTHIA 8	NNLL+NNLO	AZNLO	NNPDF3NLO	NNPDF2.3LO
	13.6	POWHEG BOX v2	PYTHIA 8	NNLL+NNLO [120–125]	A14	NNPDF3NLO	NNPDF2.3LO
VBF $H(\tau\tau)$	13	POWHEG BOX v2	PYTHIA 8	NNLO+NLO	AZNLO	NNPDF3NLO	NNPDF2.3LO
	13.6	POWHEG BOX v2	PYTHIA 8	NNLO+NLO	A14	NNPDF3NLO	NNPDF2.3LO
SUSY signal	13/13.6	MADGRAPH 3.3.1	PYTHIA 8	NNLO+NNLL [71–79]	A14	NNPDF3.0NLO	NNPDF2.3LO

lated events are corrected to match those measured in data [137].

Electron candidates are required to satisfy the "LooseAndBLayerLLH" identification criteria [138,139], and have $p_{\mathrm{T}} > 10$ GeV and $|\eta| < 2.47$. In addition, a $|z_0 \sin\theta| < 0.5$ mm selection is applied to the longitudinal impact parameter z_0 to suppress non-prompt electrons. Electron candidates have to survive the overlap removal procedure (OR, described below), to satisfy the "Tight_VarRad" isolation criterion and the "TightLLH" electron identification [138–140], and to have a transverse impact parameter d_0 significance smaller than 5 to be consider by the analysis.

Muon candidates are required to satisfy the "Medium" identification criteria [141,142], and have $p_{\mathrm{T}} > 10$ GeV, $|\eta| < 2.7$ and $|z_0 \sin\theta| < 0.5$ mm. If it survives the OR, a muon candidate is used by the analysis if it also satisfies the "PflowLoose_VarRad" isolation criteria [141,142] and has a d_0 significance smaller than 3.

Hadronically decaying τ-leptons are seeded by $R = 0.4$ anti-k_t jets reconstructed from topological cell clusters calibrated with the local hadronic cell-weighting scheme [143,144]. The production vertex of the visible part of a hadronic τ-lepton decay ($\tau_{\text{had-vis}}$) is then determined from tracks within $\Delta R = 0.2$ of the axis of the seed jet. The τ-lepton candidate is built using tracks and calorimeter-cell clusters, and undergoes a sequence of calibrations that compose the "$\tau_{\text{had-vis}}$ Energy Scale calibration" [128,145]. The τ-lepton candidates are required to have $p_{\mathrm{T}} > 20$ GeV, $|\eta| < 2.5$, and one or three tracks associated with the $\tau_{\text{had-vis}}$ vertex (as identified by a dedicated classifier [128]) with the sum of their charges equal to ± 1. The region $|\eta| \in [1.37, 1.52]$ is excluded, corresponding to the transition region between the barrel and endcap calorimeters. A classifier based on a recurrent neural network (RNN) [128] is used to separate τ-leptons from background jets, using tracking and calorimeter measurement information, including information about individual tracks and clusters, as input. The analysis uses the "medium" $\tau_{\text{had-vis}}$ identification (medium τ_{had} ID) working point, corresponding to 75% efficiency for 1-track and 60% efficiency for 3-track τ-leptons. To suppress electrons satisfying the medium τ_{had} ID selection, the "Loose" working point of a dedicated electron-veto algorithm based on an RNN classifier is used. Additionally, τ-lepton candidates that fail to satisfy the medium τ_{had} ID selection, but satisfy all other selections and a much looser RNN classifier score > 0.01 selection, are used by the analysis to estimate the fake-tau background. These objects are referred to as "anti-ID taus".

A single energy deposit in the calorimeter or a track in the inner detector can be used in the reconstruction of several analysis objects. To avoid double-counting and resolve the ambiguity, the OR procedure is performed for every event. It ensures that every detector signature is matched to at most one reconstructed object. The OR procedure used follows the one described in Ref. [146], with the addition that if a b-jet is closer than $\Delta R = 0.2$ to an anti-ID tau, the anti-ID tau is discarded, similarly to Ref. [147].

The missing transverse momentum $E_{\mathrm{T}}^{\text{miss}}$ is computed as the magnitude of $\vec{p}_{\mathrm{T}}^{\text{miss}}$, the negative vector sum of the transverse momenta of electrons, muons, τ-leptons or anti-ID taus, jets, and a "soft term" composed of tracks from the primary vertex not associated with any reconstructed objects [148]. Only anti-ID taus that are "promoted" to τ-leptons when modelling the fake-tau backgound (Sect. 7) are treated as τ-leptons instead of jets in the computation. The "tight" $E_{\mathrm{T}}^{\text{miss}}$ working point is used, defining the properties of the jets used for the calculation. Three additional variables related to $E_{\mathrm{T}}^{\text{miss}}$ are used in the analysis:

- The transverse mass m_{T} is defined as $m_{\mathrm{T}}^2(\vec{p}_{\mathrm{T}}^{\,a}, \vec{p}_{\mathrm{T}}^{\,b}) = 2\left(p_{\mathrm{T}}^a p_{\mathrm{T}}^b - \vec{p}_{\mathrm{T}}^{\,a} \cdot \vec{p}_{\mathrm{T}}^{\,b}\right)$, where a and b represent any two massless particles. When the transverse mass of a singular object is used, e.g. $m_{\mathrm{T}}^{\tau_1}$, the massless $p_{\mathrm{T}}^{\text{miss}}$ vector is used for the second object in the computation.
- The stransverse mass m_{T2} [149,150] is used to discriminate between processes where two leptons come from a resonant decay and processes where they come from non-resonant decays. The m_{T2} variable is computed as

$$m_{\mathrm{T2}} = \min_{\vec{p}_{\mathrm{T}}^{\,a} + \vec{p}_{\mathrm{T}}^{\,b} = \vec{p}_{\mathrm{T}}^{\,\text{miss}}} \left(\max\left[m_{\mathrm{T}}(\vec{p}_{\mathrm{T}}^{\,\text{lep}_1}, \vec{p}_{\mathrm{T}}^{\,a}), m_{\mathrm{T}}(\vec{p}_{\mathrm{T}}^{\,\text{lep}_2}, \vec{p}_{\mathrm{T}}^{\,b}) \right] \right),$$

  where $\vec{p}_{\mathrm{T}}^{\,\text{lep}_1}$ and $\vec{p}_{\mathrm{T}}^{\,\text{lep}_2}$ correspond to the transverse momenta of the two leading leptons, at least one of which is a τ-lepton, and (a, b) refers to two invisible massless particles assumed to be produced with transverse momenta $\vec{p}_{\mathrm{T}}^{\,a}$ and $\vec{p}_{\mathrm{T}}^{\,b}$.
- Object-based $E_{\mathrm{T}}^{\text{miss}}$ significance [151] is a variable designed to separate events where the measured $E_{\mathrm{T}}^{\text{miss}}$ is consistent with being due to detector resolution smearing alone from events where $E_{\mathrm{T}}^{\text{miss}}$ is likely to be the result of neutrinos or SUSY particles not interacting with the detector material.

Another event-level variable used is H_{T}, the scalar sum of the p_{T} of jets, τ-leptons, electrons, and muons.

6 Analysis strategy

All events considered by the analysis are required to satisfy an inclusive preselection to ensure selection in the regime where the triggers operate at full efficiency. Since $E_{\mathrm{T}}^{\text{miss}}$ performance depends on the topology of the objects, the preselection affects not only the $E_{\mathrm{T}}^{\text{miss}}$ value, but also the jet

selection. The events are required to have $E_{\mathrm{T}}^{\mathrm{miss}} > 200$ GeV, at least one hadronically decaying τ-lepton, and at least two jets, one of which has $p_{\mathrm{T}} > 120$ GeV. Additionally, to suppress contributions from QCD multijet processes, where the $E_{\mathrm{T}}^{\mathrm{miss}}$ comes from mismeasurements of jet energies, the angular separation between the two leading jets and $E_{\mathrm{T}}^{\mathrm{miss}}$ is required to be larger than 0.4 in the transverse plane.

Several signal regions (SRs) that are sensitive to the SUSY models with τ-lepton$+E_{\mathrm{T}}^{\mathrm{miss}}$ signatures are defined. The common strategy for the design of the SRs is the multi-bin approach, where not only the yields, but also the shape of the most sensitive variable is utilised. The same kinematic-variable selections are used for Run 2 and Run 3 data samples, but the binning of each variable changes to ensure that at least five events are expected in each bin before any data-driven corrections are applied. All SRs are optimised using Asimov signal significance as the metric of merit [152].

Events with τ-leptons that either originate from τ_{had} decays (true τ-leptons) or from light leptons misidentified as τ-leptons are modelled using MC simulation with data-driven corrections. Dedicated control regions (CRs) enriched in major backgrounds are used to derive normalisation factors (NFs) in simultaneous fits of MC predictions to data (further described in Sect. 8). These affect only the overall normalisation of the MC simulation (i.e. the CRs are not binned in any variable), and only the events without jets misidentified as τ-leptons. Validation regions (VRs) are defined to be kinematically closer to the SRs than the CRs. The results of the fit are propagated from the CRs to the VRs, to validate the extrapolation to the SRs. Events with jets misidentified as τ-leptons are estimated in a data-driven way, as discussed in Sect. 7. These events are not normalised to the data, and no CRs are needed for them. The following subsections describe two different approaches used to define the SRs and CRs.

6.1 Machine-learning approach

The first approach is the ML-based analysis. The key ideas for this approach are that no kinematic variables are used to further define any of the regions except the classifier scores, and that the whole data sample is used inclusively. This approach allows the classifier to fully evaluate and utilise the correlation of all variables it is trained on. A multi-class approach is chosen, with one category for signal and multiple categories for SM processes. The different scores are normalised such that they are always positive and sum to 1 for every event.

Three boosted decision trees (BDTs) are trained using the XGBoost library [153], one for each of the three channels (1TAU0LEP, 1TAU1LEP, 2TAU). Four-momentum and high-level kinematic variables associated with τ-leptons and up to three leading jets are used for training, along with event-level variables such as $E_{\mathrm{T}}^{\mathrm{miss}}$, H_{T}, and $E_{\mathrm{T}}^{\mathrm{miss}}$ significance. In particular, the addition of the transverse mass and angular separation of the τ-lepton and $E_{\mathrm{T}}^{\mathrm{miss}}$ improves the performance significantly. Lepton kinematic variables, including m_{T2} and the invariant mass of the leading lepton and τ-lepton pair, are also used for training in the 1TAU1LEP channel. Transverse masses of τ-leptons, light leptons, and jets are some of the most important variables. The total number of leptons of each flavour and the stransverse mass m_{T2} of the two τ-leptons are used as additional input variables for the 2TAU channel. The sum of the transverse masses of the τ-leptons is also used, and is one of the most powerful variables. Only simulated events are used for the training, including those with fake taus. A mixture of Run 2 and Run 3 samples is used in the training of common classifiers; this approach outperforms separate training for Run 2 and Run 3 because of the larger training samples. The training samples are rescaled with class weights such that the class distributions are balanced. All simplified SUSY model simulations are included as a common Signal class, ensuring that a wide range of kinematic signatures is covered.

Each BDT is trained using five-fold cross-validation [154] and early stopping is implemented, triggering whenever the validation loss does not improve after 100 iterations. The maximum number of trees in the ensemble, per training fold, is taken to be 10 000, but the early stopping mechanism always terminates the training before reaching this number. The typical number of iterations is around 15 000 in the 1TAU0LEP channel, 5 000 in the 1TAU1LEP channel, and below 2 000 in the 2TAU channel. The loss function is defined as the multi-class logloss [155]. Hyperparameter optimisation was studied extensively, using both traditional grid searches and a modern optimiser using the Optuna software package [156]. A tree depth of five is found to maximise performance and minimise overtraining. For the regularisation parameters, the minimum information needed to decide on a node split (γ) is found to be the most important and is taken to be 0.1. The training is stable with respect to variations of other hyperparameters, so they are set to their default values. The training is optimised separately for the three search channels. However, utilising early stopping, the channels are found to converge to stable minima using the same set of hyperparameters with a learning rate of 0.01.

The final classification of an event is done in two steps. First, a selection based on the signal score is performed, separating events with high/medium/low signal scores into SRs/VRs/CRs. The high scores are selected to maximise the sensitivity to all the possible signal models considered, while the lower scores ensure that the signal contamination is below 1% in the CRs. Then the CRs and VRs are split according to the the most likely classification if the "Signal" class is ignored, i.e. the argument of the maxima of all the non-signal scores $\hat{y} \in \{Z, W, VV, \text{Top, fake tau}\}$. For example, $\hat{y} \in \{Z, VV\}$ refers to the set of events that enter the "Z" or "VV" class when the signal score is ignored.

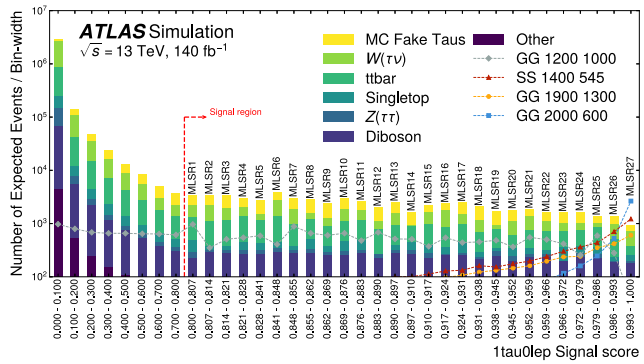

(a) Run 2 1tau0lep

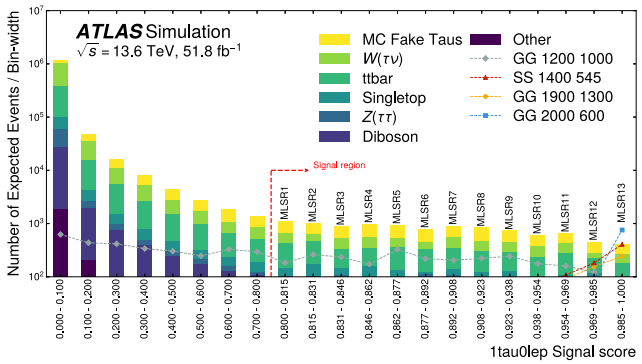

(b) Run 3 1tau0lep

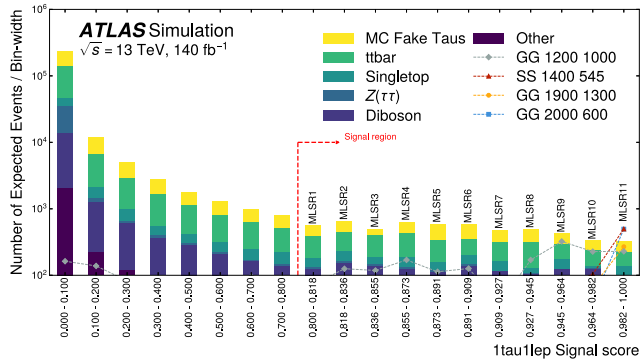

(c) Run 2 1tau1lep

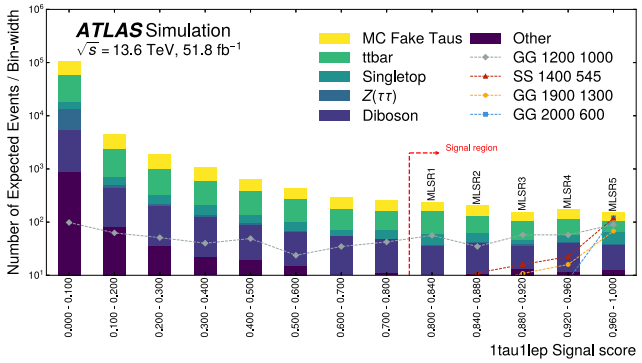

(d) Run 3 1tau1lep

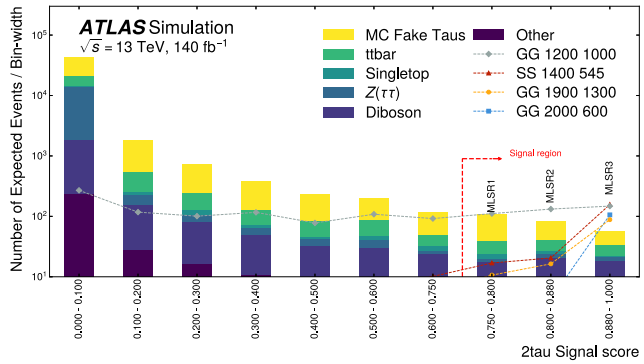

(e) Run 2 2tau

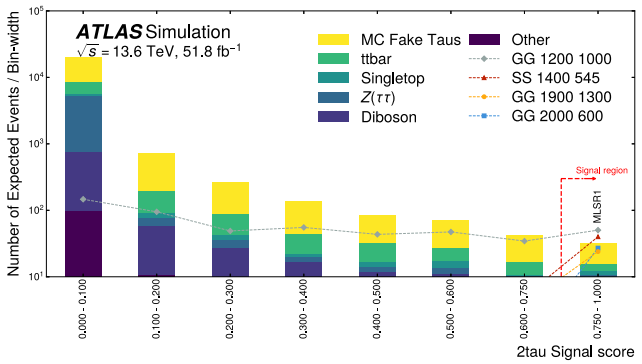

(f) Run 3 2tau

Fig. 2 Expected background composition across the range of signal scores. The numbers of events shown are normalised to their bin-width. Benchmark signal points are overlayed

In the 1tau0lep channel, six different classes are defined – W+jets, Z+jets, diboson, Top ($t\bar{t}$ + single-top-quark production), fake taus, and Signal. The SRs are defined by selecting events with a signal score larger than 0.8. The events selected in this way are then binned in signal score. This approach utilises the information encoded in the shape of the classifier score distribution, increasing the sensitivity and constraining the detector-related systematic uncertainties. Since the 1tau0lep channel has the largest yields, 27 (13) bins are defined in Run 2 (Run 3) 1tau0lep SRs. The dominant backgrounds are due to W+jets events, fake taus, and Top processes.

The contributions of W+jets events with true τ-leptons to the 1tau1lep and 2tau channels are strongly suppressed by the requirement of at least one additional lepton. Therefore, only five classes are used – Z+jets, diboson, Top, fake taus, and Signal. In the 1tau1lep channel, only events with a signal score larger than 0.8 are selected, and they are then

Table 2 Definitions of the ML-based 1TAU0LEP SRs, CRs and VRs

	Signal score	$\hat{y} = \{W, Z, VV\}$	$\hat{y} = \{\text{Top}\}$	$\hat{y} = \{Fake\}$
1TAU0LEP SR	> 0.8	–	–	–
1TAU0LEP W CR	< 0.3	True	–	–
1TAU0LEP W VR	$\in [0.3, 0.8]$	True	–	–
1TAU0LEP Top CR	< 0.3	–	True	–
1TAU0LEP Top VR	$\in [0.3, 0.8]$	–	True	–
1TAU0LEP Fake tau VR	< 0.3	–	–	True
1TAU0LEP Fake tight VR	$\in [0.3, 0.8]$	–	–	True

Table 3 Definitions of the ML-based 1TAU1LEP SRs, CRs and VRs

	Signal score	$\hat{y} = \{Z\}$	$\hat{y} = \{\text{Top}\}$	$\hat{y} = \{Fake\}$	$\hat{y} = \{VV\}$	Diboson score
1TAU1LEP SR	> 0.8	–	–	–	–	–
1TAU1LEP Z VR	< 0.8	True	–	–	–	–
1TAU1LEP Top CR	< 0.3	–	True	–	–	–
1TAU1LEP Top VR	$\in [0.3, 0.8]$	–	True	–	–	–
1TAU1LEP Fake tau VR	< 0.3	–	–	True	–	–
1TAU1LEP Fake tight VR	$\in [0.3, 0.8]$	–	–	True	–	–
1TAU1LEP VV CR	< 0.3	–	–	–	True	> 0.75
1TAU1LEP VV VR Run 2	$\in [0.15, 0.8]$	–	–	–	True	$\in [0.5, 0.75]$
1TAU1LEP VV VR Run 3	$\in [0.05, 0.8]$	–	–	–	True	$\in [0.5, 0.75]$

Table 4 Definitions of the ML-based 2TAU SRs, CRs and VRs

	Signal score	$\hat{y} = \{Z\}$	$\hat{y} = \{\text{Top}\}$	$\hat{y} = \{Fake\}$	$\hat{y} = \{VV\}$
2TAU SR	> 0.75	–	–	–	–
2TAU Z CR	< 0.75	True	–	–	–
2TAU Top VR	< 0.75	–	True	–	–
2TAU Fake tau VR	< 0.75	–	–	True	–
2TAU VV VR	< 0.75	–	–	–	True

binned in signal score. In total, 11 (5) bins are defined in the Run 2 (Run 3) 1TAU1LEP SRs. In the 2TAU channel the signal score requirement is relaxed to > 0.75 as the signal separation power of the classifier is much stronger; here, 3 bins are defined for Run 2, and 1 for Run 3.

The expected SM background distributions binned in the BDT scores for all channels are shown in Fig. 2. The binning in the SRs corresponds to the one used for the statistical analysis. The fake-tau contribution is estimated from the MC simulation on which the classifiers are trained. Yields from several benchmark signal models are overlayed, corresponding to the low-$\Delta m(\tilde{g}/\tilde{q}, \tilde{\chi}_1^0)$, high-$m(\tilde{g}/\tilde{q})$, and high-$m(\tilde{\chi}_1^0)$ signal-parameter phase space. The convention for benchmark signal-model names is "GG/SS $m(\tilde{g}/\tilde{q})$ $m(\tilde{\chi}_1^0)$" where GG/SS refers to the gluino/squark model, and the masses are given in GeV. The signal-model kinematic properties change with lower $\Delta m(\tilde{g}/\tilde{q}, \tilde{\chi}_1^0)$ values, becoming more background-like in the compressed region, which leads to a flatter classifier score distribution.

Six CRs are defined for each of the Run 2 and Run 3 data samples to derive separate sets of NFs. The split allows more freedom to treat different MC generator versions and other experimental differences. All CRs in the 1TAU0LEP and 1TAU1LEP channels are required to have signal scores < 0.3 to suppress potential signal contamination ($<1\%$ for any signal model not already excluded by previous searches). In the 2TAU channel, this requirement is relaxed to < 0.75, like in the SR definition. The definitions of all the CRs and VRs used in the ML-based approach are summarised in Tables 2, 3 and 4 and illustrated schematically in Fig. 3.

The overall yields of W+jets in the 1TAU0LEP channel are so large compared with Z+jets and diboson production that even a relatively small fraction of mislabelled events results in a large contribution to the $\hat{y} = \{Z, VV\}$ regions.

Therefore, the W+jets CR ($W(\tau\nu)$ CR 1TAU0LEP) is defined by the requirement $\hat{y} = \{W, Z, VV\}$. Even with this inclusive selection the purity of the CR is 84% (83%) in Run 2 (Run 3). The diboson CR is defined in the 1TAU1LEP channel (as this is the only channel with significant diboson production yields) by requiring a diboson classifier score > 0.75 (this automatically satisfies $\hat{y} = \{VV\}$ because the sum of scores is normalised to 1), to suppress Top and fake-tau background contamination. This selection results in a purity of 55% (49%) in Run 2 (Run 3). The Z+jets CR is then defined in the 2TAU channel, where this background makes the largest contribution to the SRs. The requirement for $Z(\tau\tau)$ CR 2TAU is $\hat{y} = \{Z\}$. The fraction of Z+jets events in these CRs is 90% in both Run 2 and Run 3. The NFs derived for these backgrounds apply to all three channels, even though the CRs are each defined only in one channel. This is motivated by the small $W(\tau\nu)$ and $Z(\tau\tau)$ background yields expected in the SRs other than 1TAU0LEP and 2TAU respectively, and similar kinematic properties of diboson processes observed across the channels.

The combined $t\bar{t}$ and single-top-quark production yield is large enough to allow a separate CR to be defined for each of the three channels by requiring $\hat{y} = \{\text{Top}\}$. These separate Top CRs allow the fit to accommodate differences between the channels. The purity of these regions is 78%/92%/71% (77%/90%/61%) in Run 2 (Run 3) in the 1TAU0LEP/1TAU1LEP/2TAU channels. The CR distributions of some important kinematic variables in data and MC simulation are shown in Fig. 4.

A validation region for W+jets is defined in the 1TAU0LEP channel by requiring a tighter selection on the signal score. Validation regions for Top backgrounds are similarly defined in the 1TAU0LEP and 1TAU1LEP channels. A diboson validation region is defined in the 1TAU1LEP channel, by requiring a diboson classifier score $\in [0.5, 0.75]$ and a signal score > 0.15 (0.05) for Run 2 (Run 3). The Z+jets validation region is defined in the 1TAU1LEP channel as well, as the yields in the 2TAU region are low. This region corresponds to $Z(\tau\tau)$ decays where one of the τ-leptons decays leptonically and the other decays hadronically. Another diboson VR is defined in the 2TAU channel by requiring $\hat{y} = VV$. This region is used for the validation of the overall modelling in the 2TAU channel because it is heavily contaminated by all major backgrounds. The VR distributions of some important kinematic variables in data and MC simulation are shown in Fig. 5.

No CRs are defined for fake taus. Instead, five VRs in total are used to validate the performance of the data-driven background modelling. These VRs are defined by requiring $\hat{y} = \{\text{fake tau}\}$. In the 1TAU0LEP and 1TAU1LEP channels the events with signal score $\in [0, 0.3]$ are used for fake-tau VRs. Signal scores $\in [0.3, 0.8]$ are used for the fake-tau tight VRs, which have significantly fewer events but are more signal-like kinematically. In the 2TAU channel, signal scores $\in [0, 0.75]$ are used to define the fake-tau VR, as the number of events available is much lower. The fake-tau VR distributions of some important kinematic variables in data and MC simulation are shown later, in Fig. 7.

6.2 Cut-and-count approach

In the cut-and-count analysis the data are split into three channels – 1TAU0LEP, 1TAU1LEP, and 2TAU, similarly to the ML-based approach. The 2TAU channel is used inclusively, targeting the higher-mass part of the signal parameter space. In the channels with exactly one τ-lepton, two different types of kinematic signatures are targeted, one corresponding to low $\Delta m(\tilde{g}/\tilde{q}, \tilde{\chi}_1^0)$, and the other to higher $m(\tilde{g}/\tilde{q})$. Unlike the ML approach, the CRs and VRs are used for all three channels inclusively.

The most powerful discriminating variables for the signal models considered in this paper are found to be related to the missing transverse momentum. For the 1TAU0LEP channel, $E_{\mathrm{T}}^{\mathrm{miss}}$ itself shows the most discrimination power and is used as the multi-bin variable, with selections on H_{T} and $m_{\mathrm{T}}^{\tau_1}$ providing suppression of SM backgrounds, while an $E_{\mathrm{T}}^{\mathrm{miss}} < 400$ GeV selection is used for CRs and VRs. Two orthogonal SRs are defined – the Compressed SR (CompSR, targeting the low-$\Delta m(\tilde{g}/\tilde{q}, \tilde{\chi}_1^0)$ signal models) and the High Mass SR (HMSR, targeting high-$m(\tilde{g}/\tilde{q})$ signal models). Their orthogonality is ensured by a requirement on the τ-lepton p_{T}. In the CompSR the small mass-splitting between the SUSY decay products results in soft τ-leptons, and the event selection requires $p_{\mathrm{T}}^{\tau_1} < 45$ GeV. In the HMSR the focus is on sensitivity to low m_{LSP} values, corresponding to larger mass-splitting and τ-leptons with higher transverse momentum. As such, all events in the HMSR are required to have $p_{\mathrm{T}}^{\tau_1} > 45$ GeV, and the requirement on $m_{\mathrm{T}}^{\tau_1}$ is set much higher than in CompSR. Another consequence of the larger mass-splitting in the signal events targeted by the HMSR is a higher jet multiplicity, which allows an $N_{\mathrm{jets}} \geq 3$ requirement to efficiently reduce the W+jets background. The exact selections used to define the 1TAU0LEP SRs are summarised in Table 5.

In the 1TAU1LEP channel the kinematic properties of the τ-leptons for the signal models remain approximately the same as in the 1TAU0LEP channel, and the same splitting into CompSR and HMSR is made by orthogonal selections on τ-lepton p_{T}. However, use of the $m_{\mathrm{T}}^{\tau_1} + m_{\mathrm{T}}^{\ell_1}$ variable, in addition to H_{T} and $m_{\mathrm{T}}^{\tau_1}$, further suppresses the Z+jets and W+jets backgrounds in the 1TAU1LEP channel. The main discriminating variable $E_{\mathrm{T}}^{\mathrm{miss}}$ is used for binning in both SRs. Due to the low lepton energies in the CompSR, the compressed-topology sensitivity is dominated by the 1TAU0LEP channel. However, in the HMSR the contribution from the 1TAU1LEP channel is significant. The exact

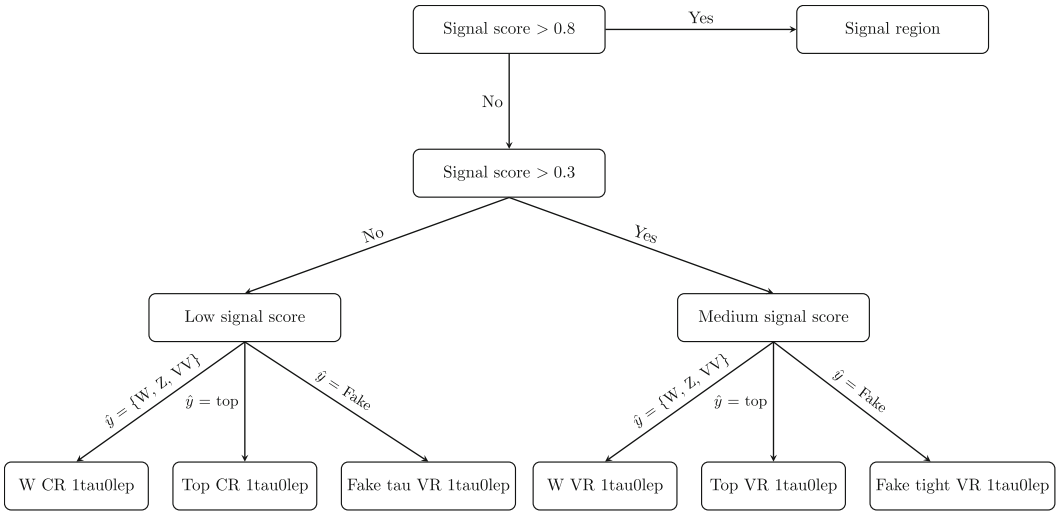

(a) 1tau0lep

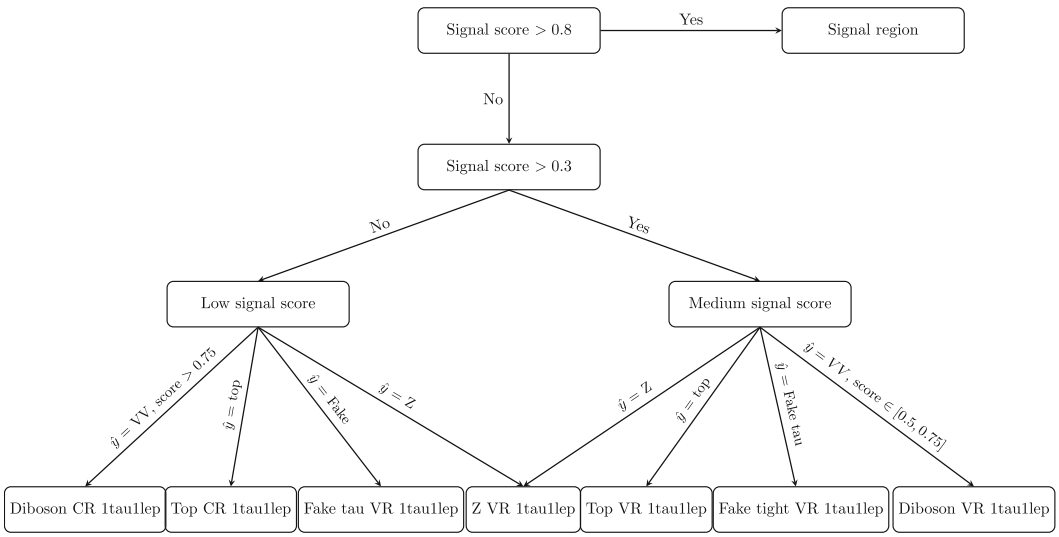

(b) 1tau1lep

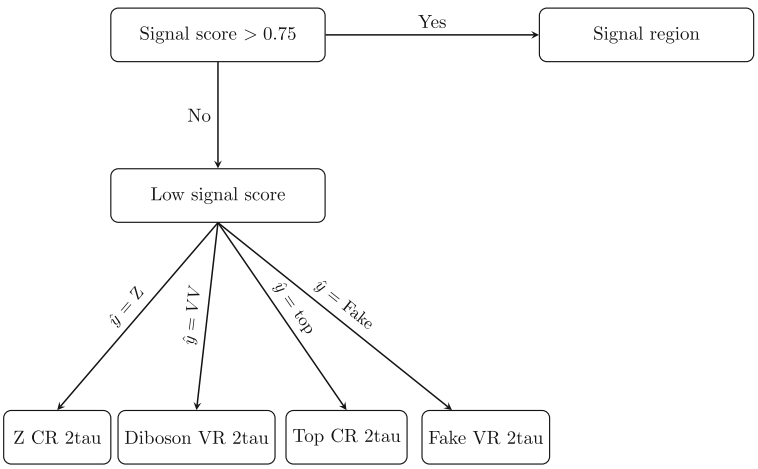

(c) 2tau

Fig. 3 Schematic definitions of the ML-based SRs, CRs and VRs. The diboson VR in the 1tau1lep channel additionally relaxes the signal score requirement to > 0.15 (0.05) for Run 2 (Run 3)

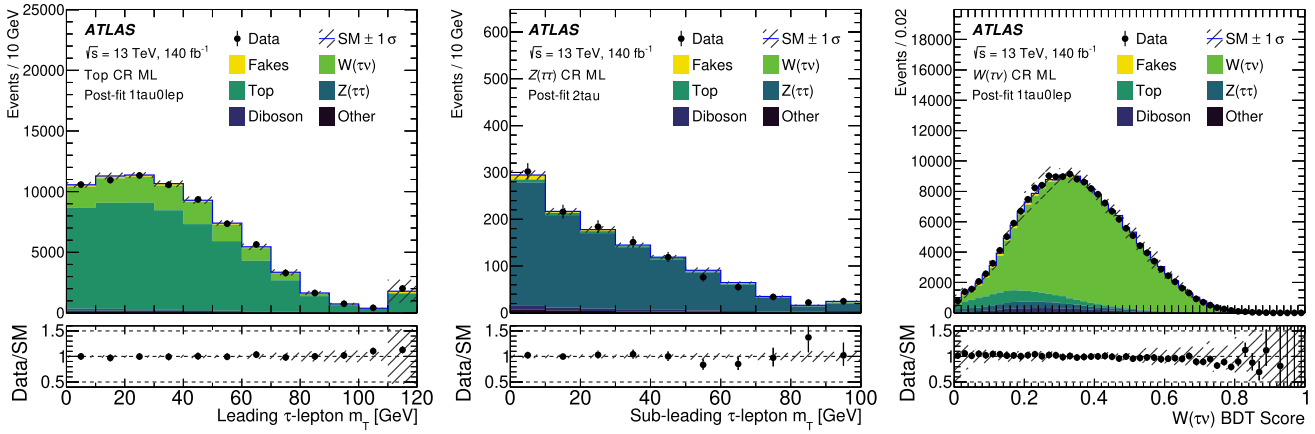

(a) Run 2, Top CR 1TAU0LEP, $m_{\mathrm{T}}^{\tau_1}$ (b) Run 2, $Z(\tau\tau)$ CR 2TAU, $m_{\mathrm{T}}^{\tau_2}$ (c) Run 2, $W(\tau\nu)$ CR, BDT score

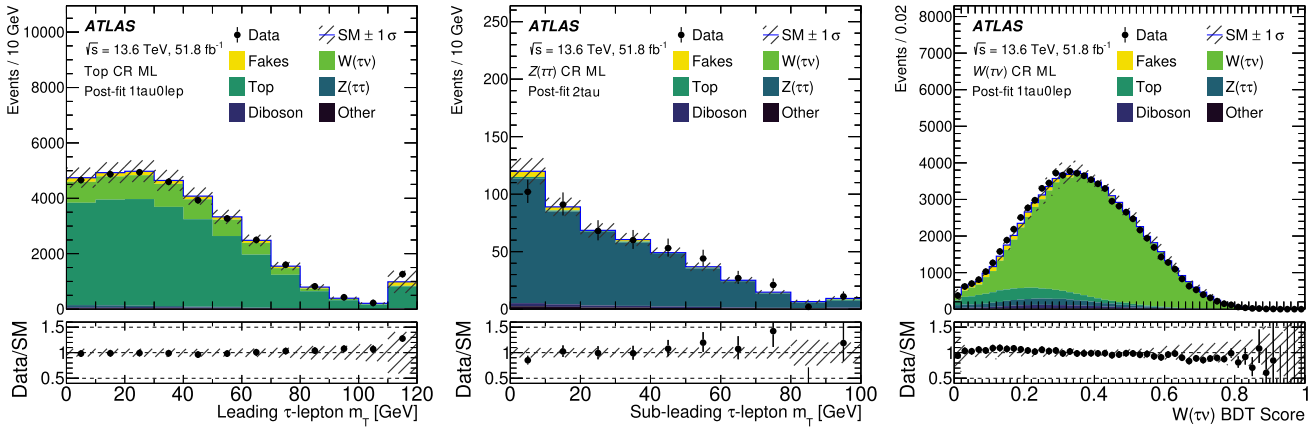

(d) Run 3, Top CR 1TAU0LEP, $m_{\mathrm{T}}^{\tau_1}$ (e) Run 3, $Z(\tau\tau)$ CR 2TAU, $m_{\mathrm{T}}^{\tau_2}$ (f) Run 3, $W(\tau\nu)$ CR, BDT score

Fig. 4 Distributions of important variables used in ML-based CRs in Run 2 (top row) and Run 3 (bottom row). The total statistical and systematic uncertainty of the SM background is shown by the hatched band. The top-quark, diboson, $W(\tau\nu)$, and $Z(\tau\tau)$ background predictions are normalised according to the background-only fit. The leftmost and rightmost bins include the underflow and overflow entries respectively. The ratio of the observed yield to the expected yield is shown in the lower panel

selections used in the 1TAU1LEP channel are summarised in Table 5.

In both the 1TAU0LEP and 1TAU1LEP channels, the main backgrounds come from $t\bar{t}$ and W+jets production. In the 1TAU0LEP channel, $W(\tau\nu)$+jets is the dominant background, while in the 1TAU1LEP channel it is $W(\ell\nu)$+jets production with one of the jets misidentified as a τ-lepton. Multijet events with a misidentified τ-lepton are another significant background in the 1TAU0LEP CompSR.

Finally, for the 2TAU channel, the $m_{\mathrm{T}}^{\tau_1} + m_{\mathrm{T}}^{\tau_2}$ variable provides the most discriminating power and is used for binning in the SR. This variable is highly correlated with $E_{\mathrm{T}}^{\mathrm{miss}}$, and no additional $E_{\mathrm{T}}^{\mathrm{miss}}$ selection beyond the preselection improves the sensitivity. Together with the H_{T} and N_{jets} requirements, it suppresses the SM backgrounds (mainly Z+jets). The selection of the two τ-leptons reduces the signal yields in the compressed region, so no splitting of the SRs is considered and the optimisation of the SR focuses on the high-$m(\tilde{g}/\tilde{q})$ scenarios only. The selections used to define the TwoTauSR are summarised in Table 5. All SRs are further binned in the most sensitive variables, $E_{\mathrm{T}}^{\mathrm{miss}}$ for 1TAU0LEP and 1TAU1LEP channels, $m_{\mathrm{T}}^{\tau_1} + m_{\mathrm{T}}^{\tau_2}$ for the 2TAU channel, with the exact values shown in Table 6.

Control regions enriched in Z+jets (Z CR) are selected by requiring the presence of exactly two τ-leptons with opposite charges. A veto on b-jets is applied to suppress Top backgrounds. To increase the purity of Z+jets and to reduce signal contamination, additional requirements on H_{T}, $m_{\mathrm{T}}^{\tau_1} + m_{\mathrm{T}}^{\tau_2}$, and m_{T2} variables are applied. The Z CRs have 82% (83%) purity in Run 2 (Run 3) and include most of the Z+jets available with the analysis preselection. No additional selection is imposed on the number of leptons – the contributions of

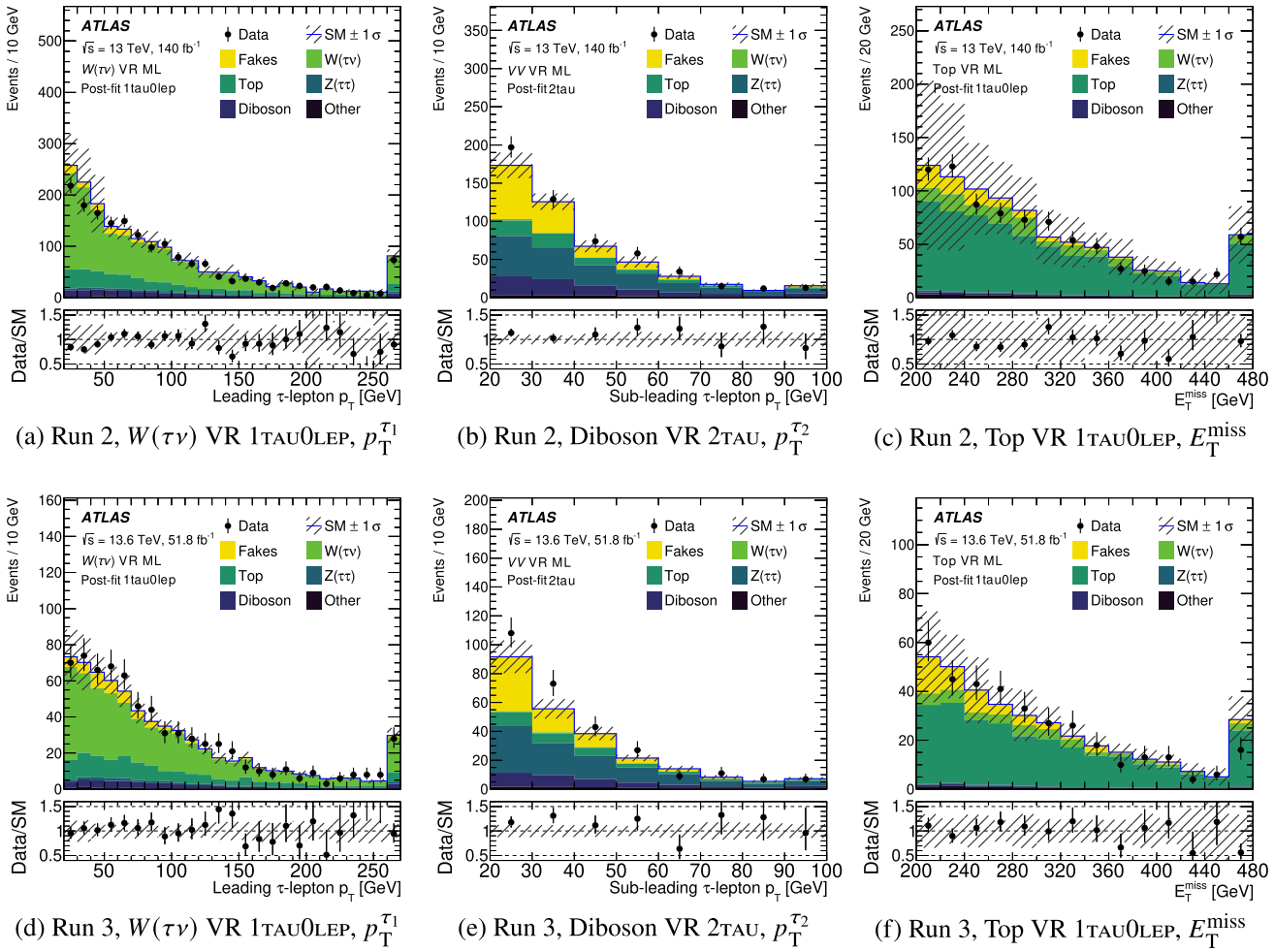

(a) Run 2, $W(\tau\nu)$ VR 1tau0lep, $p_{\mathrm{T}}^{\tau_1}$ (b) Run 2, Diboson VR 2tau, $p_{\mathrm{T}}^{\tau_2}$ (c) Run 2, Top VR 1tau0lep, $E_{\mathrm{T}}^{\mathrm{miss}}$

(d) Run 3, $W(\tau\nu)$ VR 1tau0lep, $p_{\mathrm{T}}^{\tau_1}$ (e) Run 3, Diboson VR 2tau, $p_{\mathrm{T}}^{\tau_2}$ (f) Run 3, Top VR 1tau0lep, $E_{\mathrm{T}}^{\mathrm{miss}}$

Fig. 5 Distributions of important variables used in ML-based VRs in Run 2 (top row) and Run 3 (bottom row). The total statistical and systematic uncertainty of the SM background is shown by the hatched band. The top-quark, diboson, $W(\tau\nu)$, and $Z(\tau\tau)$ background predictions are normalised according to the background-only fit. The leftmost and rightmost bins include the underflow and overflow entries respectively. The ratio of the observed yield to the expected yield is shown in the lower panel

Table 5 1tau0lep, 1tau1lep, and 2tau channel SR definitions for the cut-and-count approach

	Compressed SR		High mass SR		TwoTau SR
Channel	1tau0lep	1tau1lep	1tau0lep	1tau1lep	2tau
$N_e + N_\mu$	$= 0$	≥ 1	$= 0$	≥ 1	–
N_τ	$= 1$				2
$E_{\mathrm{T}}^{\mathrm{miss}}$ [GeV]	> 400				> 200
H_{T} [GeV]	–		> 1000		> 800
N_{jets}	≥ 2		≥ 3		≥ 3
$p_{\mathrm{T}}^{\tau_1}$ [GeV]	< 45		> 45		–
$m_{\mathrm{T}}^{\tau_1}$ [GeV]	> 80	–	> 250	> 120	–
$m_{\mathrm{T}}^{\tau_1} + m_{\mathrm{T}}^{\ell_1}$ [GeV]	–	> 350	–	> 350	–
$m_{\mathrm{T}}^{\tau_1} + m_{\mathrm{T}}^{\tau_2}$ [GeV]	–	–	–	–	> 150

Table 6 1TAU0LEP, 1TAU1LEP, and 2TAU channel SR binning for the cut-and-count approach

	$E_{\mathrm{T}}^{\mathrm{miss}}$ bins [GeV]	$m_{\mathrm{T}}^{\tau_1} + m_{\mathrm{T}}^{\tau_2}$ bins [GeV]
Run 2		
1TAU0LEP compressed SR	[400, 500, 600, 700, ∞]	–
1TAU1LEP compressed SR	[400, 550, 700, ∞]	–
1TAU0LEP high mass SR	[400, 500, 600, 700, ∞]	–
1TAU1LEP high mass SR	[400, 550, 700, ∞]	–
2TAU twoTau SR	–	[150, 200, 250, 300, 400, 500, 600, ∞]
Run 3		
1TAU0LEP compressed SR	[400, 500, 600, 700, ∞]	–
1TAU1LEP compressed SR	[400, 550, ∞]	–
1TAU0LEP high mass SR	[400, 500, 600, ∞]	–
1TAU1LEP high mass SR	[400, 550, ∞]	–
2TAU twoTau SR	–	[150, 200, 250, 300, 400, 500, ∞]

Table 7 Requirements for the cut-and-count CRs and VRs

	Z CR	W CR	Top CR	Z VR	W VR	Top VR
H_{T} [GeV]	≤ 800	≤ 800	≤ 800	≤ 800	[600, 1000]	
$E_{\mathrm{T}}^{\mathrm{miss}}$ [GeV]	–	≤ 300	≤ 300	≤ 300	[300, 400]	
N_τ	$= 2$	$= 1$	$= 1$	$= 1$	$= 1$	$= 1$
Charge	Opposite τ-lepton charge	–	–	–	–	–
$N_\mu + N_e$	–	$= 0$	$= 0$	≥ 1	$= 0$	$= 0$
$N_{\text{b-jets}}$	$= 0$	$= 0$	≥ 1	$= 0$	$= 0$	≥ 1
N_{jets}	≥ 2	≥ 3	≥ 3	≥ 2	≥ 3	≥ 3
$m_{\mathrm{T}}^{\tau_1}$ [GeV]	–	≤ 80	≤ 80	–	≤ 80	≤ 80
$m_{\mathrm{T}}^{\tau_1} + m_{\mathrm{T}}^{\tau_2}$ [GeV]	≤ 100	–	–	–	–	–
$m_{\mathrm{T}}^{\tau_1} + m_{\mathrm{T}}^{\ell_1}$ [GeV]	–	–	–	≤ 100	–	–
m_{T2} [GeV]	≤ 70	–	–	–	–	–
$m(\tau_1, \ell_1)$ [GeV]	–	–	–	< 60	–	–

Table 8 Requirements for the fake-tau validation regions in the cut-and-count channel

	Z($\nu\nu$) VR	W fake VR	Top fake VR
H_{T} [GeV]	≤ 800		
$E_{\mathrm{T}}^{\mathrm{miss}}$ [GeV]	≤ 300		
N_τ	$= 1$	$= 1$	$= 1$
$N_\mu + N_e$	$= 0$	$= 1$	$= 1$
$N_{\text{b-jets}}$	$= 0$	$= 0$	$= 1$
$m_{\mathrm{T}}^{\tau_1}$ [GeV]	$\in [100, 200]$	–	–
$m_{\mathrm{T}}^{\ell_1}$ [GeV]	–	≤ 100	≤ 100
$m(\tau_1, \ell_1)$ [GeV]	–	> 60	–
$E_{\mathrm{T}}^{\mathrm{miss}}/(E_{\mathrm{T}}^{\mathrm{miss}} + H_{\mathrm{T}})$	> 0.3	–	–
$\Delta\phi(\mathrm{jet}_1, p_{\mathrm{T}}^{\mathrm{miss}})$	> 2.0	–	–
$\Delta\phi(\tau_1, p_{\mathrm{T}}^{\mathrm{miss}})$	> 1.0	–	–

such events were studied and found to be less than 1% of the total yields.

Due to the potential signal contamination, no reasonably populated validation region can be defined for Z+jets in the 2TAU channel. Instead, the 1TAU1LEP channel is used. The events are required to have exactly one lepton and one τ-lepton, and a b-jet veto is applied. Additional requirements on $E_{\mathrm{T}}^{\mathrm{miss}}$, H_{T}, and the sum of transverse masses of the τ-lepton and ℓ are used to suppress signal and $t\bar{t}$ contamination. Finally, a selection on the visible invariant mass, $m(\tau,\ell) < 60$ GeV, suppresses the non-resonant contributions and keeps the region orthogonal to the fake-tau validation regions (described below).

Control regions enriched in W+jets background (W CR) are defined by requiring the presence of at least three jets and exactly one τ-lepton. A veto on b-jets and leptons is applied. Signal and fake tau contamination is suppressed by requirement on H_{T}, $E_{\mathrm{T}}^{\mathrm{miss}}$, and $m_{\mathrm{T}}^{\tau_1}$ variables. This results in highly populated regions with a purity of 82% (79%) in Run 2 (Run 3). The regions used to validate the W+jets corrections (W VR) are defined by tightening the $E_{\mathrm{T}}^{\mathrm{miss}}$ and H_{T} requirements of the W CR, keeping the selection orthogonal to the CR while ensuring that the kinematic selection is sufficiently similar to the SRs.

Another pair of CRs are used to correct the inclusive modelling of $t\bar{t}$ and single-top-quark backgrounds (Top CR). The dominant contribution comes from $t\bar{t}$ production, with single-top-quark production contributing 10−20% in all the analysis regions. A common normalisation factor is derived for the two backgrounds. The Top CR is defined similarly to the W CR, but with a requirement of at least one b-jet added. The purity of the Top CR is 72% (72%) in Run 2 (Run 3). The validation regions for Top backgrounds (Top VR) are defined similarly, tightening the Top CR $E_{\mathrm{T}}^{\mathrm{miss}}$ and H_{T} requirements. The CR and VR definitions are the same in Run 2 and Run 3. The definitions of the CRs and VRs are summarised in Table 7, and the modelling of important kinematic variables is shown in Fig. 6. The potential signal contamination in all CRs is below 1% for all the signal models not excluded by the previous searches.

A set of additional validation regions is defined in order to monitor the data-driven modelling of the fake-tau backgrounds. W fake-tau (Top fake-tau) VRs are defined to be kinematically similar to the W(Top) CRs. The events are required to have exactly one ℓ and one τ-lepton, with additional kinematic selections on $E_{\mathrm{T}}^{\mathrm{miss}}$, H_{T}, and the lepton transverse mass $m_{\mathrm{T}}^{\ell_1}$ to suppress signal and true tau contamination. The W(Top) fake-tau VRs are also required to have exactly $0(\geq 1)$ b-tagged jets. Finally, the dilepton visible invariant mass has to exceed 60 GeV in the W fake-tau VR, suppressing $Z(\tau_{\mathrm{had}}\tau_{\mathrm{lep}})$ contributions. The $Z(\nu\nu)$ fake-tau VR is defined by selecting events with large $m_{\mathrm{T}}^{\tau_1}$, $E_{\mathrm{T}}^{\mathrm{miss}}/(E_{\mathrm{T}}^{\mathrm{miss}} + H_{\mathrm{T}})$, and angular separation between the τ-lepton/leading jet and $E_{\mathrm{T}}^{\mathrm{miss}}$ in the transverse plane, ensuring that the main $E_{\mathrm{T}}^{\mathrm{miss}}$ contribution comes from the invisible decay of Z boson. Events containing leptons or b-jets are vetoed while $E_{\mathrm{T}}^{\mathrm{miss}}$ and H_{T} requirements suppress signal contamination. The selection criteria for the fake-tau VRs are summarised in Table 8. The modelling of some important kinematic variables in data and simulation is shown in Fig. 8.

7 Modelling of jets misidentified as τ-leptons

All of the events used by the analysis are required to have at least one object satisfying the selection criteria for a τ-lepton. These objects are often actual, true τ-leptons, but some light leptons and jets can also satisfy the selection (fake taus). Events with τ-lepton candidates coming from all three lepton generations are modelled with MC simulation, as the multiplicity of such objects is well predicted. The multiplicity of jets in an event, on the other hand, is harder to model. Therefore, a data-driven approach is used to model such events inclusively, regardless of the SM process producing them. The method is based on the Universal Fake Factor (UFF) approach [157]. A notable advantage of the data-driven approach is that the backgrounds estimated in this way include contributions from multijet production, beam noise, and other hadronic backgrounds that are traditionally hard to model with MC simulation.

The UFF approach uses dedicated fake-tau-enriched regions that are independent of the analysis phase-space to measure the fake factors (FFs), defined as

$$\mathrm{FF} = \frac{\text{Number of fake taus passing medium tau ID criteria}}{\text{Number of fake taus not passing medium tau ID criteria}}$$

as a function of several τ-lepton kinematic variables – p_{T}, $|\eta|$, and decay mode. The main assumption is that the probability of an object to satisfy the τ_{had} ID criteria depends only on the properties of the object itself, so it can be extrapolated from any measurement region. This allows the use of the same technique and FF measurements for the two different search strategies, cut-and-count and ML-based.

Three FF measurement regions are used. The first one is a back-to-back dijet selection (Multijet) with an additional low-p_{T} (relative to the leading jet) τ-lepton candidate. The second region ($Z(\ell\ell)$) requires two same-flavour opposite-charge leptons consistent with a Z-boson decay with an additional τ-lepton candidate present. Finally, the third region is based on a same-charge muon and τ-lepton selection ($W(\mu\nu)$). The $W(e\nu)$ process was also considered, but ultimately rejected due to the large $Z(ee)$ contamination. An additional selection is imposed on the NNJVT score of the jet geometrically matched to the τ-lepton candidate before

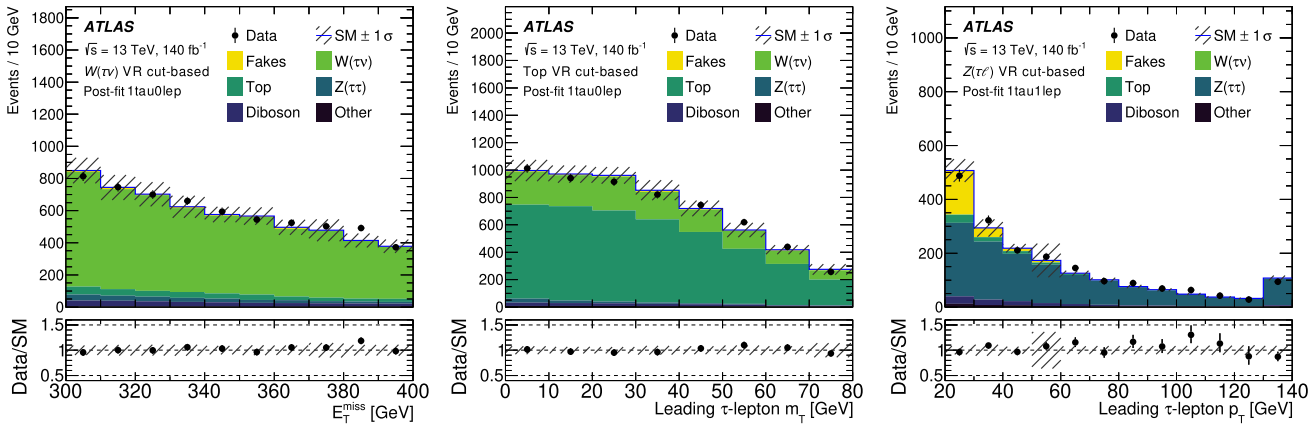

(a) Run 2, W VR, $E_{\mathrm{T}}^{\mathrm{miss}}$ (b) Run 2, Top VR, $m_{\mathrm{T}}^{\tau_1}$ (c) Run 2, Z VR, $p_{\mathrm{T}}^{\tau_1}$

(d) Run 3, W VR, $E_{\mathrm{T}}^{\mathrm{miss}}$ (e) Run 3, Top VR, $m_{\mathrm{T}}^{\tau_1}$ (f) Run 3, Z VR, $p_{\mathrm{T}}^{\tau_1}$

Fig. 6 Distributions of important variables used in cut-and-count VRs in Run 2 (top row) and Run 3 (bottom row). The total statistical and systematic uncertainty of the SM background is shown by the hatched band. The top-quark, $W(\tau\nu)$, and $Z(\tau\tau)$ background predictions are normalised according to the background-only fit. The leftmost and rightmost bins include the underflow and overflow entries respectively. The ratio of the observed yield to the expected yield is shown in the lower panel

the OR procedure is applied. This is done to further suppress/enhance contributions from the pileup jets. The details of the FF measurement regions are gathered in Table 9. In particular, the $E_{\mathrm{T}}^{\mathrm{miss}} < 50$ GeV requirement guarantees orthogonality to the analysis phase-space.

For each analysis CR, VR, and SR, an anti-ID region is defined by replacing the requirement on the number of τ-leptons with one on anti-ID taus. The contributions from τ-leptons modelled with the MC simulation are subtracted. The resulting data-minus-simulation mixture is scaled by the FFs as a function of anti-ID tau kinematic properties, giving the fake-tau background estimate in the nominal region. In the case of events with more than one τ-lepton, the data-driven approach is used if at least one of the two leading τ-leptons is a fake tau. The method described in Ref. [157] is used to avoid double-counting in events with two fake taus.

In the UFF approach, the most important variable to control is the jet origin of the fake tau. The jets can originate from gluons, light- or heavy-flavour quarks, and pileup, each having distinct properties. Several regions are used to measure FFs such that the mixture of fake tau origins is different in each of them. Templates of the track-based τ-lepton width variable

$$\frac{\Sigma p_{\mathrm{T}}^{\mathrm{track}_i} \times \Delta R(\tau, \mathrm{track}_i)}{\Sigma p_{\mathrm{T}}^{\mathrm{track}_i}},$$

which is sensitive to the jet origin mixture are also measured with the same binning as the FFs. Only the tracks matched to the $\tau_{\text{had-vis}}$ vertex or jets arising from the hard scattering interactions by a dedicated RNN-based track classifier are considered. The combined FF is determined in template fits using the track-based τ-lepton width.

Table 9 Fake-factor measurement regions. The $p_{\mathrm{T}}^{\mathrm{jet}_1}/p_{\mathrm{T}}^{\tau_1}$ requirement is relaxed to > 3 for $p_{\mathrm{T}}^{\tau_1} > 150$ GeV

Requirement	Multijet	$Z(\ell\ell)$	$W(\mu\nu)$
Single-jet trigger	Pass	–	–
Single-lepton trigger	–	Pass	Pass
N_τ	$= 1$	≥ 1	$= 1$
N_{jet}	≥ 2	–	–
$N_{\text{b-jets}}$	$= 0$	$= 0$	$= 0$
$\Delta R(\mathrm{jet}_1, \mathrm{jet}_2)$	[2.7, 3.5]	–	–
$p_{\mathrm{T}}^{\mathrm{jet}_1}/p_{\mathrm{T}}^{\tau_1}$	> 4	–	–
N_ℓ	–	$2e$ or 2μ	$0e$ and 1μ
$m(\ell_1, \ell_2)$ [GeV]	–	[70, 110]	–
Charge(τ_1, μ_1)	–	–	Same-sign
NNJVT score	> 0.8	> 0.8	< 0.8
$E_{\mathrm{T}}^{\mathrm{miss}}$ [GeV]	< 50	< 50	< 50
$E_{\mathrm{T}}^{\mathrm{miss}}$ significance	< 2	< 2	< 2
$\Delta\phi(\tau_1, p_{\mathrm{T}}^{\mathrm{miss}})$	> 1.0	> 1.0	> 1.0

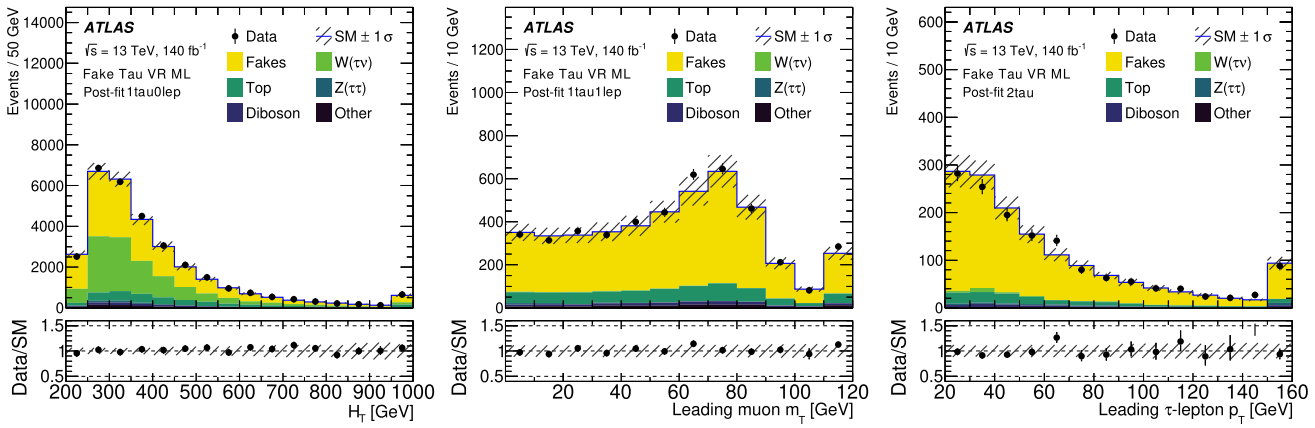

(a) Run 2, fake-tau VR 1TAU0LEP, H_{T} (b) Run 2, fake-tau VR 1TAU1LEP, $m_{\mathrm{T}}^{\mu_1}$ (c) Run 2, fake-tau VR 2TAU, $p_{\mathrm{T}}^{\tau_1}$

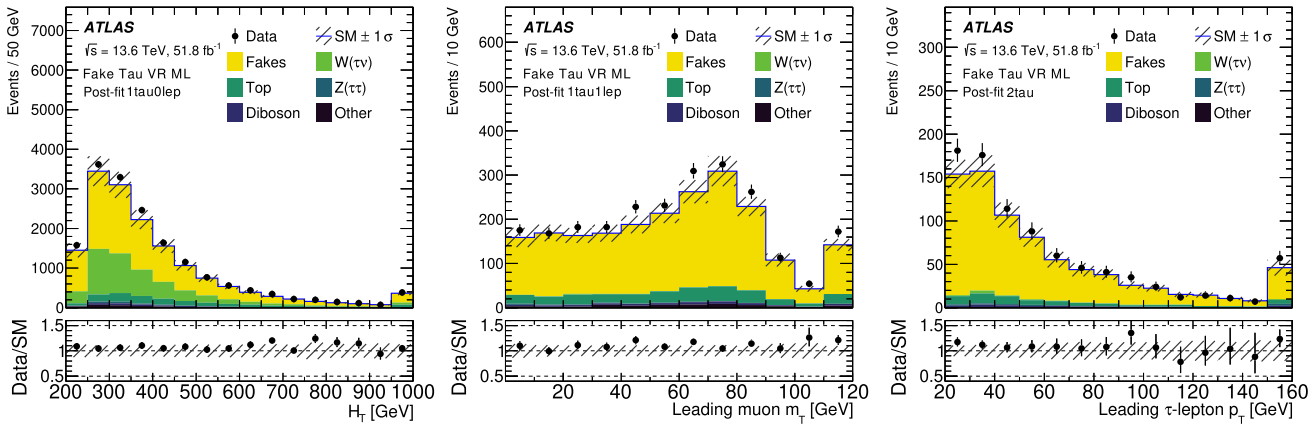

(d) Run 3, fake-tau VR 1TAU0LEP, H_{T} (e) Run 3, fake-tau VR 1TAU1LEP, $m_{\mathrm{T}}^{\mu_1}$ (f) Run 3, fake-tau VR 2TAU, $p_{\mathrm{T}}^{\tau_1}$

Fig. 7 Distributions of important variables used in the ML-based fake-tau VRs in Run 2 (top row) and Run 3 (bottom row). The total statistical and systematic uncertainty of the SM background is shown by the hatched band. The top-quark, diboson, $W(\tau\nu)$, and $Z(\tau\tau)$ background predictions are normalised according to the background-only fit. The leftmost and rightmost bins include the underflow and overflow entries respectively. The ratio of the observed yield to the expected yield is shown in the lower panel

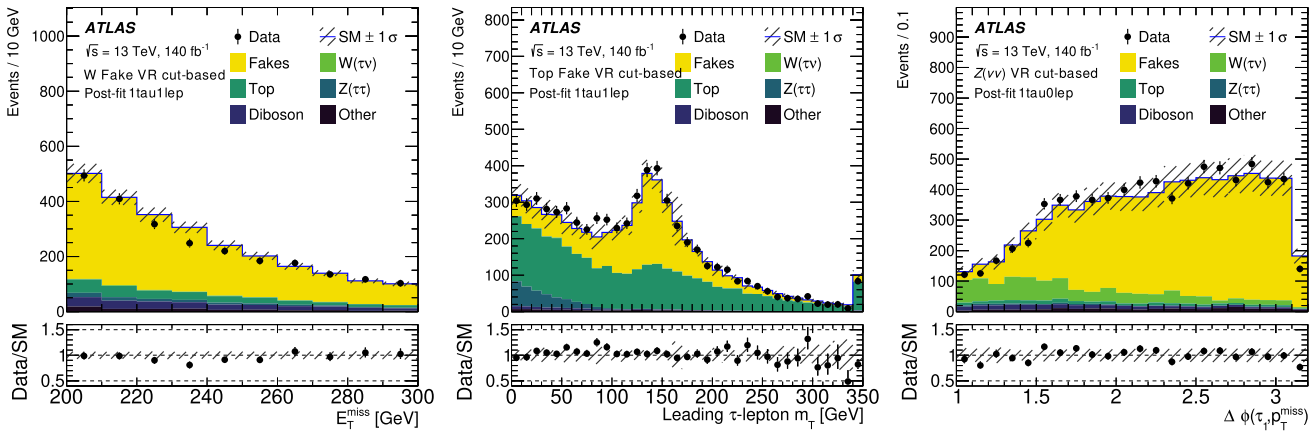

(a) Run 2, W fake-tau VR, $E_{\mathrm{T}}^{\mathrm{miss}}$ (b) Run 2, Top fake-tau VR, $m_{\mathrm{T}}^{\tau_1}$ (c) Run 2, Z($\nu\nu$) VR, $\Delta\phi(\tau_1, p_{\mathrm{T}}^{\mathrm{miss}})$

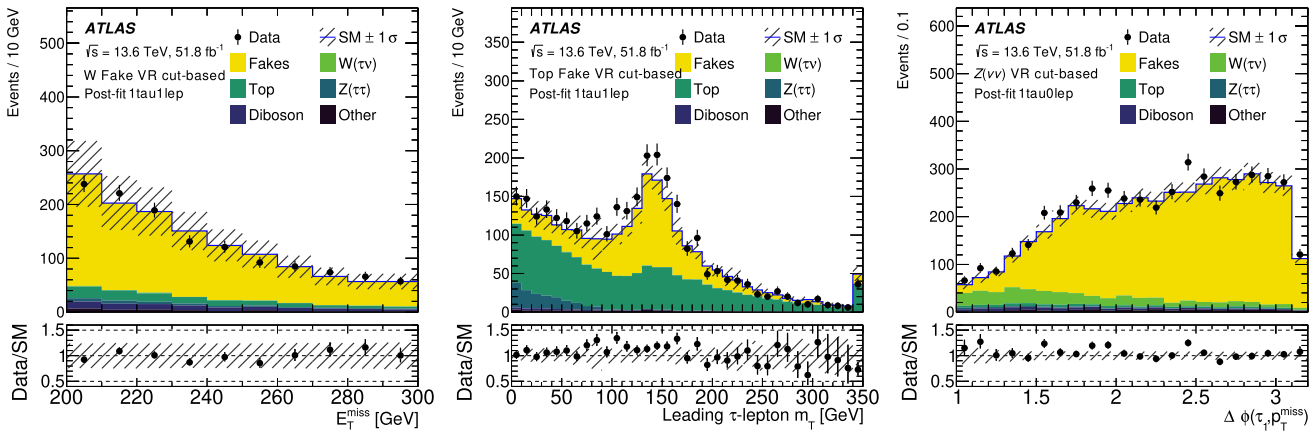

(d) Run 3, W fake-tau VR, $E_{\mathrm{T}}^{\mathrm{miss}}$ (e) Run 3, Top fake-tau VR, $m_{\mathrm{T}}^{\tau_1}$ (f) Run 3, Z($\nu\nu$) VR, $\Delta\phi(\tau_1, p_{\mathrm{T}}^{\mathrm{miss}})$

Fig. 8 Distributions of important variables used in cut-and-count fake-tau VRs in Run 2 (top row) and Run 3 (bottom row). The total statistical and systematic uncertainty of the SM background is shown by the hatched band. The top-quark, $W(\tau\nu)$, and $Z(\tau\tau)$ background predictions are normalised according to the background-only fit. The leftmost and rightmost bins include the underflow and overflow entries respectively. The ratio of the observed yield to the expected yield is shown in the lower panel

Several validation regions are defined to access the performance of the fake-tau modelling, as described in Sect. 6. The modelling of a few important kinematic variables is shown in Figs. 7 and 8 for the ML-based and cut-and-count approaches, respectively. The normalisation of the fake taus is not fitted to the data, but some of the VRs have significant contributions from $t\bar{t}$ and W+jets processes, which are corrected in the fits. The systematic uncertainties of this approach are described in Sect. 8.

8 Statistical analysis and systematic uncertainties

For the statistical analysis of the data the HISTFITTER workflow [158] is followed by using PYHF [159], the Python implementation of HISTFACTORY. Diagnostic utilities from the CABINETRY package [160] are also used. Two types of minimisation routines are used by PYHF: MINUIT (Migrad) [161] with NUMPY backend, and minimize from the SCIPY library [162] with JAX backend. As described in Sect. 6, dedicated CRs and SRs are defined and included in simultaneous likelihood fits. The binned-fit procedure is based on the HISTFACTORY [163] algorithm. It is used to build a parametric model describing the observed data, the nominal predictions, and the systematic and statistical uncertainties of these predictions, in all regions of interest. A general likelihood function L is constructed as a product of Poisson distributions, corresponding to the event counts in the binned regions, and constraint terms (Gaussian or Poisson) describing the systematic uncertainties. Signal rate(s) and normalisation factors for background processes are free within bounds in the fit, while the systematic uncertainties are subject to the con-

straints. The fit then minimises the value of $-\log(L)$. For the current analysis the asymptotic approximation [152] is assumed to be valid (and is validated by direct comparison with MC experiments). Three main fit types are used by the search, differing by the presence of different regions in the likelihood and the assumptions made about the signal model and rate.

In background-only fits, the signal contribution is assumed to be zero everywhere and the signal rate is thus decoupled from the fit. Only CRs are included in the fit, and the results are extrapolated to the VRs and SRs. The purpose of these fits is to evaluate the quality of background modelling and to allow model-independent statements to be made. All direct comparisons of data and MC modelling shown in this paper are either done before any fit or come from background-only fits.

Model-dependent (or exclusion) fits include both the CRs and SRs, which allows systematic uncertainties to be constrained more strongly. A particular signal model is assumed and the signal cross-section is included as the parameter of interest in the fit. For each of the models, the background-only and background-plus-signal hypotheses are tested and the CL_s prescription [164] is used to obtain results corresponding to an exclusion region defined by $CL_s < 0.05$. These fits are used to construct the exclusion contours that are presented in Sect. 9.

Finally, model-independent fits are used to make qualitative (and model-independent) statements about whether the measurements in single-bin regions are consistent with the SM predictions or not. All the CRs and one chosen SR are included in each of these fits. A signal contribution of zero is assumed in the CRs, and a signal contribution equal to the fitted signal strength is assumed in the SR. The signal rate derived from the fit is then interpreted as the allowed/excluded cross-section of the signal. The selection of the regions tested and the results are further discussed in Sect. 9.

For all of the fits, Run 2 and Run 3 data samples are first treated separately in individual fits. Combined Run 2 and Run 3 exclusion fits are then performed to obtain the most stringent limits.

The analysis considers three main types of systematic uncertainties. The experimental uncertainties include systematic uncertainties related to the reconstruction, identification, calibration, and corrections applied to the physical objects used in the analysis. Theoretical uncertainties comprise uncertainties of the MC generators and PDF sets. The third type of uncertainties considered are statistical uncertainties, related to the limited number of MC simulated events or limited number of data events used in the data-driven fake-tau estimations. The following correlation scheme is used:

- detector uncertainties are correlated across regions and samples;
- theory uncertainties are correlated across regions, but not samples;
- fake-tau uncertainties are uncorrelated across regions and samples, as they are largely statistical;
- no uncertainties are correlated between Run 2 and Run 3.

In the cases where correlation between Run 2 and Run 3 is expected (primarily jet and theory uncertainties), both correlation schemes were tested and no significant difference was observed. Thus, it is more practical to treat them as uncorrelated, simplifying the fitting procedures.

The experimental uncertainties are grouped according to the object they are applied to. Jet uncertainties include uncertainties from the energy scale calibration [165] and resolution [132], and the NNJVT jet-vertex-tagging uncertainties [166]. The jet flavour-tagging uncertainties [137,167,168] are also considered. Experimental uncertainties for τ-leptons consist of uncertainties from reconstruction and identification algorithms, energy scale calibrations, and the electron veto [145,169]. The experimental uncertainties for electrons and muons include uncertainties from reconstruction, isolation, and identification algorithms [138,139,141,142]. The resolution and energy scale uncertainties for all the objects used in the analysis are propagated into the $E_{\mathrm{T}}^{\mathrm{miss}}$ calculations, and uncertainties in the modelling of the underlying event and tracks not matched to any of the reconstructed objects are used to compute dedicated soft-term uncertainties [148].

The uncertainty in the combined Run 2 (Run 3) integrated luminosity is 0.83% (2.0%) [56,170,171], obtained from luminosity measurements with the LUCID-2 detector. Pileup reweighting is applied to all simulated events to match the observed conditions in data and is also assigned systematic uncertainties.

Dedicated uncertainties are applied to the fake-factor method for fake taus. The statistical uncertainty of the FFs due to the limited number of events in the measurement regions is one such uncertainty. The statistical uncertainty due to the limited number of data events in the anti-ID regions used for the measurements is also considered. The MC-simulated number of true τ-leptons in the anti-ID regions is varied by $\pm 30\%$ (as a conservative estimate of expected detector uncertainty), and the effect of this variation is included as a separate uncertainty. The shape uncertainty of the templates used to determine the flavour composition of the fake-tau seed jets and the uncertainty of the flavour composition itself are also considered. Given that most of the fake-tau uncertainties are statistical, no correlation between regions is assumed. Alternative correlation schemes were tested, and no significant difference was observed, so the no-correlation scheme is selected as the most conservative and straightforward approach.

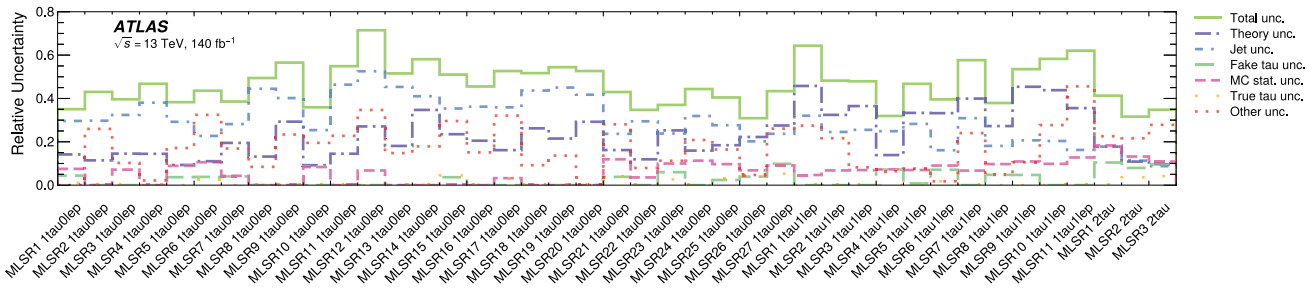

(a) Run 2 ML-based SRs

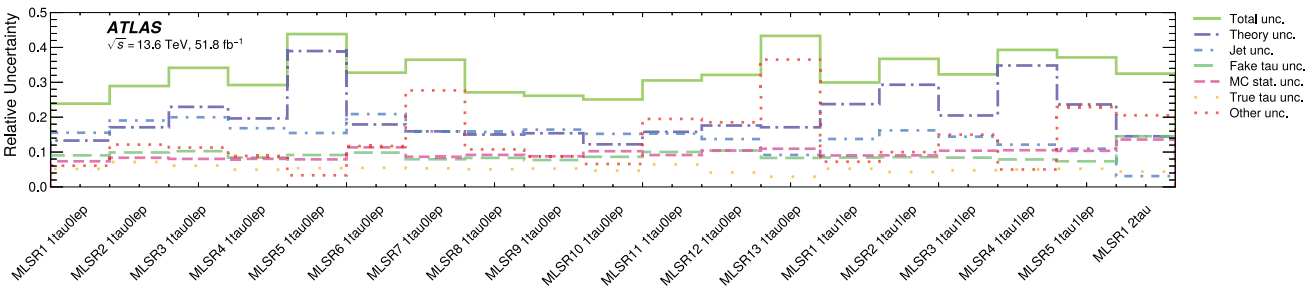

(b) Run 3 ML-based SRs

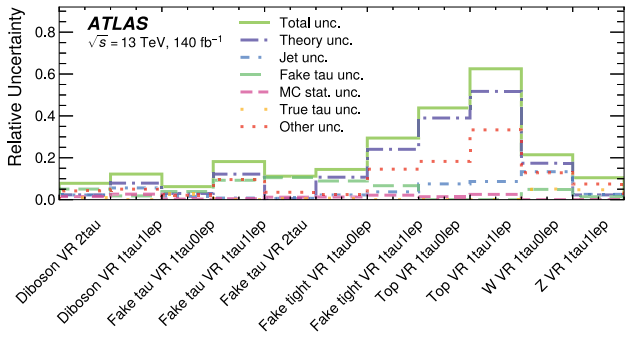

(c) Run 2 ML-based VRs

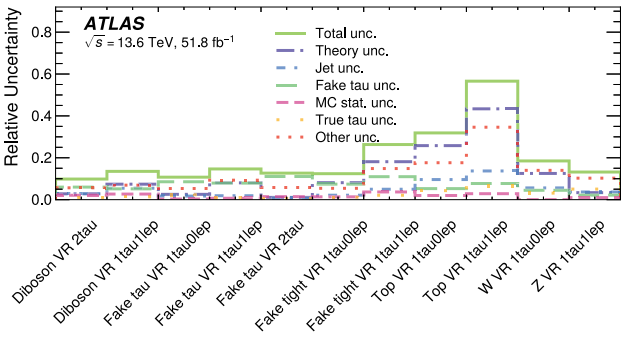

(d) Run 3 ML-based VRs

Fig. 9 Comparison of the dominant groups of systematic uncertainties in the total background prediction after the background-only fit for the ML-based approach, relative to the total yields. The total uncertainty is calculated using all the available systematic and statistical uncertainties. "Other" refers to $E_{\mathrm{T}}^{\mathrm{miss}}$, muon, electron, and pileup uncertainties. "True tau" refers to the experimental uncertainties of τ-leptons. The individual uncertainties can be correlated and do not necessarily add in quadrature to the total uncertainty

Variations of the factorisation and renormalisation scales (μ_{f} and μ_{r}) are used to estimate uncertainties due to the lack of higher-order corrections in the simulations. The standard 7-point scale-variation scheme is used, where $\{\mu_{\mathrm{r}}, \mu_{\mathrm{f}}\}$ are varied from their nominal values by factors of {0.5, 0.5}, {0.5, 1}, {1, 0.5}, {2, 1}, {1, 2}, and {2, 2}. These variations are implemented as alternative weights. The envelope of the effects of the six variations is used as the final uncertainty. For the NNPDF sets the standard prescription is followed [172], using the LHAPDF library to evaluate the effect of 100 alternative PDF variations. The effect of the PDF uncertainties is then combined in quadrature with the effect of varying the strong coupling constant α_{s}. Theoretical systematic uncertainties related to the PDF and scale variations are applied to all samples except the signal samples, for which dedicated higher-order cross-section uncertainties are available.

Additional theory uncertainties related to final-state radiation variations, variations of the A14 tune due to varying α_{s} for initial-state radiation, and variations of the merging parameter and resummation scale in SHERPA-generated samples [88,89] are considered where appropriate. For $t\bar{t}$ samples, a direct comparison is made with alternative samples generated such that the p_{T} of the POWHEG emission is tested against all other incoming and outgoing partons, and

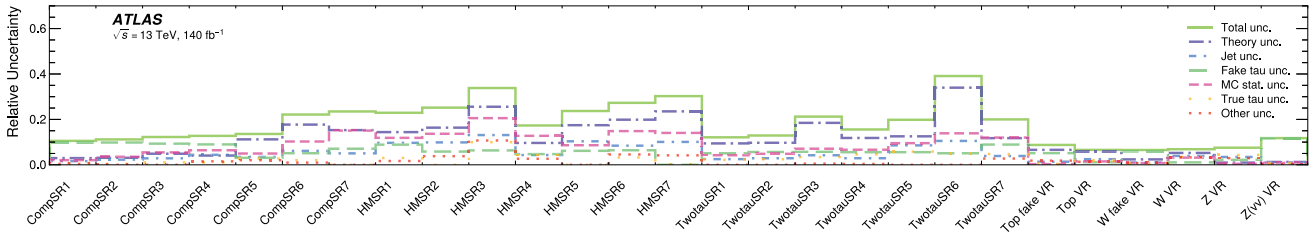

(a) Run 2 cut-and-count SRs and VRs

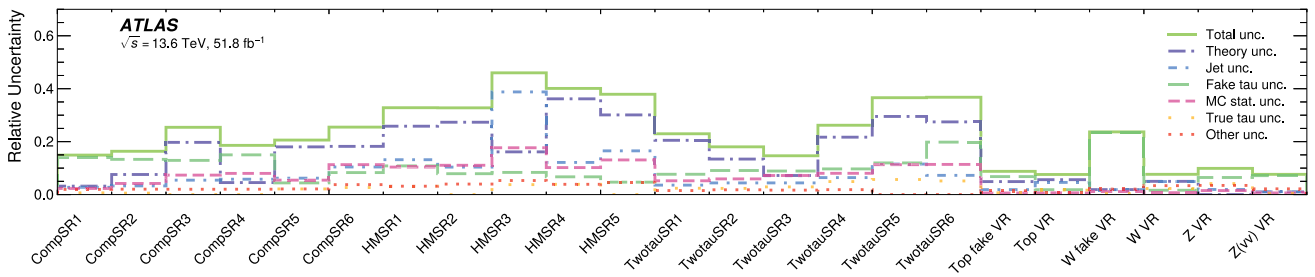

(b) Run 3 cut-and-count SRs and VRs

Fig. 10 Comparison of the dominant groups of systematic uncertainties in the total background prediction after the background-only fit for the cut-and-count approach, relative to the total yields. The total uncertainty is calculated using all the available systematic and statistical uncertainties. "Other" refers to $E_{\mathrm{T}}^{\mathrm{miss}}$, muon, electron, and pileup uncertainties. "True tau" refers to the experimental uncertainties of τ-leptons. The individual uncertainties can be correlated and do not necessarily add in quadrature to the total uncertainty

the minimum value is chosen as the *pThard* scale (i.e. the *pThard* parameter is set to option 1 in PYTHIA 8). Another comparison uses $t\bar{t}$ samples generated with the h_{damp} (first-emission damping parameter) value set to $3 \times m_{\mathrm{top}}$ instead of the nominal $1.5 \times m_{\mathrm{top}}$. The uncertainty from the parton-shower approach is estimated by comparing the nominal $t\bar{t}$ samples (POWHEG+PYTHIA) with POWHEG+HERWIG samples [173,174]. For single-top-quark production a comparison is made between samples produced using the diagram removal (nominal) and diagram subtraction schemes, which are used to remove the overlap with the $t\bar{t}$ production in the next-to-leading-order calculations.

For signal MC production, general simulation variations not affected by the cross-section uncertainties are also considered. These uncertainties include the radiation uncertainty and the effect of varying the factorisation and renormalisation scales, merging scales, and parton-shower tuning. The combined uncertainty from the signal theory uncertainties is estimated by using envelopes around the nominal result. From the comparisons the 68% (95%) confidence intervals generally lie within the 1σ (2σ) Poisson uncertainty of the nominal sample, indicating that no statistically significant effect is expected. A conservative upper limit of 10% is used for all signal models.

The largest individual contributions to the total uncertainty in the ML-based SRs come from the factorisation and renormalisation scale uncertainties for W+jets and Z+jets backgrounds, and comparisons with alternative generators for $t\bar{t}$ and single-top-quark MC samples. In the 1TAU0LEP channel the cumulative effect of experimental jet uncertainties is sizeable. Statistical uncertainties and modelling of the τ-leptons (true and fake) also contribute significantly in most SRs. In most of the cut-and-count SRs, Top theory uncertainties (mainly from comparisons with alternative generators) are dominant. In the HMSR 1TAU0LEP channel, factorisation and renormalisation scale uncertainties for W+jets backgrounds are important as well. The CompSR 1TAU0LEP channel is dominated by fake taus, leading to a large contribution from the fake-tau uncertainties.

The breakdown of the effects of different sources of systematic uncertainty in the VRs and SRs is shown in Figs. 9 and 10. To find the effect of a group of uncertainties, its square is evaluated as the difference between the squares of the total uncertainty and the uncertainty computed without this group. In the ML-based analysis the Run 2 SRs tend to have larger total uncertainties than the Run 3 ones, due to the effects of several experimental jet and $E_{\mathrm{T}}^{\mathrm{miss}}$ uncertainties in the 1TAU0LEP channel. The contribution of theory uncertainties is on average larger in Run 2 than in Run 3 in all channels. This can also be seen in the uncertainties of the Top VRs of Run 2 and Run 3. In the cut-and-count SRs, the Top theory uncertainties and jet non-closure uncertainties are more dominant in the Run 3 SRs, leading to larger total uncertainties overall. The fake-tau uncertainties are also larger in Run 3

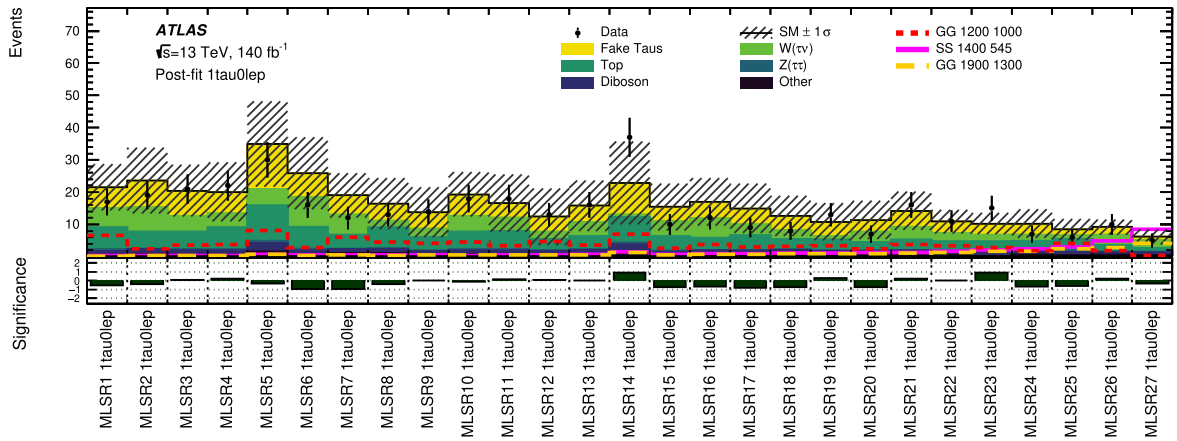

(a) Run 2 1TAU0LEP

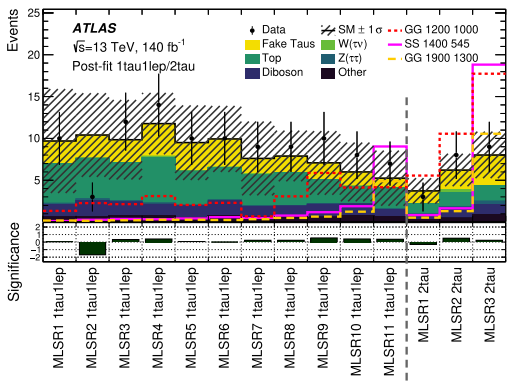

(b) Run 2 1TAU1LEP and 2TAU

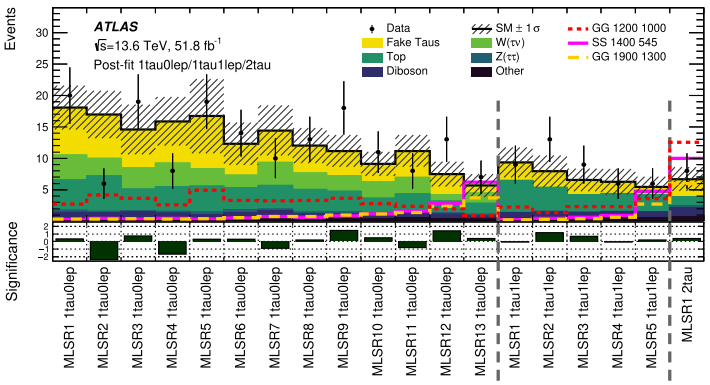

(c) Run 3

Fig. 11 A comparison of the observed and expected yields in the bins of the **a** Run 2 1TAU0LEP, **b** Run 2 1TAU1LEP and 2TAU, and **c** Run 3 ML SRs used in the analysis is shown in the upper panel. The lower panel shows the statistical significance [175] of the observation given the predicted number of events. The top-quark, $W(\tau\nu)$, and $Z(\tau\tau)$ background predictions are normalised according to the background-only fit. The total statistical and systematic uncertainty of the SM background is shown by the hatched band. Benchmark signal models are overlayed

because fewer events are available for measurements of the fake factors; this is the leading contribution in the CompSR 1TAU0LEP channel.

9 Results

The observed and expected yields in all the SRs used by the analysis are shown in Figs. 11 and 12. The NFs are determined with the background-only fit procedure described in Sect. 8. No significant deviations from the SM are observed. The largest excess of events has less than 2σ significance, in the Run 2 HMSR 1TAU0LEP $E_{\mathrm{T}}^{\mathrm{miss}} \in [400, 500]$ GeV bin. The largest deficit of events has just over 2σ significance, in the second bin of the Run 3 1TAU0LEP ML SR. Benchmark signal models are overlayed, showing that the minor excesses seen are not compatible with the expected SUSY signal yields. A slight tendency to overestimate the SM background is seen in the Run 2 CompSR 1TAU1LEP.

An exclusion fit is performed for every simplified SUSY model considered by the analysis. All of the relevant SRs are included in the fit together with the CRs. In addition to the NFs, the signal strength parameter μ is included as the parameter of interest. A comparison of the background-only ($\mu = 0$) and signal-plus-background ($\mu = 1$) hypothesis tests is performed. A common value of μ is used for Run 2 and Run 3 data. The signal model most compatible with the observed data is GG 1300 1200 in the ML-based SRs, with local p-value of 0.00058 ($Z = 3.2$). Following the convention adopted for ATLAS SUSY searches, the SUSY cross-section uncertainty due to missing higher-order corrections is not included in the fit directly. Instead, the effects of raising and lowering the nominal cross-section by its theoretical uncertainty are shown. The results are presented in the two-

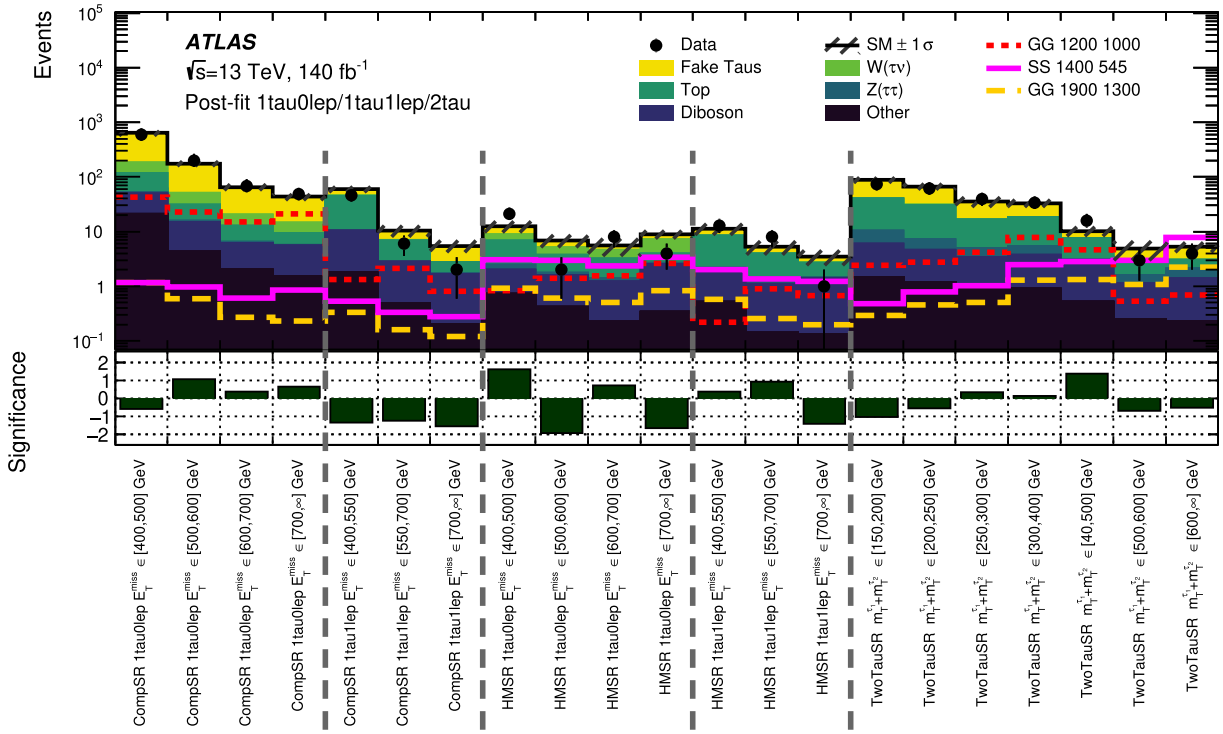

(a) Run 2

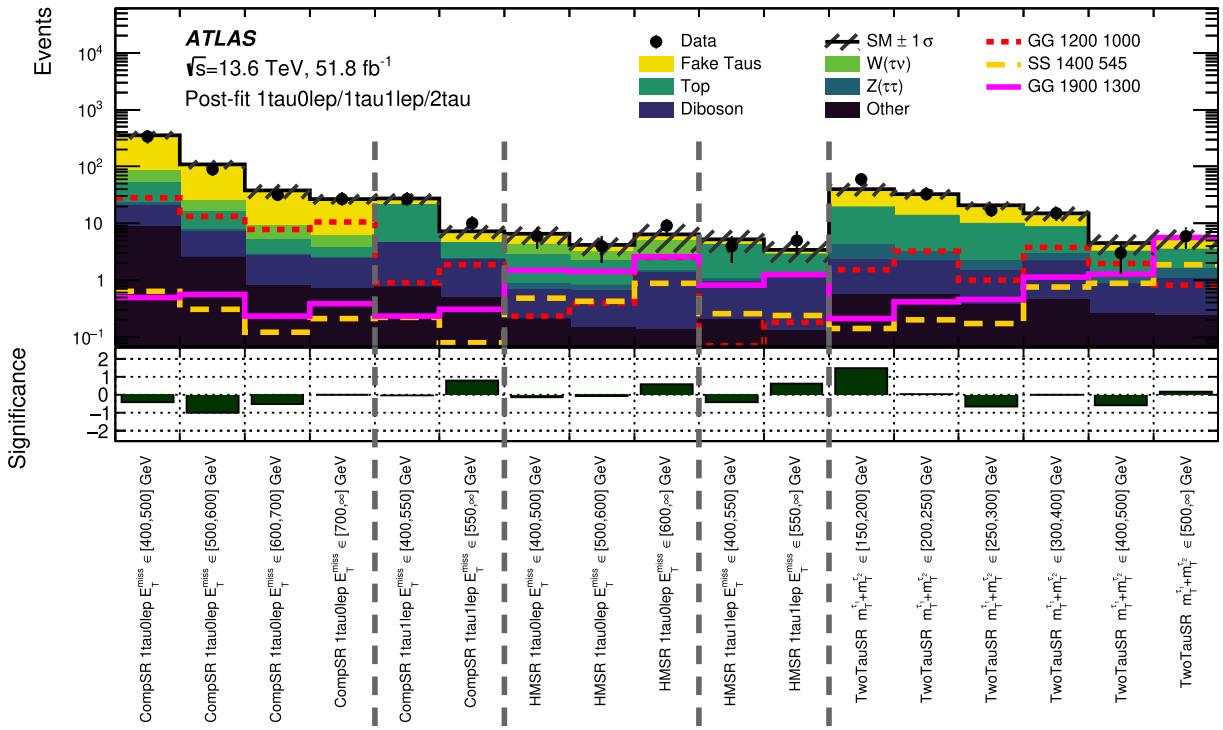

(b) Run 3

Fig. 12 A comparison of the observed and expected yields in the bins of the **a** Run 2 and **b** Run 3 cut-and-count SRs used in the analysis is shown in the upper panel. The lower panel shows the statistical significance [175] of the observation given the predicted number of events. The top-quark, $W(\tau\nu)$, and $Z(\tau\tau)$ background predictions are normalised according to the background-only fit. The total statistical and systematic uncertainty of the SM background is shown by the hatched band. Benchmark signal models are overlayed

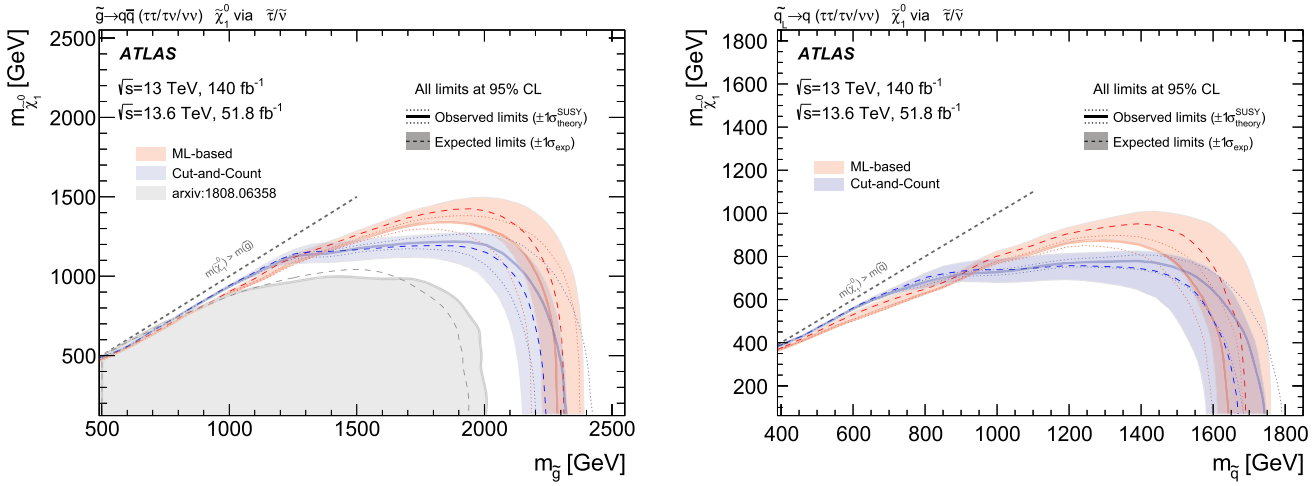

(a) Gluino models (b) Squark models

Fig. 13 The exclusion contours from the ML-based and cut-and-count approaches, for **a** gluino pair production and **b** squark pair production. The results are obtained using the CL_s prescription. The gluino limits are overlayed with the previous, partial Run 2, search

dimensional parameter spaces, as exclusion contours at 95% confidence level (CL) following the CL_s prescription, and as upper limits on $\sigma_{\text{obs}}/\sigma_{\text{SUSY}}$. The ML-based and cut-and-count analysis results are shown in Fig. 13 for both gluino and squark pair production. The ML approach has better sensitivity in the high-$m(\tilde{g}/\tilde{q})$ and high-$m(\tilde{\chi}_1^0)$ parts of the phase space, excluding gluino masses up to 2.25 TeV and $m(\tilde{\chi}_1^0)$ up to 1.35 TeV. For squark models, $m(\tilde{\chi}_1^0)$ values up to 0.85 TeV are excluded. The cut-and-count approach has stronger sensitivity towards the compressed, low-$\Delta m(\tilde{g}/\tilde{q}, \tilde{\chi}_1^0)$ region of the parameter space because of the dedicated CompSR regions, excluding models with $\Delta m(\tilde{g}, \tilde{\chi}_1^0) > 150$ GeV and $\Delta m(\tilde{q}, \tilde{\chi}_1^0) > 130$ GeV. The observed limits from the cut-and-count analysis also reach gluino masses of 2.3 TeV and squark masses of 1.7 TeV for the $m(\tilde{\chi}_1^0) = 0.1$ TeV models. A comparison of the presented results with the previous searches targeting similar final states with data collected in 2015–2016 is shown in Fig. 13a. The improvement is mainly due to the more sophisticated τ-lepton reconstruction and identification techniques, the larger data sample, and the use of ML techniques. Upper limits on the signal cross-section are shown in Fig. 14 for the ML-based and cut-and-count approaches. The upper limits are normalised to the theory SUSY cross-section for the corresponding $m(\tilde{g}/\tilde{q})$ pair production. Compared to Run 2 only, the combined Run 2 and Run 3 fits in the ML-based (cut-and-count) analysis strengthen the upper limits on the observed cross-section by up to 10% (30%) in the high-$m(\tilde{\chi}_1^0)$ regions, up to 20% (50%) in the low-$\Delta m(\tilde{g}/\tilde{q}, \tilde{\chi}_1^0)$ regions, and up to 10% (10%) in the low-m_{LSP} region.

Model-independent statements about the presence of new physics are made for several regions. A generic new signal is assumed to be present in one particular region, a signal-plus-background fit is performed over all CRs and the selected region, and the profile-likelihood-ratio test statistic is evaluated. The final bin of every individual SR is used for this procedure (one at a time) together with all the CRs. In the cut-and-count approach, these bins are the tails of kinematic distributions, sensitive to any new physics with τ-leptons and $E_{\text{T}}^{\text{miss}}$. For the ML-based approach the classifier score is intrinsically tuned to be sensitive to a particular class of SUSY models. If the new physics is sufficiently similar to the models the classifiers are trained on, the sensitivity is maximised. The limits are set independently for Run 2 and Run 3, not assuming any particular cross-section dependence for the new physics. The results, including the upper limit on the visible cross-section σ_{vis} at 95% CL, number of signal events given the observed and predicted numbers of background events, confidence level for the background-only hypothesis, and the discovery p-value and its associated significance, are presented in Table 10. Upper limits of 0.02−0.31 fb are placed on the cross-section of a new physics process appearing in these regions.

10 Conclusion

A search for pair production of supersymmetric particles with cascade decays in events with hadronically decaying τ-leptons, jets, and missing transverse momentum is presented, performed both with ML-based and cut-and-count approaches. Final states with exactly one τ-lepton and no other leptons, exactly one τ-lepton and at least one other lepton, or at least two τ-leptons are considered. The search

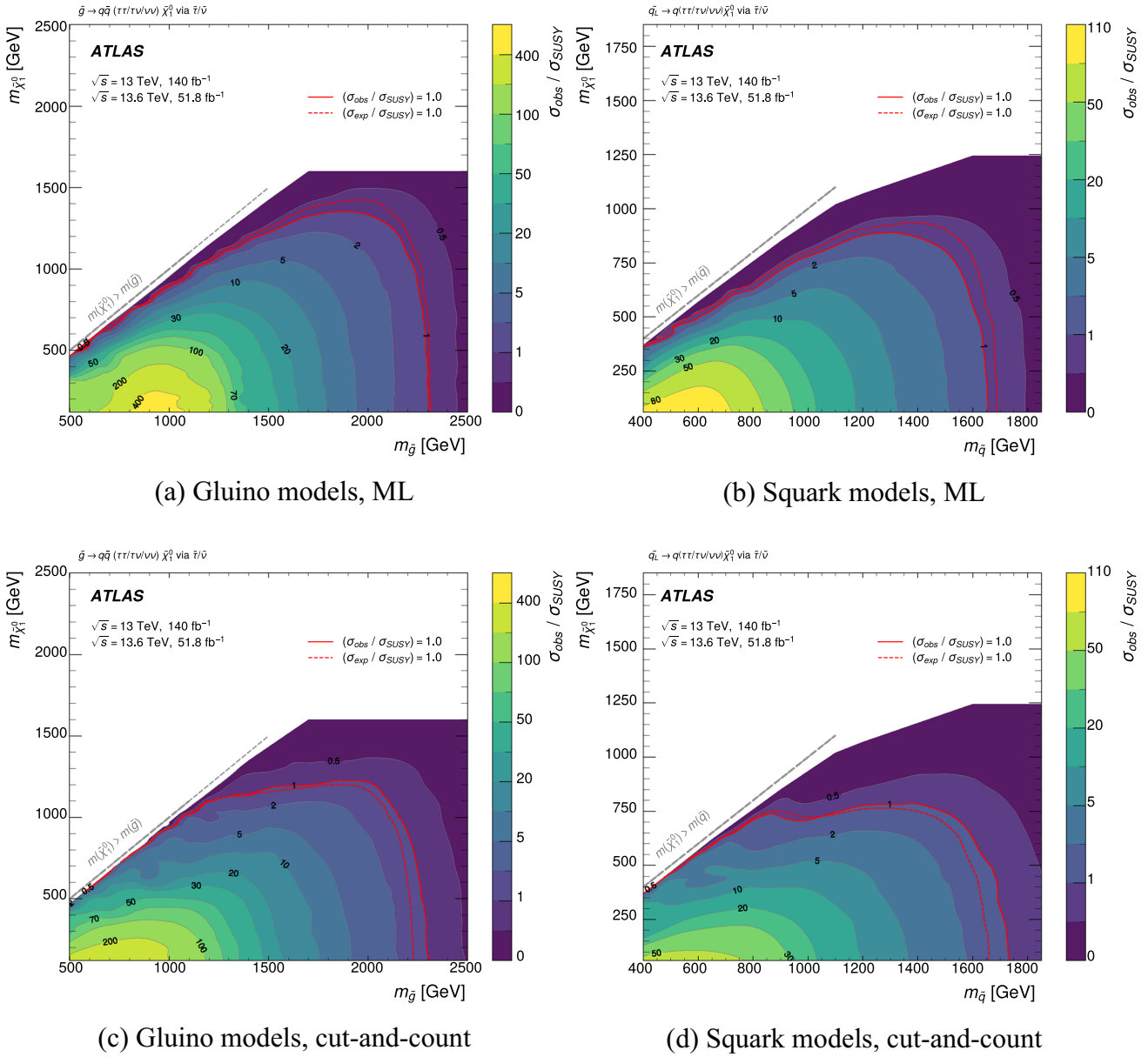

(a) Gluino models, ML

(b) Squark models, ML

(c) Gluino models, cut-and-count

(d) Squark models, cut-and-count

Fig. 14 Upper limit on the observed cross-section normalised to the theory-predicted SUSY cross-section, obtained with the ML-based (top row) and cut-and-count (bottom row) approaches

uses pp collisions at $\sqrt{s} = 13$ TeV and 13.6 TeV delivered by the Large Hadron Collider to collect data with the ATLAS detector in 2015–2018 and 2022–2023 respectively, corresponding to integrated luminosities of 140 fb^{-1} and 51.8 fb^{-1}. The enhanced calibration and identification algorithms, data sample, and analysis techniques improve the sensitivity across the whole range of masses considered compared to the previous searches. No significant deviations from the SM predictions are observed in either a cut-and-count or ML-based approach. The results are interpreted in the context of simplified supersymmetric models, setting the most stringent limits for these channels. For gluino pair-production models, gluino masses below 2.25 GeV are excluded, and LSP masses below 1.35 TeV are excluded for gluino masses around 2 TeV. Squark pair-production models with squark masses up to 1.7 TeV, and LSP masses up to 0.85 TeV are excluded.

Table 10 Upper limits at 95% CL on the visible cross-section σ_{vis}, on the number of signal events (S^{95}_{obs}), and on the number of signal events given the expected number (and $\pm 1\sigma$ excursions of the expectation) of background events (S^{95}_{exp}). The last two columns indicate the CL_b value (i.e. the confidence level observed for the background-only hypothesis), the discovery p-value (p_0), and its associated significance Z

Signal region	Bin	Total bkg	Data	σ_{vis} [fb]	S^{95}_{obs}	S^{95}_{exp}	CL_b	p_0 (Z)
Run 2 cut-and-count								
CompSR 1TAU0LEP	$E_{\text{T}}^{\text{miss}} > 700$ GeV	45 ± 4.3	49	0.16	22.2	$17.9^{+7.1}_{-5.2}$	0.73	0.26 (0.6)
CompSR 1TAU1LEP	$E_{\text{T}}^{\text{miss}} > 700$ GeV	4.6 ± 1.1	2	0.026	3.7	$6.0^{+3.1}_{-1.9}$	0.1	0.50 (0.0)
HMSR 1TAU0LEP	$E_{\text{T}}^{\text{miss}} > 700$ GeV	7.9 ± 1.3	4	0.031	4.3	$7.3^{+3.6}_{-2.3}$	0.08	0.50 (0.0)
HMSR 1TAU1LEP	$E_{\text{T}}^{\text{miss}} > 700$ GeV	2.6 ± 1.0	1	0.024	3.3	$5.1^{+2.7}_{-1.7}$	0.14	0.50 (0.0)
TwoTauSR 2TAU	$m_{\text{T}}^{\tau_1} + m_{\text{T}}^{\tau_2} > 600$ GeV	5.0 ± 0.9	4	0.036	5.0	$6.0^{+3.1}_{-1.9}$	0.33	0.50 (0.0)
Run 3 cut-and-count								
CompSR 1TAU0LEP	$E_{\text{T}}^{\text{miss}} > 700$ GeV	27 ± 3.6	27	0.29	14.8	$14.9^{+6.2}_{-4.3}$	0.5	0.50 (0.0)
CompSR 1TAU1LEP	$E_{\text{T}}^{\text{miss}} > 550$ GeV	8.1 ± 1.6	10	0.20	10.2	$7.8^{+3.7}_{-2.4}$	0.76	0.21 (0.8)
HMSR 1TAU0LEP	$E_{\text{T}}^{\text{miss}} > 600$ GeV	7.7 ± 1.9	9	0.31	16.0	$12.6^{+12.4}_{-5.5}$	0.63	0.26 (0.6)
HMSR 1TAU1LEP	$E_{\text{T}}^{\text{miss}} > 550$ GeV	3.9 ± 1.1	5	0.14	7.2	$5.8^{+3.0}_{-1.8}$	0.71	0.26 (0.6)
TwoTauSR 2TAU	$m_{\text{T}}^{\tau_1} + m_{\text{T}}^{\tau_2} > 550$ GeV	5.7 ± 1.5	6	0.14	7.4	$7.0^{+3.4}_{-2.2}$	0.55	0.44 (0.2)
Run 2 ML								
1TAU0LEP SR	MLSR27	5.5 ± 1.3	5	0.07	10.1	$11.3^{+6.7}_{-4.2}$	0.41	0.50 (0.0)
1TAU1LEP SR	MLSR11	6.3 ± 1.9	7	0.15	20.3	$18.2^{+6.8}_{-9.1}$	0.55	0.34 (0.4)
2TAU SR	MLSR3	8.5 ± 2.2	9	0.09	13.3	$12.4^{+6.9}_{-5.1}$	0.53	0.41 (0.2)
Run 3 ML								
1TAU0LEP SR	MLSR13	6.3 ± 1.7	7	0.29	15.1	$14.1^{+10.9}_{-6.7}$	0.54	0.35 (0.4)
1TAU1LEP SR	MLSR5	5.7 ± 1.5	6	0.20	10.6	$10.0^{+11.0}_{-4.4}$	0.53	0.43 (0.2)
2TAU SR	MLSR1	7.2 ± 1.7	8	0.17	8.9	$7.9^{+4.1}_{-2.6}$	0.61	0.36 (0.4)

Acknowledgements We thank CERN for the very successful operation of the LHC and its injectors, as well as the support staff at CERN and at our institutions worldwide without whom ATLAS could not be operated efficiently. The crucial computing support from all WLCG partners is acknowledged gratefully, in particular from CERN, the ATLAS Tier-1 facilities at TRIUMF/SFU (Canada), NDGF (Denmark, Norway, Sweden), CC-IN2P3 (France), KIT/GridKA (Germany), INFN-CNAF (Italy), NL-T1 (Netherlands), PIC (Spain), RAL (UK) and BNL (USA), the Tier-2 facilities worldwide and large non-WLCG resource providers. Major contributors of computing resources are listed in Ref. [176]. We gratefully acknowledge the support of ANPCyT, Argentina; YerPhI, Armenia; ARC, Australia; BMWFW and FWF, Austria; ANAS, Azerbaijan; CNPq and FAPESP, Brazil; NSERC, NRC and CFI, Canada; CERN; ANID, Chile; CAS, MOST and NSFC, China; Minciencias, Colombia; MEYS CR, Czech Republic; DNRF and DNSRC, Denmark; IN2P3-CNRS and CEA-DRF/IRFU, France; SRNSFG, Georgia; BMFTR, HGF and MPG, Germany; GSRI, Greece; RGC and Hong Kong SAR, China; ICHEP and Academy of Sciences and Humanities, Israel; INFN, Italy; MEXT and JSPS, Japan; CNRST, Morocco; NWO, Netherlands; RCN, Norway; MNiSW, Poland; FCT, Portugal; MNE/IFA, Romania; MSTDI, Serbia; MSSR, Slovakia; ARIS and MVZI, Slovenia; DSI/NRF, South Africa; MICIU/AEI, Spain; SRC and Wallenberg Foundation, Sweden; SERI, SNSF and Cantons of Bern and Geneva, Switzerland; NSTC, Taipei; TENMAK, Türkiye; STFC/UKRI, United Kingdom; DOE and NSF, United States of America. Individual groups and members have received support from BCKDF, CANARIE, CRC and DRAC, Canada; CERN-CZ, FORTE and PRIMUS, Czech Republic; COST, ERC, ERDF, Horizon 2020, ICSC-NextGenerationEU and Marie Skłodowska-Curie Actions, European Union; Investissements d'Avenir Labex, Investissements d'Avenir Idex and ANR, France; DFG and AvH Foundation, Germany; Herakleitos, Thales and Aristeia programmes co-financed by EU-ESF and the Greek NSRF, Greece; BSF-NSF and MINERVA, Israel; NCN and NAWA, Poland; La Caixa Banking Foundation, CERCA Programme Generalitat de Catalunya and PROMETEO and GenT Programmes Generalitat Valenciana, Spain; Göran Gustafssons Stiftelse, Sweden; The Royal Society and Leverhulme Trust, United Kingdom. In addition, individual members wish to acknowledge support from CERN: European Organization for Nuclear Research (CERN DOCT); Chile: Agencia Nacional de Investigación y Desarrollo (FONDECYT 1230812, FONDECYT 1240864, Fondecyt 3240661); China: Chinese Ministry of Science and Technology (MOST-2023YFA1605700, MOST-2023YFA1609300), National Natural Science Foundation of China (NSFC - 12175119, NSFC 12275265); Czech Republic: Czech Science Foundation (GACR - 24-11373 S), Ministry of Education Youth and Sports (ERC-CZ-LL2327, FORTE CZ.02.01.01/00/22_008/0004632), PRIMUS Research Programme (PRIMUS/21/SCI/017); EU: H2020 European Research Council (ERC - 101002463); European Union: European Research Council (BARD No. 101116429, ERC - 948254, ERC 101089007), European Regional Development Fund (SMASH COFUND 101081355, SLO ERDF), Horizon 2020 Framework Programme (MUCCA - CHIST-ERA-19-XAI-00), European Union, Future Artificial Intelligence Research (FAIR-NextGenerationEU PE00000013), Italian Center for High Performance Computing, Big Data and Quantum Computing (ICSC, NextGenerationEU); France: Agence Nationale de la Recherche (ANR-21-CE31-0022, ANR-22-EDIR-0002); Germany: Baden-Württemberg Stiftung (BW Stiftung-Postdoc Eliteprogramme),

Deutsche Forschungsgemeinschaft (DFG - 469666862, DFG - CR 312/5-2); China: Research Grants Council (GRF); Italy: Istituto Nazionale di Fisica Nucleare (ICSC, NextGenerationEU), Ministero dell'Università e della Ricerca (NextGenEU 153D23001490006 M4C2.1.1, NextGenEU I53D23000820006 M4C2.1.1, NextGenEU I53D23001490006 M4C2.1.1, SOE2024_0000023); Japan: Japan Society for the Promotion of Science (JSPS KAKENHI JP22H01227, JSPS KAKENHI JP22H04944, JSPS KAKENHI JP22KK0227, JSPS KAKENHI JP24K23939, JSPS KAKENHI JP25H00650, JSPS KAKENHI JP25H01291, JSPS KAKENHI JP25K01023); Norway: Research Council of Norway (RCN-314472); Poland: Ministry of Science and Higher Education (IDUB AGH, POB8, D4 no 9722), Polish National Science Centre (NCN 2021/42/E/ST2/00350, NCN OPUS 2023/51/B/ST2/02507, NCN OPUS nr 2022/47/B/ST2/03059, NCN UMO-2019/34/E/ST2/00393, UMO-2022/47/O/ST2/00148, UMO-2023/49/B/ST2/04085, UMO-2023/51/B/ST2/00920, UMO -2024/53/N/ST2/00869); Portugal: Foundation for Science and Technology (FCT); Spain: Ministry of Science and Innovation (MCIN & NextGenEU PCI2022-135018-2, MICIN & FEDER PID2021-125273NB, RYC2019-028510-I, RYC2020-030254-I, RYC2021-031273-I, RYC2022-038164-I); Sweden: Carl Trygger Foundation (Carl Trygger Foundation CTS 22:2312), Swedish Research Council (Swedish Research Council 2023-04654, VR 2021-03651, VR 2022-03845, VR 2022-04683, VR 2023-03403, VR 2024-05451), Knut and Alice Wallenberg Foundation (KAW 2018.0458, KAW 2022.0358, KAW 2023.0366); Switzerland: Swiss National Science Foundation (SNSF - PCEFP2_194658); United Kingdom: Leverhulme Trust (Leverhulme Trust RPG-2020-004), Royal Society (NIF-R1-231091); United States of America: U.S. Department of Energy (ECA DE-AC02-76SF00515), Neubauer Family Foundation.

Data Availability Statement This manuscript has associated data in a data repository. [Author's comment: "All ATLAS scientific output is published in journals, and preliminary results are made available in Conference Notes. All are openly available, without restriction on use by external parties beyond copyright law and the standard conditions agreed by CERN. Data associated with journal publications are also made available: tables and data from plots (e.g. cross section values, likelihood profiles, selection efficiencies, cross section limits, ...) are stored inappropriate repositories such as HEPDATA (http://hepdata.cedar.ac.uk/). ATLAS also strives to make additional material related to the paper available that allows a reinterpretation of the data in the context of new theoretical models. For example, an extended encapsulation of the analysis is often provided for measurements in the framework of RIVET (http://rivet.hepforge.org/)." This information is taken from the ATLAS Data Access Policy, which is a public document that can be downloaded from http://opendata.cern.ch/record/413 [opendata.cern.ch].]

Code Availability Statement This manuscript has associated code/software in a data repository. [Author's comment: ATLAS collaboration software is open source, and all code necessary to recreate an analysis is publicly available. The Athena (http://gitlab.cern.ch/atlas/athena) software repository provides all code needed for calibration and uncertainty application, with configuration files that are also publicly available via Docker containers and cvmfs. The specific code and configurations written in support of this analysis are not public; however, these are internally preserved.]

Funded by SCOAP[3].

References

1. ATLAS Collaboration, Observation of a new particle in the search for the Standard Model Higgs boson with the ATLAS detector at the LHC. Phys. Lett. B **716**, 1 (2012). https://doi.org/10.1016/j.physletb.2012.08.020. arXiv:1207.7214 [hep-ex]
2. CMS Collaboration, Observation of a new boson at a mass of 125 GeV with the CMS experiment at the LHC. Phys. Lett. B **716**, 30 (2012). https://doi.org/10.1016/j.physletb.2012.08.021. arXiv:1207.7235 [hep-ex]
3. L. Evans, P. Bryant, L.H.C. Machine, JINST **3**, S08001 (2008). https://doi.org/10.1088/1748-0221/3/08/S08001
4. D. Clowe, A. Gonzalez, M. Markevitch, Weak-lensing mass reconstruction of the interacting cluster 1E 0657–558: direct evidence for the existence of dark matter*. ApJ **604**, 596 (2004). https://doi.org/10.1086/381970
5. G. Bertone, D. Hooper, J. Silk, Particle dark matter: evidence, candidates and constraints. Phys. Rep. **405**, 279 (2005). https://doi.org/10.1016/j.physrep.2004.08.031. arXiv:hep-ph/0404175
6. Particle Data Group, P. Zyla et al., Review of particle physics. Prog. Theor. Exp. Phys. **2020**, 083C01 (2020). https://doi.org/10.1093/ptep/ptaa104
7. S.R. Coleman, J. Mandula, All possible symmetries of the S matrix. Phys. Rev. **159**, 1251 (1967). https://doi.org/10.1103/PhysRev.159.1251
8. R. Haag, J.T. Lopuszanski, M. Sohnius, All possible generators of supersymmetries of the s matrix. Nucl. Phys. B **88**, 257 (1975). https://doi.org/10.1016/0550-3213(75)90279-5
9. Y. Gol'fand, E. Likhtman, Extension of the algebra of Poincare group generators and violation of P invariance. JETP Lett. **13**, 20 (1971). https://doi.org/10.1142/9789814542340_0001. [Pisma Zh. Eksp. Teor. Fiz. 13 (1971) 452]
10. D.V. Volkov, V.P. Akulov, Is the neutrino a goldstone particle? Phys. Lett. B **46**, 109 (1973). https://doi.org/10.1016/0370-2693(73)90490-5
11. J. Wess, B. Zumino, Supergauge transformations in four dimensions. Nucl. Phys. B **70**, 39 (1974). https://doi.org/10.1016/0550-3213(74)90355-1
12. J. Wess, B. Zumino, Supergauge invariant extension of quantum electrodynamics. Nucl. Phys. B **78**, 1 (1974). https://doi.org/10.1016/0550-3213(74)90112-6
13. S. Ferrara, B. Zumino, Supergauge invariant Yang–Mills theories. Nucl. Phys. B **79**, 413 (1974). https://doi.org/10.1016/0550-3213(74)90559-8
14. A. Salam, J. Strathdee, Super-symmetry and non-Abelian gauges. Phys. Lett. B **51**, 353 (1974). https://doi.org/10.1016/0370-2693(74)90226-3
15. E. Witten, Introduction to supersymmetry. in 19th International School of Subnuclear Physics: The Unity of the Fundamental Interactions, vol. 305 (1983)
16. N. Sakai, Naturalness in supersymmetric GUTS. Z. Phys. C **11**, 153 (1981). https://doi.org/10.1007/BF01573998
17. S. Dimopoulos, S. Raby, F. Wilczek, Supersymmetry and the scale of unification. Phys. Rev. D **24**, 1681 (1981). https://doi.org/10.1103/PhysRevD.24.1681

18. L.E. Ibáñez, G.G. Ross, Low-energy predictions in supersymmetric grand unified theories. Phys. Lett. B **105**, 439 (1981). https://doi.org/10.1016/0370-2693(81)91200-4
19. S. Dimopoulos, H. Georgi, Softly broken supersymmetry and SU(5). Nucl. Phys. B **193**, 150 (1981). https://doi.org/10.1016/0550-3213(81)90522-8
20. G.R. Farrar, P. Fayet, Phenomenology of the production, decay, and detection of new hadronic states associated with supersymmetry. Phys. Lett. B **76**, 575 (1978). https://doi.org/10.1016/0370-2693(78)90858-4
21. H. Goldberg, Constraint on the photino mass from cosmology. Phys. Rev. Lett. **50**, 1419 (1983). https://doi.org/10.1103/PhysRevLett.103.099905. (**Erratum: Phys. Rev. Lett. 103 (2009) 099905**)
22. J. Ellis, J. Hagelin, D.V. Nanopoulos, K.A. Olive, M. Srednicki, Supersymmetric relics from the big bang. Nucl. Phys. B **238**, 453 (1984). https://doi.org/10.1016/0550-3213(84)90461-9
23. S.P. Martin, A supersymmetry primer. Adv. Ser. Direct. High Energy Phys. **18**, 1 (1998). https://doi.org/10.1142/9789812839657_0001. arXiv:hep-ph/9709356
24. D. Albornoz Vásquez, G. Bélanger, C. Bæhm, Revisiting light neutralino scenarios in the MSSM. Phys. Rev. D **84**, 095015 (2011). https://doi.org/10.1103/PhysRevD.84.095015
25. D. Alves et al., Simplified models for LHC new physics searches. J. Phys. G **39**, 105005 (2012). https://doi.org/10.1088/0954-3899/39/10/105005. arXiv:1105.2838 [hep-ph]
26. J. Alwall, P.C. Schuster, N. Toro, Simplified models for a first characterization of new physics at the LHC. Phys. Rev. D **79**, 075020 (2009). https://doi.org/10.1103/PhysRevD.79.075020. arXiv:0810.3921 [hep-ph]
27. L. Covi, S. Kraml, Collider signatures of gravitino dark matter with a sneutrino NLSP. JHEP **08**, 015 (2007). https://doi.org/10.1088/1126-6708/2007/08/015. arXiv:hep-ph/0703130
28. J. Ellis, K.A. Olive, Y. Santoso, Sneutrino NLSP scenarios in the NUHM with gravitino dark matter. JHEP **10**, 005 (2008). https://doi.org/10.1088/1126-6708/2008/10/005. arXiv:0807.3736 [hep-ph]
29. T. Figy, K. Rolbiecki, Y. Santoso, Tau-Sneutrino NLSP and multilepton signatures at the LHC. Phys. Rev. D **82**, 075016 (2010). https://doi.org/10.1103/PhysRevD.82.075016. arXiv:1005.5136 [hep-ph]
30. A. Katz, B. Tweedie, Signals of a Sneutrino (N)LSP at the LHC. Phys. Rev. D **81**, 035012 (2010). https://doi.org/10.1103/PhysRevD.81.035012. arXiv:0911.4132 [hep-ph]
31. A. Katz, B. Tweedie, Leptophilic signals of a Sneutrino (N)LSP and flavor biases from flavor-blind SUSY. Phys. Rev. D **81**, 115003 (2010). https://doi.org/10.1103/PhysRevD.81.115003. arXiv:1003.5664 [hep-ph]
32. S. Bhattacharya, S. Biswas, B. Mukhopadhyaya, M.M. Nojiri, Signatures of supersymmetry with non-universal Higgs mass at the Large Hadron Collider. JHEP **02**, 104 (2012). https://doi.org/10.1007/JHEP02(2012)104. arXiv: 1105.3097 [hep-ph]
33. M. Chala, A. Delgado, G. Nardini, M. Quirós, A light sneutrino rescues the light stop. JHEP **04**, 097 (2017). https://doi.org/10.1007/JHEP04(2017)097. arXiv:1702.07359 [hep-ph]
34. D. Alvestad, N. Fomin, J. Kersten, S. Maeland, I. Strümke, Beyond cuts in small signal scenarios. Eur. Phys. J. C **83**, 379 (2023). https://doi.org/10.1140/epjc/s10052-023-11532-9. arXiv: 2108.03125 [hep-ph]
35. ATLAS Collaboration, The quest to discover supersymmetry at the ATLAS experiment. Phys. Rep. **1116**, 261 (2025). https://doi.org/10.1016/j.physrep.2024.09.010. arXiv:2403.02455 [hep-ex]
36. ATLAS Collaboration, Summary of the searches for squarks and gluinos using $\sqrt{s} = 8\,TeV$ pp collisions with the ATLAS experiment at the LHC. JHEP **10**, 054 (2015). https://doi.org/10.1007/JHEP10(2015)054. arXiv:1507.05525 [hep-ex]
37. J. Alwall, M.-P. Le, M. Lisanti, J.G. Wacker, Searching for directly decaying gluinos at the Tevatron. Phys. Lett. B **666**, 34 (2008). https://doi.org/10.1016/j.physletb.2008.06.065. arXiv:0803.0019 [hep-ph]
38. ATLAS Collaboration, Summary of the ATLAS experiment's sensitivity to supersymmetry after LHC Run 1 – interpreted in the phenomenological MSSM. JHEP **10**, 134 (2015). https://doi.org/10.1007/JHEP10(2015)134. arXiv:1508.06608 [hep-ex]
39. ATLAS Collaboration, Search for squarks and gluinos in events with hadronically decaying tau leptons, jets and missing transverse momentum in proton-proton collisions at $\sqrt{s} = 13\,TeV$ recorded with the ATLAS detector. Eur. Phys. J. C **76**, 683 (2016). https://doi.org/10.1140/epjc/s10052-016-4481-2. arXiv:1607.05979 [hep-ex]
40. ATLAS Collaboration, Search for squarks and gluinos in final states with hadronically decaying τ-leptons, jets, and missing transverse momentum using pp collisions at $\sqrt{s} = 13$ TeV with the ATLAS detector. Phys. Rev. D **99**, 012009 (2019). https://doi.org/10.1103/PhysRevD.99.012009. arXiv: 1808.06358 [hep-ex]
41. CMS Collaboration, Search for physics beyond the standard model in events with τ leptons, jets, and large transverse momentum imbalance in pp collisions at $\sqrt{s} = 7$ TeV. Eur. Phys. J. C **73**, 2493 (2013). https://doi.org/10.1140/epjc/s10052-013-2493-8. arXiv:1301.3792 [hep-ex]
42. ATLAS Collaboration, The ATLAS experiment at the CERN Large Hadron Collider. JINST **3**, S08003 (2008). https://doi.org/10.1088/1748-0221/3/08/S08003
43. ATLAS Collaboration, Search for new phenomena in final states with large jet multiplicities and missing transverse momentum using $\sqrt{s} = 13$ TeV proton-proton collisions recorded by ATLAS in Run 2 of the LHC. JHEP **10**, 062 (2020). https://doi.org/10.1007/JHEP10(2020)062. arXiv:2008.06032 [hep-ex]
44. ATLAS Collaboration, Search for squarks and gluinos in final states with jets and missing transverse momentum using $139\,fb^{-1}$ of $\sqrt{s} = 13\,TeV$ pp collision data with the ATLAS detector. JHEP **02**, 143 (2021). https://doi.org/10.1007/JHEP02(2021)143. arXiv:2010.14293 [hep-ex]
45. D. Matalliotakis, H.P. Nilles, Implications of nonuniversality of soft terms in supersymmetric grand unified theories. Nucl. Phys. B **435**, 115 (1995). https://doi.org/10.1016/0550-3213(94)00487-Y. arXiv:hep-ph/9407251
46. J.R. Ellis, T. Falk, K.A. Olive, Y. Santoso, Exploration of the MSSM with nonuniversal Higgs masses. Nucl. Phys. B **652**, 259 (2003). https://doi.org/10.1016/S0550-3213(02)01144-6. arXiv:hep-ph/0210205
47. A.H. Chamseddine, R.L. Arnowitt, P. Nath, Locally supersymmetric grand unification. Phys. Rev. Lett. **49**, 970 (1982). https://doi.org/10.1103/PhysRevLett.49.970
48. G.F. Giudice, R. Rattazzi, Theories with gauge mediated supersymmetry breaking. Phys. Rep. **322**, 419 (1999). https://doi.org/10.1016/S0370-1573(99)00042-3. arXiv:hep-ph/9801271
49. ATLAS Collaboration, Search for squarks and gluinos in final states with one isolated lepton, jets, and missing transverse momentum at $\sqrt{s} = 13$ TeV with the ATLAS detector. Eur. Phys. J. C **81**, 600 (2021). https://doi.org/10.1140/epjc/s10052-021-09344-w. arXiv:2101.01629 [hep-ex]. [Erratum: Eur. Phys. J. C 81 (2021) 956]
50. A.T.L.A.S. Collaboration, The ATLAS experiment at the CERN Large Hadron Collider: a description of the detector configuration for Run 3. JINST **19**, P05063 (2024). https://doi.org/10.1088/1748-0221/19/05/P05063. arXiv: 2305.16623 [physics.ins-det]
51. ATLAS Collaboration, ATLAS Insertable B-Layer Technical Design Report, ATLAS-TDR-19; CERN-LHCC-2010-013, 2010, Addendum: ATLAS-TDR-19-ADD-1; CERN-LHCC-2012-009 (2012). https://cds.cern.ch/record/1451888

52. B. Abbott et al., Production and integration of the ATLAS Insertable B-Layer. JINST **13**, T05008 (2018). https://doi.org/10.1088/1748-0221/13/05/T05008. arXiv: 1803.00844 [physics.ins-det]
53. ATLAS Collaboration, Performance of the ATLAS trigger system in 2015. Eur. Phys. J. C **77**, 317 (2017). https://doi.org/10.1140/epjc/s10052-017-4852-3. arXiv:1611.09661 [hep-ex]
54. ATLAS Collaboration, The ATLAS trigger system for LHC Run 3 and trigger performance in 2022. JINST **19**, P06029 (2024). https://doi.org/10.1088/1748-0221/19/06/P06029. arXiv:2401.06630 [hep-ex]
55. ATLAS Collaboration, The ATLAS Collaboration Software and Firmware, ATL-SOFT-PUB-2021-001 (2021). https://cds.cern.ch/record/2767187
56. G. Avoni et al., The new LUCID-2 detector for luminosity measurement and monitoring in ATLAS. JINST **13**, P07017 (2018). https://doi.org/10.1088/1748-0221/13/07/P07017
57. ATLAS Collaboration, ATLAS data quality operations and performance for 2015–2018 data-taking. JINST **15**, P04003 (2020). https://doi.org/10.1088/1748-0221/15/04/P04003. arXiv:1911.04632 [physics.ins-det]
58. ATLAS Collaboration, Performance of the missing transverse momentum triggers for the ATLAS detector during Run-2 data taking. JHEP **08**, 080 (2020). https://doi.org/10.1007/JHEP08(2020)080. arXiv:2005.09554 [hep-ex]
59. ATLAS Collaboration, Performance of the ATLAS muon triggers in Run 2. JINST **15**, P09015 (2020). https://doi.org/10.1088/1748-0221/15/09/p09015. arXiv:2004.13447 [physics.ins-det]
60. ATLAS Collaboration, Performance of electron and photon triggers in ATLAS during LHC Run 2. Eur. Phys. J. C **80**, 47 (2020). https://doi.org/10.1140/epjc/s10052-019-7500-2. arXiv:1909.00761 [hep-ex]
61. ATLAS Collaboration, The performance of the jet trigger for the ATLAS detector during 2011 data taking. Eur. Phys. J. C **76**, 526 (2016). https://doi.org/10.1140/epjc/s10052-016-4325-0. arXiv:1606.07759 [hep-ex]
62. ATLAS Collaboration, The ATLAS simulation infrastructure. Eur. Phys. J. C **70**, 823 (2010). https://doi.org/10.1140/epjc/s10052-010-1429-9. arXiv:1005.4568 [physics.ins-det]
63. ATLAS Collaboration, Software and computing for Run 3 of the ATLAS experiment at the LHC. Eur. Phys. J. C **85**, 234 (2025). https://doi.org/10.1140/epjc/s10052-024-13701-w. arXiv:2404.06335 [hep-ex]
64. S. Agostinelli et al., Geant4 – a simulation toolkit. Nucl. Instrum. Methods A **506**, 250 (2003). https://doi.org/10.1016/S0168-9002(03)01368-8
65. S. Porteboeuf, T. Pierog, K. Werner, Producing hard processes regarding the complete event: the EPOS event generator. in 45th Rencontres de Moriond on QCD and High Energy Interactions, Gioi Publishers (2010). arXiv:1006.2967 [hep-ph]
66. T. Sjöstrand, S. Mrenna, P. Skands, A brief introduction to PYTHIA 8.1. Comput. Phys. Commun. **178**, 852 (2008). https://doi.org/10.1016/j.cpc.2008.01.036. arXiv:0710.3820 [hep-ph]
67. ATLAS Collaboration, The Pythia 8 A3 tune description of ATLAS minimum bias and inelastic measurements incorporating the Donnachie–Landshoff diffractive model. ATL-PHYS-PUB-2016-017 (2016). https://cds.cern.ch/record/2206965
68. N.N.P.D.F. Collaboration, R.D. Ball et al., Parton distributions with LHC data. Nucl. Phys. B **867**, 244 (2013). https://doi.org/10.1016/j.nuclphysb.2012.10.003. arXiv:1207.1303 [hep-ph]
69. L. Lönnblad, Correcting the colour-dipole cascade model with fixed order matrix elements. JHEP **05**, 046 (2002). https://doi.org/10.1088/1126-6708/2002/05/046. arXiv:hep-ph/0112284
70. L. Lönnblad, S. Prestel, Matching tree-level matrix elements with interleaved showers. JHEP **03**, 019 (2012). https://doi.org/10.1007/JHEP03(2012)019. arXiv:1109.4829 [hep-ph]
71. W. Beenakker et al., NNLL-fast 2.0: coloured sparticle production at the LHC Run 3 with $\sqrt{S} = 13.6$ TeV. SciPost Phys. Core **7**, 072 (2024). https://doi.org/10.21468/SciPostPhysCore.7.4.072. arXiv:2404.18837 [hep-ph]
72. W. Beenakker, C. Borschensky, M. Krämer, A. Kulesza, E. Laenen, NNLL-fast: predictions for coloured supersymmetric particle production at the LHC with threshold and Coulomb resummation. JHEP **12**, 133 (2016). https://doi.org/10.1007/JHEP12(2016)133. arXiv:1607.07741 [hep-ph]
73. W. Beenakker et al., NNLL resummation for squark and gluino production at the LHC. JHEP **12**, 023 (2014). https://doi.org/10.1007/JHEP12(2014)023. arXiv:1404.3134 [hep-ph]
74. W. Beenakker et al., Towards NNLL resummation: hard matching coefficients for squark and gluino hadroproduction. JHEP **10**, 120 (2013). https://doi.org/10.1007/JHEP10(2013)120. arXiv:1304.6354 [hep-ph]
75. W. Beenakker et al., NNLL resummation for squark-antisquark pair production at the LHC. JHEP **01**, 076 (2012). https://doi.org/10.1007/JHEP01(2012)076. arXiv:1110.2446 [hep-ph]
76. W. Beenakker et al., Soft-gluon resummation for squark and gluino hadroproduction. JHEP **12**, 041 (2009). https://doi.org/10.1088/1126-6708/2009/12/041. arXiv:0909.4418 [hep-ph]
77. A. Kulesza, L. Motyka, Soft gluon resummation for the production of gluino-gluino and squark-antisquark pairs at the LHC. Phys. Rev. D **80**, 095004 (2009). https://doi.org/10.1103/PhysRevD.80.095004. arXiv:0905.4749 [hep-ph]
78. A. Kulesza, L. Motyka, Threshold resummation for squark-antisquark and gluino-pair production at the LHC. Phys. Rev. Lett. **102**, 111802 (2009). https://doi.org/10.1103/PhysRevLett.102.111802. arXiv:0807.2405 [hep-ph]
79. W. Beenakker, R. Höpker, M. Spira, P. Zerwas, Squark and gluino production at hadron colliders. Nucl. Phys. B **492**, 51 (1997). https://doi.org/10.1016/S0550-3213(97)00084-9. arXiv:hep-ph/9610490
80. R.D. Ball et al., The PDF4LHC21 combination of global PDF fits for the LHC Run III. J. Phys. G **49**, 080501 (2022). https://doi.org/10.1088/1361-6471/ac7216. arXiv:2203.05506 [hep-ph]
81. E. Bothmann et al., Event generation with Sherpa 2.2. SciPost Phys. **7**, 034 (2019). https://doi.org/10.21468/SciPostPhys.7.3.034. arXiv:1905.09127 [hep-ph]
82. S. Schumann, F. Krauss, A parton shower algorithm based on Catani–Seymour dipole factorisation. JHEP **03**, 038 (2008). https://doi.org/10.1088/1126-6708/2008/03/038. arXiv:0709.1027 [hep-ph]
83. C. Anastasiou, L. Dixon, K. Melnikov, F. Petriello, High-precision QCD at hadron colliders: electroweak gauge boson rapidity distributions at next-to-next-to leading order. Phys. Rev. D **69**, 094008 (2004). https://doi.org/10.1103/PhysRevD.69.094008. arXiv:hep-ph/0312266
84. N.N.P.D.F. Collaboration, R.D. Ball et al., Parton distributions for the LHC Run II. JHEP **04**, 040 (2015). https://doi.org/10.1007/JHEP04(2015)040. arXiv:1410.8849 [hep-ph]
85. S. Carrazza, S. Forte, Z. Kassabov, J.I. Latorre, J. Rojo, An unbiased Hessian representation for Monte Carlo PDFs. Eur. Phys. J. C **75**, 369 (2015). https://doi.org/10.1140/epjc/s10052-015-3590-7. arXiv:1505.06736 [hep-ph]
86. S. Höche, F. Krauss, M. Schönherr, F. Siegert, A critical appraisal of NLO+PS matching methods. JHEP **09**, 049 (2012). https://doi.org/10.1007/JHEP09(2012)049. arXiv:1111.1220 [hep-ph]
87. S. Höche, F. Krauss, M. Schönherr, F. Siegert, QCD matrix elements + parton showers. The NLO case. JHEP **04**, 027 (2013). https://doi.org/10.1007/JHEP04(2013)027. arXiv:1207.5030 [hep-ph]
88. S. Catani, F. Krauss, B.R. Webber, R. Kuhn, QCD matrix elements + parton showers. JHEP **11**, 063 (2001). https://doi.org/10.1088/1126-6708/2001/11/063. arXiv:hep-ph/0109231

89. S. Höche, F. Krauss, S. Schumann, F. Siegert, QCD matrix elements and truncated showers. JHEP **05**, 053 (2009). https://doi.org/10.1088/1126-6708/2009/05/053. arXiv:0903.1219 [hep-ph]
90. S. Frixione, G. Ridolfi, P. Nason, A positive-weight next-to-leading-order Monte Carlo for heavy flavour hadroproduction. JHEP **09**, 126 (2007). https://doi.org/10.1088/1126-6708/2007/09/126. arXiv:0707.3088 [hep-ph]
91. P. Nason, A new method for combining NLO QCD with shower Monte Carlo algorithms. JHEP **11**, 040 (2004). https://doi.org/10.1088/1126-6708/2004/11/040. arXiv:hep-ph/0409146
92. S. Frixione, P. Nason, C. Oleari, Matching NLO QCD computations with parton shower simulations: the POWHEG method. JHEP **11**, 070 (2007). https://doi.org/10.1088/1126-6708/2007/11/070. arXiv:0709.2092 [hep-ph]
93. S. Alioli, P. Nason, C. Oleari, E. Re, A general framework for implementing NLO calculations in shower Monte Carlo programs: the POWHEG BOX. JHEP **06**, 043 (2010). https://doi.org/10.1007/JHEP06(2010)043. arXiv:1002.2581 [hep-ph]
94. T. Sjöstrand et al., An introduction to PYTHIA 8.2. Comput. Phys. Commun. **191**, 159 (2015). https://doi.org/10.1016/j.cpc.2015.01.024. arXiv:1410.3012 [hep-ph]
95. M. Beneke, P. Falgari, S. Klein, C. Schwinn, Hadronic top-quark pair production with NNLL threshold resummation. Nucl. Phys. B **855**, 695 (2012). https://doi.org/10.1016/j.nuclphysb.2011.10.021. arXiv:1109.1536 [hep-ph]
96. M. Cacciari, M. Czakon, M. Mangano, A. Mitov, P. Nason, Top-pair production at hadron colliders with next-to-next-to-leading logarithmic soft-gluon resummation. Phys. Lett. B **710**, 612 (2012). https://doi.org/10.1016/j.physletb.2012.03.013. arXiv:1111.5869 [hep-ph]
97. P. Bärnreuther, M. Czakon, A. Mitov, Percent-level-precision physics at the tevatron: next-to-next-to-leading order QCD corrections to $q\bar{q} \rightarrow t\bar{t} + X$. Phys. Rev. Lett. **109**, 132001 (2012). https://doi.org/10.1103/PhysRevLett.109.132001. arXiv:1204.5201 [hep-ph]
98. M. Czakon, A. Mitov, NNLO corrections to top-pair production at hadron colliders: the all-fermionic scattering channels. JHEP **12**, 054 (2012). https://doi.org/10.1007/JHEP12(2012)054. arXiv:1207.0236 [hep-ph]
99. M. Czakon, A. Mitov, NNLO corrections to top pair production at hadron colliders: the quark-gluon reaction. JHEP **01**, 080 (2013). https://doi.org/10.1007/JHEP01(2013)080. arXiv:1210.6832 [hep-ph]
100. M. Czakon, P. Fiedler, A. Mitov, Total top-quark pair-production cross section at hadron colliders through $mathcal O(\alpha_S^4)$. Phys. Rev. Lett. **110**, 252004 (2013). https://doi.org/10.1103/PhysRevLett.110.252004. arXiv:1303.6254 [hep-ph]
101. M. Czakon, A. Mitov, Top++: a program for the calculation of the top-pair cross-section at hadron colliders. Comput. Phys. Commun. **185**, 2930 (2014). https://doi.org/10.1016/j.cpc.2014.06.021. arXiv:1112.5675 [hep-ph]
102. ATLAS Collaboration, ATLAS Pythia 8 tunes to 7 TeV data. ATL-PHYS-PUB-2014-021 (2014). https://cds.cern.ch/record/1966419
103. N. Kidonakis, Two-loop soft anomalous dimensions for single top quark associated production with a W^- or H^-. Phys. Rev. D **82**, 054018 (2010). https://doi.org/10.1103/PhysRevD.82.054018. arXiv:1005.4451 [hep-ph]
104. N. Kidonakis, Top quark production. in Proceedings, Helmholtz International Summer School on Physics of Heavy Quarks and Hadrons (HQ2013) (JINR, Dubna, Russia, 15th–28th July), vol. 139 (2013). arXiv:1311.0283 [hep-ph]
105. M. Aliev et al., HATHOR - HAdronic top and heavy quarks crOss section calculatoR. Comput. Phys. Commun. **182**, 1034 (2011). https://doi.org/10.1016/j.cpc.2010.12.040. arXiv:1007.1327 [hep-ph]
106. P. Kant et al., HatHor for single top-quark production: updated predictions and uncertainty estimates for single top-quark production in hadronic collisions. Comput. Phys. Commun. **191**, 74 (2015). https://doi.org/10.1016/j.cpc.2015.02.001. arXiv:1406.4403 [hep-ph]
107. J. Alwall et al., The automated computation of tree-level and next-to-leading order differential cross sections, and their matching to parton shower simulations. JHEP **07**, 079 (2014). https://doi.org/10.1007/JHEP07(2014)079. arXiv:1405.0301 [hep-ph]
108. D. de Florian et al., Handbook of LHC Higgs cross sections: 4. Deciphering the nature of the Higgs sector. FERMILAB-FN-1025-T, CERN-2017-002-M (2017). https://doi.org/10.23731/CYRM-2017-002 arXiv:1610.07922 [hep-ph]
109. H.B. Hartanto, B. Jäger, L. Reina, D. Wackeroth, Higgs boson production in association with top quarks in the POWHEG BOX. Phys. Rev. D **91**, 094003 (2015). https://doi.org/10.1103/PhysRevD.91.094003. arXiv:1501.04498 [hep-ph]
110. K. Hamilton, P. Nason, E. Re, G. Zanderighi, NNLOPS simulation of Higgs boson production. JHEP **10**, 222 (2013). https://doi.org/10.1007/JHEP10(2013)222. arXiv:1309.0017 [hep-ph]
111. K. Hamilton, P. Nason, G. Zanderighi, Finite quark-mass effects in the NNLOPS POWHEG+MiNLO Higgs generator. JHEP **05**, 140 (2015). https://doi.org/10.1007/JHEP05(2015)140. arXiv:1501.04637 [hep-ph]
112. M.L. Ciccolini, S. Dittmaier, M. Krämer, Electroweak radiative corrections to associated WH and ZH production at hadron colliders. Phys. Rev. D **68**, 073003 (2003). https://doi.org/10.1103/PhysRevD.68.073003. arXiv:hep-ph/0306234
113. O. Brein, A. Djouadi, R. Harlander, NNLO QCD corrections to the Higgs-Strahlung processes at hadron colliders. Phys. Lett. B **579**, 149 (2004). https://doi.org/10.1016/j.physletb.2003.10.112. arXiv:hep-ph/0307206
114. O. Brein, R.V. Harlander, M. Wiesemann, T. Zirke, Top-quark mediated effects in hadronic Higgs-Strahlung. Eur. Phys. J. C **72**, 1868 (2012). https://doi.org/10.1140/epjc/s10052-012-1868-6. arXiv:1111.0761 [hep-ph]
115. L. Altenkamp, S. Dittmaier, R.V. Harlander, H. Rzehak, T.J.E. Zirke, Gluon-induced Higgs-Strahlung at next-to-leading order QCD. JHEP **02**, 078 (2013). https://doi.org/10.1007/JHEP02(2013)078. arXiv:1211.5015 [hep-ph]
116. A. Denner, S. Dittmaier, S. Kallweit, A. Mück, HAWK 2.0: a Monte Carlo program for Higgs production in vector-boson fusion and Higgs Strahlung at hadron colliders. Comput. Phys. Commun. **195**, 161 (2015). https://doi.org/10.1016/j.cpc.2015.04.021. arXiv:1412.5390 [hep-ph]
117. O. Brein, R.V. Harlander, T.J.E. Zirke, vh@nnlo – Higgs Strahlung at hadron colliders. Comput. Phys. Commun. **184**, 998 (2013). https://doi.org/10.1016/j.cpc.2012.11.002. arXiv:1210.5347 [hep-ph]
118. R.V. Harlander, A. Kulesza, V. Theeuwes, T. Zirke, Soft gluon resummation for gluon-induced Higgs Strahlung. JHEP **11**, 082 (2014). https://doi.org/10.1007/JHEP11(2014)082. arXiv:1410.0217 [hep-ph]
119. ATLAS Collaboration, Measurement of the Z/γ^* boson transverse momentum distribution in pp collisions at $\sqrt{s} = 7\,TeV$ with the ATLAS detector. JHEP **09**, 145 (2014). https://doi.org/10.1007/JHEP09(2014)145. arXiv:1406.3660 [hep-ex]
120. K. Hamilton, P. Nason, G. Zanderighi, MINLO: multi-scale improved NLO. JHEP **10**, 155 (2012). https://doi.org/10.1007/JHEP10(2012)155. arXiv:1206.3572 [hep-ph]
121. J.M. Campbell et al., NLO Higgs boson production plus one and two jets using the POWHEG BOX, MadGraph4 and MCFM. JHEP **07**, 092 (2012). https://doi.org/10.1007/JHEP07(2012)092. arXiv:1202.5475 [hep-ph]
122. K. Hamilton, P. Nason, C. Oleari, G. Zanderighi, Merging H/W/Z + 0 and 1 jet at NLO with no merging scale: a path to parton

shower + NNLO matching. JHEP **05**, 082 (2013). https://doi.org/10.1007/JHEP05(2013)082. arXiv:1212.4504 [hep-ph]
123. S. Catani, M. Grazzini, Next-to-next-to-leading-order subtraction formalism in hadron collisions and its application to Higgs–Boson production at the Large Hadron Collider. Phys. Rev. Lett. **98**, 222002 (2007). https://doi.org/10.1103/PhysRevLett.98.222002. arXiv:hep-ph/0703012
124. G. Bozzi, S. Catani, D. de Florian, M. Grazzini, Transverse-momentum resummation and the spectrum of the Higgs boson at the LHC. Nucl. Phys. B **737**, 73 (2006). https://doi.org/10.1016/j.nuclphysb.2005.12.022. arXiv:hep-ph/0508068
125. D. de Florian, G. Ferrera, M. Grazzini, D. Tommasini, Transverse-momentum resummation: Higgs boson production at the tevatron and the LHC. JHEP **11**, 064 (2011). https://doi.org/10.1007/JHEP11(2011)064. arXiv:1109.2109 [hep-ph]
126. ATLAS Collaboration, Reconstruction of primary vertices at the ATLAS experiment in Run 1 proton-proton collisions at the LHC. Eur. Phys. J. C **77**, 332 (2017). https://doi.org/10.1140/epjc/s10052-017-4887-5. arXiv:1611.10235 [physics.ins-det]
127. ATLAS Collaboration, Development of ATLAS primary vertex reconstruction for LHC Run 3. ATL-PHYS-PUB-2019-015 (2019). https://cds.cern.ch/record/2670380
128. ATLAS Collaboration, Reconstruction, identification, and calibration of hadronically decaying tau leptons with the ATLAS detector for the LHC Run 3 and reprocessed Run 2 data. ATL-PHYS-PUB-2022-044 (2022). https://cds.cern.ch/record/2827111
129. ATLAS Collaboration, Jet reconstruction and performance using particle flow with the ATLAS detector. Eur. Phys. J. C **77**, 466 (2017). https://doi.org/10.1140/epjc/s10052-017-5031-2. arXiv:1703.10485 [hep-ex]
130. M. Cacciari, G.P. Salam, G. Soyez, The anti-k_t jet clustering algorithm. JHEP **04**, 063 (2008). https://doi.org/10.1088/1126-6708/2008/04/063. arXiv:0802.1189 [hep-ph]
131. M. Cacciari, G.P. Salam, G. Soyez, FastJet user manual. Eur. Phys. J. C **72**, 1896 (2012). https://doi.org/10.1140/epjc/s10052-012-1896-2. arXiv:1111.6097 [hep-ph]
132. ATLAS Collaboration, Jet energy scale and resolution measured in proton-proton collisions at $\sqrt{s} = 13$ TeV with the ATLAS detector. Eur. Phys. J. C **81**, 689 (2021). https://doi.org/10.1140/epjc/s10052-021-09402-3. arXiv:2007.02645 [hep-ex]
133. ATLAS Collaboration, Performance of pile-up mitigation techniques for jets in pp collisions at $\sqrt{s} = 8$ TeV using the ATLAS detector. Eur. Phys. J. C **76**, 581 (2016). https://doi.org/10.1140/epjc/s10052-016-4395-z. arXiv:1510.03823 [hep-ex]
134. ATLAS Collaboration, Neural network jet flavour tagging with the upgraded ATLAS inner tracker detector at the high-luminosity LHC. ATL-PHYS-PUB-2022-047 (2022). https://cds.cern.ch/record/2839913
135. ATLAS Collaboration, Deep sets based neural networks for impact parameter flavour tagging in ATLAS. ATL-PHYS-PUB-2020-014 (2020). https://cds.cern.ch/record/2718948
136. ATLAS Collaboration, ATLAS flavour-tagging algorithms for the LHC Run 2 pp collision dataset. Eur. Phys. J. C **83**, 681 (2023). https://doi.org/10.1140/epjc/s10052-023-11699-1. arXiv:2211.16345 [physics.data-an]
137. ATLAS Collaboration, ATLAS b-jet identification performance and efficiency measurement with $t\bar{t}$ events in pp collisions at $\sqrt{s} = 13$ TeV. Eur. Phys. J. C **79**, 970 (2019). https://doi.org/10.1140/epjc/s10052-019-7450-8. arXiv:1907.05120 [hep-ex]
138. ATLAS Collaboration, Electron and photon performance measurements with the ATLAS detector using the 2015–2017 LHC proton-proton collision data. JINST **14**, P12006 (2019). https://doi.org/10.1088/1748-0221/14/12/P12006. arXiv:1908.00005 [hep-ex]
139. ATLAS Collaboration, Electron and photon energy calibration with the ATLAS detector using LHC Run 2 data. JINST **19**, P02009 (2024). https://doi.org/10.1088/1748-0221/19/02/P02009. arXiv:2309.05471 [hep-ex]
140. ATLAS Collaboration, Electron reconstruction and identification in the ATLAS experiment using the 2015 and 2016 LHC proton-proton collision data at $\sqrt{s} = 13$ TeV. Eur. Phys. J. C **79**, 639 (2019). https://doi.org/10.1140/epjc/s10052-019-7140-6. arXiv:1902.04655 [physics.ins-det]
141. ATLAS Collaboration, Muon reconstruction and identification efficiency in ATLAS using the full Run 2 pp collision data set at $\sqrt{s} = 13$ TeV. Eur. Phys. J. C **81**, 578 (2021). https://doi.org/10.1140/epjc/s10052-021-09233-2. arXiv:2012.00578 [hep-ex]
142. ATLAS Collaboration, Studies of the muon momentum calibration and performance of the ATLAS detector with pp collisions at $\sqrt{s} = 13$ TeV. Eur. Phys. J. C **83**, 686 (2023). https://doi.org/10.1140/epjc/s10052-023-11584-x. arXiv:2212.07338 [hep-ex]
143. ATLAS Collaboration, Topological cell clustering in the ATLAS calorimeters and its performance in LHC Run 1. Eur. Phys. J. C **77**, 490 (2017). https://doi.org/10.1140/epjc/s10052-017-5004-5. arXiv:1603.02934 [hep-ex]
144. T. Barillari et al., Local hadronic calibration. ATL-LARG-PUB-2009-001-2 (2008). https://cds.cern.ch/record/1112035
145. ATLAS Collaboration, Reconstruction, energy calibration, and identification of hadronically decaying tau leptons in the ATLAS experiment for Run-2 of the LHC. ATL-PHYS-PUB-2015-045 (2015). https://cds.cern.ch/record/2064383
146. ATLAS Collaboration, Measurements of Higgs boson production cross-sections in the $H \to \tau^+\tau^-$ decay channel in pp collisions at $\sqrt{s} = 13\,TeV$ with the ATLAS detector. JHEP **08**, 175 (2022). https://doi.org/10.1007/JHEP08(2022)175. arXiv:2201.08269 [hep-ex]
147. ATLAS Collaboration, Search for resonant and non-resonant Higgs boson pair production in the $b\bar{b}\tau^+\tau^-$ decay channel using $\sqrt{s} = 13\,TeV$ pp collision data from the ATLAS detector. JHEP **07**, 040 (2023). https://doi.org/10.1007/JHEP07(2023)040. arXiv:2209.10910 [hep-ex]
148. ATLAS Collaboration, The performance of missing transverse momentum reconstruction and its significance with the ATLAS detector using $140\,fb^{-1}$ of $\sqrt{s} = 13\,TeV$ pp collisions. Eur. Phys. J. C **85**, 606 (2025). https://doi.org/10.1140/epjc/s10052-025-14062-8. arXiv:2402.05858 [hep-ex]
149. C.G. Lester, D.J. Summers, Measuring masses of semi-invisibly decaying particle pairs produced at hadron colliders. Phys. Lett. B **463**, 99 (1999). https://doi.org/10.1016/S0370-2693(99)00945-4. arXiv:hep-ph/9906349 [hep-ph]
150. C.G. Lester, B. Nachman, Bisection-based asymmetric M_{T2} computation: a higher precision calculator than existing symmetric methods. JHEP **03**, 100 (2015). https://doi.org/10.1007/JHEP03(2015)100. arXiv:1411.4312 [hep-ph]
151. ATLAS Collaboration, Object-based missing transverse momentum significance in the ATLAS detector. ATLAS-CONF-2018-038 (2018). https://cds.cern.ch/record/2630948
152. G. Cowan, K. Cranmer, E. Gross, O. Vitells, Asymptotic formulae for likelihood-based tests of new physics. Eur. Phys. J. C **71**, 1554 (2011). https://doi.org/10.1140/epjc/s10052-011-1554-0. arXiv:1007.1727 [physics.data-an]. [Erratum: Eur. Phys. J. C 73 (2013) 2501]
153. T. Chen, C. Guestrin, XGBoost: a scalable tree boosting system. in Proceedings of the 22nd ACM SIGKDD International Conference on Knowledge Discovery and Data Mining, KDD '16, San Francisco, California, USA: ACM, vol. 785 (2016). https://doi.org/10.1145/2939672.2939785. (ISBN: 978-1-4503-4232-2)
154. R. Kohavi, A study of cross-validation and bootstrap for accuracy estimation and model selection. in Proceedings of the 14th International Joint Conference on Artificial Intelligence - Volume

2, IJCAI'95, Montreal, Quebec, Canada, 1137 (1995). (ISBN: 1558603638)
155. I.J. Good, Rational decisions. J. R. Stat. Soc. Ser. B Methodol. **14**, 107 (1952)
156. T. Akiba, S. Sano, T. Yanase, T. Ohta, M. Koyama, Optuna: a next-generation hyperparameter optimization framework. in Proceedings of the 25th ACM SIGKDD International Conference on Knowledge Discovery and Data Mining (2019)
157. ATLAS Collaboration, Estimation of backgrounds from jets misidentified as τ-leptons using the Universal Fake Factor method with the ATLAS detector (2025). arXiv:2502.04156 [hep-ex]
158. M. Baak et al., HistFitter software framework for statistical data analysis. Eur. Phys. J. C **75**, 153 (2015). https://doi.org/10.1140/epjc/s10052-015-3327-7. arXiv:1410.1280 [hep-ex]
159. L. Heinrich, M. Feickert, G. Stark, K. Cranmer, pyhf: pure-Python implementation of HistFactory statistical models. J. Open Source Softw. **6**, 2823 (2021). https://doi.org/10.21105/joss.02823
160. K. Cranmer, A. Held, Building and steering binned template fits with cabinetry. EPJ Web Conf. **251**, 03067 (2021). https://doi.org/10.1051/epjconf/202125103067
161. F. James, MINUIT function minimization and error analysis: reference manual version 94.1 (1994)
162. P. Virtanen et al., SciPy 1.0: fundamental algorithms for scientific computing in Python. Nat. Methods **17**, 261 (2020)
163. R. Collaboration, HistFactory: a tool for creating statistical models for use with RooFit and RooStats. Tech. Rep., New York (2012). https://cds.cern.ch/record/1456844
164. A.L. Read, Presentation of search results: the CL_s technique. J. Phys. G **28**, 2693 (2002). https://doi.org/10.1088/0954-3899/28/10/313
165. ATLAS Collaboration, Jet energy scale measurements and their systematic uncertainties in proton-proton collisions at $\sqrt{s}$ = 13 TeV with the ATLAS detector. Phys. Rev. D **96**, 072002 (2017). https://doi.org/10.1103/PhysRevD.96.072002. arXiv:1703.09665 [hep-ex]
166. ATLAS Collaboration, Tagging and suppression of pileup jets with the ATLAS detector. ATLAS-CONF-2014-018 (2014). https://cds.cern.ch/record/1700870
167. ATLAS Collaboration, Measurement of b-tagging efficiency of c-jets in $t\bar{t}$ events using a likelihood approach with the ATLAS detector. ATLAS-CONF-2018-001 (2018). https://cds.cern.ch/record/2306649
168. ATLAS Collaboration, Calibration of light-flavour b-jet mistagging rates using ATLAS proton–proton collision data at $\sqrt{s}$ = 13 TeV. ATLAS-CONF-2018-006 (2018). https://cds.cern.ch/record/2314418
169. ATLAS Collaboration, Measurement of the tau lepton reconstruction and identification performance in the ATLAS experiment using pp collisions at $\sqrt{s}$ = 13 TeV. ATLAS-CONF-2017-029 (2017). https://cds.cern.ch/record/2261772
170. A.T.L.A.S. Collaboration, Luminosity determination in pp collisions at $\sqrt{s}$ = 13 TeV using the ATLAS detector at the LHC. Eur. Phys. J. C **83**, 982 (2023). https://doi.org/10.1140/epjc/s10052-023-11747-w. arXiv:2212.09379 [hep-ex]
171. ATLAS Collaboration, Preliminary analysis of the luminosity calibration for the ATLAS 13.6 TeV data recorded in 2023. ATL-DAPR-PUB-2024-001 (2024). https://cds.cern.ch/record/2900949
172. J. Butterworth et al., PDF4LHC recommendations for LHC Run II. J. Phys. G **43**, 023001 (2016). https://doi.org/10.1088/0954-3899/43/2/023001. arXiv:1510.03865 [hep-ph]
173. M. Bähr et al., Herwig++ physics and manual. Eur. Phys. J. C **58**, 639 (2008). https://doi.org/10.1140/epjc/s10052-008-0798-9. arXiv:0803.0883 [hep-ph]
174. J. Bellm et al., Herwig 7.0/Herwig++ 3.0 release note. Eur. Phys. J. C **76**, 196 (2016). https://doi.org/10.1140/epjc/s10052-016-4018-8. arXiv:1512.01178 [hep-ph]
175. R.D. Cousins, J.T. Linnemann, J. Tucker, Evaluation of three methods for calculating statistical significance when incorporating a systematic uncertainty into a test of the background-only hypothesis for a Poisson process. Nucl. Instrum. Methods A **595**, 480 (2008). https://doi.org/10.1016/j.nima.2008.07.086
176. ATLAS Collaboration, ATLAS computing acknowledgements. ATL-SOFT-PUB-2025-001 (2025). https://cds.cern.ch/record/2922210

ATLAS Collaboration[★]

G. Aad[104], E. Aakvaag[17], B. Abbott[123], S. Abdelhameed[119a], K. Abeling[55], N. J. Abicht[49], S. H. Abidi[30], M. Aboelela[45], A. Aboulhorma[36e], H. Abramowicz[157], Y. Abulaiti[120], B. S. Acharya[69a,69b,m], A. Ackermann[63a], C. Adam Bourdarios[4], L. Adamczyk[87a], S. V. Addepalli[149], M. J. Addison[103], J. Adelman[118], A. Adiguzel[22c], T. Adye[137], A. A. Affolder[139], Y. Afik[40], M. N. Agaras[13], A. Aggarwal[102], C. Agheorghiesei[28c], F. Ahmadov[39,ad], S. Ahuja[97], X. Ai[143b], G. Aielli[76a,76b], A. Aikot[169], M. Ait Tamlihat[36e], B. Aitbenchikh[36a], M. Akbiyik[102], T. P. A. Åkesson[100], A. V. Akimov[151], D. Akiyama[174], N. N. Akolkar[25], S. Aktas[172], G. L. Alberghi[24b], J. Albert[171], U. Alberti[20], P. Albicocco[53], G. L. Albouy[60], S. Alderweireldt[52], Z. L. Alegria[124], M. Aleksa[37], I. N. Aleksandrov[39], C. Alexa[28b], T. Alexopoulos[10], F. Alfonsi[24b], M. Algren[56], M. Alhroob[173], B. Ali[135], H. M. J. Ali[93,w], S. Ali[32], S. W. Alibocus[94], M. Aliev[34c], G. Alimonti[71a], W. Alkakhi[55], C. Allaire[66], B. M. M. Allbrooke[152], J. S. Allen[103], J. F. Allen[52], P. P. Allport[21], A. Aloisio[72a,72b], F. Alonso[92], C. Alpigiani[142], Z. M. K. Alsolami[93], A. Alvarez Fernandez[102], M. Alves Cardoso[56], M. G. Alviggi[72a,72b], M. Aly[103], Y. Amaral Coutinho[83b], A. Ambler[106], C. Amelung[37], M. Amerl[103], C. G. Ames[111], T. Amezza[130], D. Amidei[108], B. Amini[54], K. Amirie[161], A. Amirkhanov[39], S. P. Amor Dos Santos[133a], K. R. Amos[169], D. Amperiadou[158], S. An[84], C. Anastopoulos[145], T. Andeen[11], J. K. Anders[94], A. C. Anderson[59], A. Andreazza[71a,71b], S. Angelidakis[9], A. Angerami[42], A. V. Anisenkov[39], A. Annovi[74a], C. Antel[37], E. Antipov[151], M. Antonelli[53], F. Anulli[75a], M. Aoki[84], T. Aoki[159], M. A. Aparo[152], L. Aperio Bella[48], M. Apicella[31], C. Appelt[157], A. Apyan[27], M. Arampatzi[10], S. J. Arbiol Val[88], C. Arcangeletti[53], A. T. H. Arce[51], J. -F. Arguin[110], S. Argyropoulos[158], J. -H. Arling[48], O. Arnaez[4], H. Arnold[151], G. Artoni[75a,75b], H. Asada[113], K. Asai[121], S. Asatryan[179], N. A. Asbah[37], R. A. Ashby Pickering[173], A. M. Aslam[97], K. Assamagan[30], R. Astalos[29a], K. S. V. Astrand[100], S. Atashi[165], R. J. Atkin[34a], H. Atmani[36f], P. A. Atmasiddha[131], K. Augsten[135], A. D. Auriol[41], V. A. Austrup[103], G. Avolio[37], K. Axiotis[56], A. Azzam[13], D. Babal[29b], H. Bachacou[138], K. Bachas[158,q], A. Bachiu[35], E. Bachmann[50], M. J. Backes[63a], A. Badea[40], T. M. Baer[108], P. Bagnaia[75a,75b], M. Bahmani[19], D. Bahner[54], K. Bai[126], J. T. Baines[137], L. Baines[96], O. K. Baker[178], E. Bakos[16], D. Bakshi Gupta[8], L. E. Balabram Filho[83b], V. Balakrishnan[123], R. Balasubramanian[4], E. M. Baldin[38], P. Balek[87a], E. Ballabene[24a,24b], F. Balli[138], L. M. Baltes[63a], W. K. Balunas[33], J. Balz[102], I. Bamwidhi[119b], E. Banas[88], M. Bandieramonte[132], A. Bandyopadhyay[25], S. Bansal[25], L. Barak[157], M. Barakat[48], E. L. Barberio[107], D. Barberis[18b], M. Barbero[104], M. Z. Barel[117], T. Barillari[112], M. -S. Barisits[37], T. Barklow[149], P. Baron[136], D. A. Baron Moreno[103], A. Baroncelli[62], A. J. Barr[129], J. D. Barr[98], F. Barreiro[101], J. Barreiro Guimarães da Costa[14], M. G. Barros Teixeira[133a], S. Barsov[38], F. Bartels[63a], R. Bartoldus[149], A. E. Barton[93], P. Bartos[29a], A. Basan[102], M. Baselga[49], S. Bashiri[88], A. Bassalat[66,b], M. J. Basso[162a], S. Bataju[45], R. Bate[170], R. L. Bates[59], S. Batlamous[101], M. Battaglia[139], D. Battulga[19], M. Bauce[75a,75b], M. Bauer[79], P. Bauer[25], L. T. Bayer[48], L. T. Bazzano Hurrell[31], J. B. Beacham[112], T. Beau[130], J. Y. Beaucamp[92], P. H. Beauchemin[164], P. Bechtle[25], H. P. Beck[20,p], K. Becker[173], A. J. Beddall[82], V. A. Bednyakov[39], C. P. Bee[151], L. J. Beemster[16], M. Begalli[83d], M. Begel[30], J. K. Behr[48], J. F. Beirer[37], F. Beisiegel[25], M. Belfkir[119b], G. Bella[157], L. Bellagamba[24b], A. Bellerive[35], C. D. Bellgraph[68], P. Bellos[21], K. Beloborodov[38], I. Benaoumeur[21], D. Benchekroun[36a], F. Bendebba[36a], Y. Benhammou[157], K. C. Benkendorfer[61], L. Beresford[48], M. Beretta[53], E. Bergeaas Kuutmann[167], N. Berger[4], B. Bergmann[135], J. Beringer[18a], G. Bernardi[5], C. Bernius[149], F. U. Bernlochner[25], F. Bernon[37], A. Berrocal Guardia[13], T. Berry[97], P. Berta[136], A. Berthold[50], A. Berti[133a], R. Bertrand[104], S. Bethke[112], A. Betti[75a,75b], A. J. Bevan[96], L. Bezio[56], N. K. Bhalla[54], S. Bharthuar[112], S. Bhatta[151], P. Bhattarai[149], Z. M. Bhatti[120], K. D. Bhide[54], V. S. Bhopatkar[124], R. M. Bianchi[132], G. Bianco[24a,24b], O. Biebel[111], M. Biglietti[77a], C. S. Billingsley[45], Y. Bimgdi[36f], M. Bindi[55], A. Bingham[177], A. Bingul[22b], C. Bini[75a,75b], G. A. Bird[33], M. Birman[175], M. Biros[136], S. Biryukov[152], T. Bisanz[49], E. Bisceglie[24a,24b], J. P. Biswal[137], D. Biswas[147], I. Bloch[48], A. Blue[59], U. Blumenschein[96], V. S. Bobrovnikov[39], L. Boccardo[57a,57b], M. Boehler[54], B. Boehm[172], D. Bogavac[13], A. G. Bogdanchikov[38], L. S. Boggia[130], V. Boisvert[97], P. Bokan[37], T. Bold[87a], M. Bomben[5], M. Bona[96], M. Boonekamp[138], A. G. Borbély[59], I. S. Bordulev[38], G. Borissov[93], D. Bortoletto[129], D. Boscherini[24b], M. Bosman[13], K. Bouaouda[36a], N. Bouchhar[169], L. Boudet[4], J. Boudreau[132], E. V. Bouhova-Thacker[93], D. Boumediene[41], R. Bouquet[57a,57b], A. Boveia[122], J. Boyd[37], D. Boye[30], I. R. Boyko[39], L. Bozianu[56], J. Bracinik[21], N. Brahimi[4], G. Brandt[177], O. Brandt[33], B. Brau[105], J. E. Brau[126], R. Brener[175], L. Brenner[117], R. Brenner[167], S. Bressler[175], G. Brianti[78a,78b],

D. Britton[59], D. Britzger[112], I. Brock[25], R. Brock[109], G. Brooijmans[42], A. J. Brooks[68], E. M. Brooks[162b], E. Brost[30], L. M. Brown[162a,171], L. E. Bruce[61], T. L. Bruckler[129], P. A. Bruckman de Renstrom[88], B. Brüers[48], A. Bruni[24b], G. Bruni[24b], D. Brunner[47a,47b], M. Bruschi[24b], N. Bruscino[75a,75b], T. Buanes[17], Q. Buat[142], D. Buchin[112], A. G. Buckley[59], O. Bulekov[82], B. A. Bullard[149], S. Burdin[94], C. D. Burgard[49], A. M. Burger[91], B. Burghgrave[8], O. Burlayenko[54], J. Burleson[168], J. C. Burzynski[148], E. L. Busch[42], V. Büscher[102], P. J. Bussey[59], J. M. Butler[26], C. M. Buttar[59], J. M. Butterworth[98], W. Buttinger[137], C. J. Buxo Vazquez[109], A. R. Buzykaev[39], S. Cabrera Urbán[169], L. Cadamuro[66], H. Cai[37], Y. Cai[24a,24b,114c], Y. Cai[114a], V. M. M. Cairo[37], O. Cakir[3a], N. Calace[37], P. Calafiura[18a], G. Calderini[130], P. Calfayan[35], L. Calic[100], G. Callea[59], L. P. Caloba[83b], D. Calvet[41], S. Calvet[41], R. Camacho Toro[130], S. Camarda[37], D. Camarero Munoz[27], P. Camarri[76a,76b], C. Camincher[171], M. Campanelli[98], A. Camplani[43], V. Canale[72a,72b], A. C. Canbay[3a], E. Canonero[97], J. Cantero[169], Y. Cao[168], F. Capocasa[27], M. Capua[44a,44b], A. Carbone[71a,71b], R. Cardarelli[76a], J. C. J. Cardenas[8], M. P. Cardiff[27], G. Carducci[44a,44b], T. Carli[37], G. Carlino[72a], J. I. Carlotto[13], B. T. Carlson[132,r], E. M. Carlson[171], J. Carmignani[94], L. Carminati[71a,71b], A. Carnelli[4], M. Carnesale[37], S. Caron[116], E. Carquin[140g], I. B. Carr[107], S. Carrá[73a,73b], G. Carratta[24a,24b], C. Carrion Martinez[169], A. M. Carroll[126], M. P. Casado[13,h], P. Casolaro[72a,72b], M. Caspar[48], F. L. Castillo[4], L. Castillo Garcia[13], V. Castillo Gimenez[169], N. F. Castro[133a,133e], A. Catinaccio[37], J. R. Catmore[128], T. Cavaliere[4], V. Cavaliere[30], L. J. Caviedes Betancourt[23b], E. Celebi[82], S. Cella[37], V. Cepaitis[56], K. Cerny[125], A. S. Cerqueira[83a], A. Cerri[74a,74b,am], L. Cerrito[76a,76b], F. Cerutti[18a], B. Cervato[71a,71b], A. Cervelli[24b], G. Cesarini[53], S. A. Cetin[82], P. M. Chabrillat[130], R. Chakkappai[66], S. Chakraborty[173], A. Chambers[61], J. Chan[18a], W. Y. Chan[159], J. D. Chapman[33], E. Chapon[138], B. Chargeishvili[155b], D. G. Charlton[21], C. Chauhan[136], Y. Che[114a], S. Chekanov[6], S. V. Chekulaev[162a], G. A. Chelkov[39,a], B. Chen[157], B. Chen[171], H. Chen[114a], H. Chen[30], J. Chen[144a], J. Chen[148], M. Chen[129], S. Chen[89], S. J. Chen[114a], X. Chen[144a], X. Chen[15,ah], Z. Chen[62], C. L. Cheng[176], H. C. Cheng[64a], S. Cheong[149], A. Cheplakov[39], E. Cherepanova[117], R. Cherkaoui El Moursli[36e], E. Cheu[7], K. Cheung[65], L. Chevalier[138], V. Chiarella[53], G. Chiarelli[74a], G. Chiodini[70a], A. S. Chisholm[21], A. Chitan[28b], M. Chitishvili[169], M. V. Chizhov[39,s], K. Choi[11], Y. Chou[142], E. Y. S. Chow[116], K. L. Chu[175], M. C. Chu[64a], X. Chu[14,114c], Z. Chubinidze[53], J. Chudoba[134], J. J. Chwastowski[88], D. Cieri[112], K. M. Ciesla[87a], V. Cindro[95], A. Ciocio[18a], F. Cirotto[72a,72b], Z. H. Citron[175], M. Citterio[71a], D. A. Ciubotaru[28b], A. Clark[56], P. J. Clark[52], N. Clarke Hall[98], C. Clarry[161], S. E. Clawson[48], C. Clement[47a,47b], Y. Coadou[104], M. Cobal[69a,69c], A. Coccaro[57b], R. F. Coelho Barrue[133a], R. Coelho Lopes De Sa[105], S. Coelli[71a], L. S. Colangeli[161], B. Cole[42], P. Collado Soto[101], J. Collot[60], R. Coluccia[70a,70b], P. Conde Muiño[133a,133g], M. P. Connell[34c], S. H. Connell[34c], E. I. Conroy[129], M. Contreras Cossio[11], F. Conventi[72a,aj], A. M. Cooper-Sarkar[129], L. Corazzina[75a,75b], F. A. Corchia[24a,24b], A. Cordeiro Oudot Choi[142], L. D. Corpe[41], M. Corradi[75a,75b], F. Corriveau[106,ab], A. Cortes-Gonzalez[159], M. J. Costa[169], F. Costanza[4], D. Costanzo[145], B. M. Cote[122], J. Couthures[4], G. Cowan[97], K. Cranmer[176], L. Cremer[49], D. Cremonini[24a,24b], S. Crépé-Renaudin[60], F. Crescioli[130], T. Cresta[73a,73b], M. Cristinziani[147], M. Cristoforetti[78a,78b], V. Croft[117], G. Crosetti[44a,44b], A. Cueto[101], H. Cui[98], Z. Cui[7], B. M. Cunnett[152], W. R. Cunningham[59], F. Curcio[169], J. R. Curran[52], M. J. Da Cunha Sargedas De Sousa[57a,57b], J. V. Da Fonseca Pinto[83b], C. Da Via[103], W. Dabrowski[87a], T. Dado[37], S. Dahbi[154], T. Dai[108], D. Dal Santo[20], C. Dallapiccola[105], M. Dam[43], G. D'amen[30], V. D'Amico[111], J. Damp[102], J. R. Dandoy[35], M. D'Andrea[57a,57b], D. Dannheim[37], G. D'anniballe[74a,74b], M. Danninger[148], V. Dao[151], G. Darbo[57b], S. J. Das[30], F. Dattola[48], S. D'Auria[71a,71b], A. D'Avanzo[72a,72b], T. Davidek[136], J. Davidson[173], I. Dawson[96], K. De[8], C. De Almeida Rossi[161], R. De Asmundis[72a], N. De Biase[48], S. De Castro[24a,24b], N. De Groot[116], P. de Jong[117], H. De la Torre[118], A. De Maria[114a], A. De Salvo[75a], U. De Sanctis[76a,76b], F. De Santis[70a,70b], A. De Santo[152], J. B. De Vivie De Regie[60], J. Debevc[95], D. V. Dedovich[39], J. Degens[94], A. M. Deiana[45], J. Del Peso[101], L. Delagrange[130], F. Deliot[138], C. M. Delitzsch[49], M. Della Pietra[72a,72b], D. Della Volpe[56], A. Dell'Acqua[37], L. Dell'Asta[71a,71b], M. Delmastro[4], C. C. Delogu[102], P. A. Delsart[60], S. Demers[178], M. Demichev[39], S. P. Denisov[38], H. Denizli[22a,l], L. D'Eramo[41], D. Derendarz[88], F. Derue[130], P. Dervan[94,*], A. M. Desai[1], K. Desch[25], F. A. Di Bello[57a,57b], A. Di Ciaccio[76a,76b], L. Di Ciaccio[4], A. Di Domenico[75a,75b], C. Di Donato[72a,72b], A. Di Girolamo[37], G. Di Gregorio[37], A. Di Luca[78a,78b], B. Di Micco[77a,77b], R. Di Nardo[77a,77b], K. F. Di Petrillo[40], M. Diamantopoulou[35], F. A. Dias[117], M. A. Diaz[140a,140b], A. R. Didenko[39], M. Didenko[169], S. D. Diefenbacher[18a], E. B. Diehl[108], S. Díez Cornell[48], C. Diez Pardos[147], C. Dimitriadi[150], A. Dimitrievska[21], A. Dimri[151], Y. Ding[62], J. Dingfelder[25], T. Dingley[129], I. -M. Dinu[28b], S. J. Dittmeier[63b],

F. Dittus[37], M. Divisek[136], B. Dixit[94], F. Djama[104], T. Djobava[155b], C. Doglioni[100,103], A. Dohnalova[29a], Z. Dolezal[136], K. Domijan[87a], K. M. Dona[40], M. Donadelli[83d], B. Dong[109], J. Donini[41], A. D'Onofrio[72a,72b], M. D'Onofrio[94], J. Dopke[137], A. Doria[72a], N. Dos Santos Fernandes[133a], I. A. Dos Santos Luz[83e], P. Dougan[103], M. T. Dova[92], A. T. Doyle[59], M. P. Drescher[55], E. Dreyer[175], I. Drivas-koulouris[10], M. Drnevich[120], D. Du[62], T. A. du Pree[117], Z. Duan[114a], M. Dubau[4], F. Dubinin[39], M. Dubovsky[29a], E. Duchovni[175], G. Duckeck[111], P. K. Duckett[98], O. A. Ducu[28b], D. Duda[52], A. Dudarev[37], M. M. Dudek[88], E. R. Duden[27], M. D'uffizi[103], L. Duflot[66], M. Dührssen[37], I. Duminica[28g], A. E. Dumitriu[28b], M. Dunford[63a], K. Dunne[47a,47b], A. Duperrin[104], H. Duran Yildiz[3a], A. Durglishvili[155b], G. I. Dyckes[18a], M. Dyndal[87a], B. S. Dziedzic[37], Z. O. Earnshaw[152], G. H. Eberwein[129], B. Eckerova[29a], S. Eggebrecht[55], E. Egidio Purcino De Souza[83e], G. Eigen[17], K. Einsweiler[18a], T. Ekelof[167], P. A. Ekman[100], S. El Farkh[36b], Y. El Ghazali[62], H. El Jarrari[37], A. El Moussaouy[36a], D. Elitez[37], M. Ellert[167], F. Ellinghaus[177], T. A. Elliot[97], N. Ellis[37], J. Elmsheuser[30], M. Elsawy[119a], M. Elsing[37], D. Emeliyanov[137], Y. Enari[84], I. Ene[18a], S. Epari[110], D. Ernani Martins Neto[88], F. Ernst[37], M. Errenst[177], M. Escalier[66], C. Escobar[169], E. Etzion[157], G. Evans[133a,133b], H. Evans[68], L. S. Evans[48], A. Ezhilov[38], S. Ezzarqtouni[36a], F. Fabbri[24a,24b], L. Fabbri[24a,24b], G. Facini[98], V. Fadeyev[139], R. M. Fakhrutdinov[38], D. Fakoudis[102], S. Falciano[75a], L. F. Falda Ulhoa Coelho[133a], F. Fallavollita[112], G. Falsetti[44a,44b], J. Faltova[136], C. Fan[168], K. Y. Fan[64b], Y. Fan[14], Y. Fang[14,114c], M. Fanti[71a,71b], M. Faraj[69a,69b], Z. Farazpay[99], A. Farbin[8], A. Farilla[77a], K. Farman[154], T. Farooque[109], J. N. Farr[178], S. M. Farrington[52,137], F. Fassi[36e], D. Fassouliotis[9], L. Fayard[66], P. Federic[136], P. Federicova[134], O. L. Fedin[38,a], M. Feickert[176], L. Feligioni[104], D. E. Fellers[18a], C. Feng[143a], Y. Feng[14], Z. Feng[117], M. J. Fenton[165], L. Ferencz[48], B. Fernandez Barbadillo[93], P. Fernandez Martinez[67], M. J. V. Fernoux[104], J. Ferrando[93], A. Ferrari[167], P. Ferrari[116,117], R. Ferrari[73a], D. Ferrere[56], C. Ferretti[108], M. P. Fewell[1], D. Fiacco[75a,75b], F. Fiedler[102], P. Fiedler[135], S. Filimonov[39], M. S. Filip[28b,t], A. Filipčič[95], E. K. Filmer[162a], F. Filthaut[116], M. C. N. Fiolhais[133a,133c,c], L. Fiorini[169], W. C. Fisher[109], T. Fitschen[103], P. M. Fitzhugh[138], I. Fleck[147], P. Fleischmann[108], T. Flick[177], M. Flores[34d,ag], L. R. Flores Castillo[64a], L. Flores Sanz De Acedo[37], F. M. Follega[78a,78b], N. Fomin[33], J. H. Foo[161], A. Formica[138], A. C. Forti[103], E. Fortin[37], A. W. Fortman[18a], L. Foster[18a], L. Fountas[9,i], D. Fournier[66], H. Fox[93], P. Francavilla[74a,74b], S. Francescato[61], S. Franchellucci[56], M. Franchini[24a,24b], S. Franchino[63a], D. Francis[37], L. Franco[116], L. Franconi[48], M. Franklin[61], G. Frattari[27], Y. Y. Frid[157], J. Friend[59], N. Fritzsche[37], A. Froch[56], D. Froidevaux[37], J. A. Frost[129], Y. Fu[109], S. Fuenzalida Garrido[140g], M. Fujimoto[104], K. Y. Fung[64a], E. Furtado De Simas Filho[83e], M. Furukawa[159], J. Fuster[169], A. Gaa[55], A. Gabrielli[24a,24b], A. Gabrielli[161], P. Gadow[37], G. Gagliardi[57a,57b], L. G. Gagnon[18a], S. Gaid[85b], S. Galantzan[157], J. Gallagher[1], E. J. Gallas[129], A. L. Gallen[167], B. J. Gallop[137], K. K. Gan[122], S. Ganguly[159], Y. Gao[52], A. Garabaglu[142], F. M. Garay Walls[140a,140b], C. García[169], A. Garcia Alonso[117], A. G. Garcia Caffaro[178], J. E. García Navarro[169], M. A. Garcia Ruiz[23b], M. Garcia-Sciveres[18a], G. L. Gardner[131], R. W. Gardner[40], N. Garelli[164], R. B. Garg[149], J. M. Gargan[52], C. A. Garner[161], C. M. Garvey[34a], V. K. Gassmann[164], G. Gaudio[73a], V. Gautam[13], P. Gauzzi[75a,75b], J. Gavranovic[95], I. L. Gavrilenko[133a], A. Gavrilyuk[38], C. Gay[170], G. Gaycken[126], E. N. Gazis[10], A. Gekow[122], C. Gemme[57b], M. H. Genest[60], A. D. Gentry[115], S. George[97], T. Geralis[46], A. A. Gerwin[123], P. Gessinger-Befurt[37], M. E. Geyik[177], M. Ghani[173], K. Ghorbanian[96], A. Ghosal[147], A. Ghosh[165], A. Ghosh[7], B. Giacobbe[24b], S. Giagu[75a,75b], T. Giani[117], A. Giannini[62], S. M. Gibson[97], M. Gignac[139], D. T. Gil[87b], A. K. Gilbert[87a], B. J. Gilbert[42], D. Gillberg[35], G. Gilles[117], D. M. Gingrich[2,ai], M. P. Giordani[69a,69c], P. F. Giraud[138], G. Giugliarelli[69a,69c], D. Giugni[71a], F. Giuli[76a,76b], I. Gkialas[9,i], L. K. Gladilin[38], C. Glasman[101], M. Glazewska[20], R. M. Gleason[165], G. Glemža[48], M. Glisic[126], I. Gnesi[44b], Y. Go[30], M. Goblirsch-Kolb[37], B. Gocke[49], D. Godin[110], B. Gokturk[22a], S. Goldfarb[107], T. Golling[56], M. G. D. Gololo[34c], D. Golubkov[38], J. P. Gombas[109], A. Gomes[133a,133b], G. Gomes Da Silva[147], A. J. Gomez Delegido[37], R. Gonçalo[133a], L. Gonella[21], A. Gongadze[155c], F. Gonnella[21], J. L. Gonski[149], R. Y. González Andana[52], S. González de la Hoz[169], M. V. Gonzalez Rodrigues[48], R. Gonzalez Suarez[167], S. Gonzalez-Sevilla[56], L. Goossens[37], B. Gorini[37], E. Gorini[70a,70b], A. Gorišek[95], T. C. Gosart[131], A. T. Goshaw[51], M. I. Gostkin[39], S. Goswami[124], C. A. Gottardo[37], S. A. Gotz[111], M. Gouighri[36b], A. G. Goussiou[142], N. Govender[34c], R. P. Grabarczyk[129], I. Grabowska-Bold[87a], K. Graham[35], E. Gramstad[128], S. Grancagnolo[70a,70b], C. M. Grant[1], P. M. Gravila[28f], F. G. Gravili[70a,70b], H. M. Gray[18a], M. Greco[112], M. J. Green[1], C. Grefe[25], A. S. Grefsrud[17], I. M. Gregor[48], K. T. Greif[165], P. Grenier[149], S. G. Grewe[112], A. A. Grillo[139], K. Grimm[32], S. Grinstein[13,x], J. -F. Grivaz[66], E. Gross[175], J. Grosse-Knetter[55], L. Guan[108], G. Guerrieri[37], R. Guevara[128], R. Gugel[102], J. A. M. Guhit[108],

A. Guida[19], E. Guilloton[173], S. Guindon[37], F. Guo[14,114c], J. Guo[144a], L. Guo[48], L. Guo[114b,v], Y. Guo[108], A. Gupta[49], R. Gupta[132], S. Gupta[27], S. Gurbuz[25], S. S. Gurdasani[48], G. Gustavino[75a,75b], P. Gutierrez[123], L. F. Gutierrez Zagazeta[131], M. Gutsche[50], C. Gutschow[98], C. Gwenlan[129], C. B. Gwilliam[94], E. S. Haaland[128], A. Haas[120], M. Habedank[59], C. Haber[18a], H. K. Hadavand[8], A. Haddad[41], A. Hadef[50], A. I. Hagan[93], J. J. Hahn[147], E. H. Haines[98], M. Haleem[172], J. Haley[124], G. D. Hallewell[104], K. Hamano[171], H. Hamdaoui[167], M. Hamer[25], S. E. D. Hammoud[66], E. J. Hampshire[97], J. Han[143a], L. Han[114a], L. Han[62], S. Han[14], K. Hanagaki[84], M. Hance[139], D. A. Hangal[42], H. Hanif[148], M. D. Hank[131], J. B. Hansen[43], P. H. Hansen[43], D. Harada[56], T. Harenberg[177], S. Harkusha[179], M. L. Harris[105], Y. T. Harris[25], J. Harrison[13], N. M. Harrison[122], P. F. Harrison[173], M. L. E. Hart[98], N. M. Hartman[112], N. M. Hartmann[111], R. Z. Hasan[97,137], Y. Hasegawa[146], F. Haslbeck[129], S. Hassan[17], R. Hauser[109], M. Haviernik[136], C. M. Hawkes[21], R. J. Hawkings[37], Y. Hayashi[159], D. Hayden[109], C. Hayes[108], R. L. Hayes[117], C. P. Hays[129], J. M. Hays[96], H. S. Hayward[94], M. He[14,114c], Y. He[48], Y. He[98], N. B. Heatley[96], V. Hedberg[100], C. Heidegger[54], K. K. Heidegger[54], J. Heilman[35], S. Heim[48], T. Heim[18a], J. G. Heinlein[131], J. J. Heinrich[126], L. Heinrich[112], J. Hejbal[134], M. Helbig[50], A. Held[176], S. Hellesund[17], C. M. Helling[170], S. Hellman[47a,47b], A. M. Henriques Correia[37], H. Herde[100], Y. Hernández Jiménez[151], L. M. Herrmann[25], T. Herrmann[50], G. Herten[54], R. Hertenberger[111], L. Hervas[37], M. E. Hesping[102], N. P. Hessey[162a], J. Hessler[112], M. Hidaoui[36b], N. Hidic[136], E. Hill[161], T. S. Hillersoy[17], S. J. Hillier[21], J. R. Hinds[109], F. Hinterkeuser[25], M. Hirose[127], S. Hirose[163], D. Hirschbuehl[177], T. G. Hitchings[103], B. Hiti[95], J. Hobbs[151], R. Hobincu[28e], N. Hod[175], A. M. Hodges[168], M. C. Hodgkinson[145], B. H. Hodkinson[129], A. Hoecker[37], D. D. Hofer[108], J. Hofer[169], M. Holzbock[37], L. B. A. H. Hommels[33], V. Homsak[129], B. P. Honan[103], J. J. Hong[68], T. M. Hong[132], B. H. Hooberman[168], W. H. Hopkins[6], M. C. Hoppesch[168], Y. Horii[113], M. E. Horstmann[112], S. Hou[154], M. R. Housenga[168], J. Howarth[59], J. Hoya[6], M. Hrabovsky[125], T. Hryn'ova[4], P. J. Hsu[65], S. -C. Hsu[142], T. Hsu[66], M. Hu[18a], Q. Hu[62], S. Huang[33], X. Huang[14,114c], Y. Huang[136], Y. Huang[114b], Y. Huang[14], Z. Huang[66], Z. Hubacek[135], F. Huegging[25], T. B. Huffman[129], M. Hufnagel Maranha De Faria[83a], C. A. Hugli[48], M. Huhtinen[37], S. K. Huiberts[17], R. Hulsken[106], C. E. Hultquist[18a], D. L. Humphreys[105], N. Huseynov[12], J. Huston[109], J. Huth[61], L. Huth[48], R. Hyneman[7], G. Iacobucci[56], G. Iakovidis[30], L. Iconomidou-Fayard[66], J. P. Iddon[37], P. Iengo[72a,72b], R. Iguchi[159], Y. Iiyama[159], T. Iizawa[159], Y. Ikegami[84], D. Iliadis[158], N. Ilic[161], H. Imam[36a], G. Inacio Goncalves[83d], S. A. Infante Cabanas[140c], T. Ingebretsen Carlson[47a,47b], J. M. Inglis[96], G. Introzzi[73a,73b], M. Iodice[77a], V. Ippolito[75a,75b], R. K. Irwin[94], M. Ishino[159], W. Islam[176], C. Issever[19], S. Istin[22a,ao], K. Itabashi[84], H. Ito[174], R. Iuppa[78a,78b], A. Ivina[175], V. Izzo[72a], P. Jacka[135], P. Jackson[1], P. Jain[48], K. Jakobs[54], T. Jakoubek[175], J. Jamieson[59], W. Jang[159], S. Jankovych[136], M. Javurkova[105], P. Jawahar[103], L. Jeanty[126], J. Jejelava[155a,ae], P. Jenni[54,f], C. E. Jessiman[35], C. Jia[143a], H. Jia[170], J. Jia[151], X. Jia[112,114c], Z. Jia[114a], C. Jiang[52], Q. Jiang[64b], S. Jiggins[48], M. Jimenez Ortega[169], J. Jimenez Pena[13], S. Jin[114a], A. Jinaru[28b], O. Jinnouchi[141], P. Johansson[145], K. A. Johns[7], J. W. Johnson[139], F. A. Jolly[48], D. M. Jones[152], E. Jones[48], K. S. Jones[8], P. Jones[33], R. W. L. Jones[93], T. J. Jones[94], H. L. Joos[55], R. Joshi[122], J. Jovicevic[16], X. Ju[18a], J. J. Junggeburth[37], T. Junkermann[63a], A. Juste Rozas[13,x], M. K. Juzek[88], S. Kabana[140f], A. Kaczmarska[88], S. A. Kadir[149], M. Kado[112], H. Kagan[122], M. Kagan[149], A. Kahn[131], C. Kahra[102], T. Kaji[159], E. Kajomovitz[156], N. Kakati[175], N. Kakoty[13], I. Kalaitzidou[54], S. Kandel[8], N. J. Kang[139], D. Kar[34h], E. Karentzos[25], K. Karki[8], O. Karkout[117], S. N. Karpov[39], Z. M. Karpova[39], V. Kartvelishvili[93], A. N. Karyukhin[38], E. Kasimi[158], J. Katzy[48], S. Kaur[35], K. Kawade[146], M. P. Kawale[123], C. Kawamoto[89], T. Kawamoto[62], E. F. Kay[37], F. I. Kaya[164], S. Kazakos[109], V. F. Kazanin[38], J. M. Keaveney[34a], R. Keeler[171], G. V. Kehris[61], J. S. Keller[35], J. M. Kelly[171], J. J. Kempster[152], O. Kepka[134], J. Kerr[162b], B. P. Kerridge[137], B. P. Kerševan[95], L. Keszeghova[29a], R. A. Khan[132], A. Khanov[124], A. G. Kharlamov[38], T. Kharlamova[38], E. E. Khoda[142], M. Kholodenko[133a], T. J. Khoo[19], G. Khoriauli[172], Y. Khoulaki[36a], J. Khubua[155b,*], Y. A. R. Khwaira[130], B. Kibirige[34h], D. Kim[6], D. W. Kim[47a,47b], Y. K. Kim[40], N. Kimura[98], M. K. Kingston[55], A. Kirchhoff[55], C. Kirfel[25], F. Kirfel[25], J. Kirk[137], A. E. Kiryunin[112], S. Kita[163], O. Kivernyk[25], M. Klassen[164], C. Klein[35], L. Klein[172], M. H. Klein[45], S. B. Klein[56], U. Klein[94], A. Klimentov[30], T. Klioutchnikova[37], P. Kluit[117], S. Kluth[112], E. Kneringer[79], T. M. Knight[161], A. Knue[49], M. Kobel[50], D. Kobylianskii[175], S. F. Koch[129], M. Kocian[149], P. Kodyš[136], D. M. Koeck[126], T. Koffas[35], O. Kolay[50], I. Koletsou[4], T. Komarek[88], K. Köneke[55], A. X. Y. Kong[1], T. Kono[121], N. Konstantinidis[98], P. Kontaxakis[56], B. Konya[100], R. Kopeliansky[42], S. Koperny[87a], K. Korcyl[88], K. Kordas[158,d], A. Korn[98], S. Korn[55], I. Korolkov[13],

N. Korotkova[38], B. Kortman[117], O. Kortner[112], S. Kortner[112], W. H. Kostecka[118], M. Kostov[29a], V. V. Kostyukhin[147], A. Kotsokechagia[37], A. Kotwal[51], A. Koulouris[37], A. Kourkoumeli-Charalampidi[73a,73b], C. Kourkoumelis[9], E. Kourlitis[112], O. Kovanda[126], R. Kowalewski[171], W. Kozanecki[126], A. S. Kozhin[38], V. A. Kramarenko[38], G. Kramberger[95], P. Kramer[25], M. W. Krasny[130], A. Krasznahorkay[105], A. C. Kraus[118], J. W. Kraus[177], J. A. Kremer[48], N. B. Krengel[147], T. Kresse[50], L. Kretschmann[177], J. Kretzschmar[94], P. Krieger[161], K. Krizka[21], K. Kroeninger[49], H. Kroha[112], J. Kroll[134], J. Kroll[131], K. S. Krowpman[109], U. Kruchonak[39], H. Krüger[25], N. Krumnack[81], M. C. Kruse[51], O. Kuchinskaia[39], S. Kuday[3a], S. Kuehn[37], R. Kuesters[54], T. Kuhl[48], V. Kukhtin[39], Y. Kulchitsky[39], S. Kuleshov[140b,140d], J. Kull[1], E. V. Kumar[111], M. Kumar[34h], N. Kumari[48], P. Kumari[162b], A. Kupco[134], A. Kupich[38], O. Kuprash[54], H. Kurashige[86], L. L. Kurchaninov[162a], O. Kurdysh[4], Y. A. Kurochkin[38], A. Kurova[38], M. Kuze[141], A. K. Kvam[105], J. Kvita[125], N. G. Kyriacou[142], C. Lacasta[169], F. Lacava[75a,75b], H. Lacker[19], D. Lacour[130], N. N. Lad[98], E. Ladygin[39], A. Lafarge[41], B. Laforge[130], T. Lagouri[178], F. Z. Lahbabi[36a], S. Lai[37,55], W. S. Lai[98], J. E. Lambert[171], S. Lammers[68], W. Lampl[7], C. Lampoudis[158,d], G. Lamprinoudis[102], A. N. Lancaster[118], E. Lançon[30], U. Landgraf[54], M. P. J. Landon[96], V. S. Lang[54], O. K. B. Langrekken[128], A. J. Lankford[165], F. Lanni[37], K. Lantzsch[25], A. Lanza[73a], M. Lanzac Berrocal[169], J. F. Laporte[138], T. Lari[71a], D. Larsen[17], L. Larson[11], F. Lasagni Manghi[24b], M. Lassnig[37], S. D. Lawlor[145], R. Lazaridou[165], M. Lazzaroni[71a,71b], H. D. M. Le[109], E. M. Le Boulicaut[178], L. T. Le Pottier[18a], B. Leban[24a,24b], F. Ledroit-Guillon[60], T. F. Lee[162b], L. L. Leeuw[34c], M. Lefebvre[171], C. Leggett[18a], G. Lehmann Miotto[37], M. Leigh[56], W. A. Leight[105], W. Leinonen[116], A. Leisos[158,u], M. A. L. Leite[83c], C. E. Leitgeb[19], R. Leitner[136], K. J. C. Leney[45], T. Lenz[25], S. Leone[74a], C. Leonidopoulos[52], A. Leopold[150], J. H. Lepage Bourbonnais[35], R. Les[109], C. G. Lester[33], M. Levchenko[38], J. Levêque[4], L. J. Levinson[175], G. Levrini[24a,24b], M. P. Lewicki[88], C. Lewis[142], D. J. Lewis[4], L. Lewitt[145], A. Li[30], B. Li[143a], C. Li[108], C. -Q. Li[112], H. Li[143a], H. Li[103], H. Li[15], H. Li[62], H. Li[143a], J. Li[144a], K. Li[14], L. Li[144a], R. Li[178], S. Li[14,114c], S. Li[144a,144b], T. Li[5], X. Li[106], Y. Li[14], Z. Li[159], Z. Li[14,114c], Z. Li[62], S. Liang[14,114c], Z. Liang[14], M. Liberatore[138], B. Liberti[76a], G. B. Libotte[83d], K. Lie[64c], J. Lieber Marin[83e], H. Lien[68], H. Lin[108], S. F. Lin[151], L. Linden[111], R. E. Lindley[7], J. H. Lindon[37], J. Ling[61], E. Lipeles[131], A. Lipniacka[17], A. Lister[170], J. D. Little[68], B. Liu[14], B. X. Liu[114b], D. Liu[144a,144b], D. Liu[139], E. H. L. Liu[21], J. K. K. Liu[120], K. Liu[144b], K. Liu[144a,144b], M. Liu[62], M. Y. Liu[62], P. Liu[14], Q. Liu[142,144a,144b], S. Liu[151], X. Liu[62], X. Liu[143a], Y. Liu[114b,114c], Y. L. Liu[143a], Y. W. Liu[62], Z. Liu[66,k], S. L. Lloyd[96], E. M. Lobodzinska[48], P. Loch[7], E. Lodhi[161], K. Lohwasser[145], E. Loiacono[48], J. D. Lomas[21], J. D. Long[42], I. Longarini[165], R. Longo[168], A. Lopez Solis[13], N. A. Lopez-canelas[7], N. Lorenzo Martinez[4], A. M. Lory[111], M. Losada[119a], G. Löschcke Centeno[4], X. Lou[47a,47b], X. Lou[14,114c], A. Lounis[66], P. A. Love[93], M. Lu[66], S. Lu[131], Y. J. Lu[154], H. J. Lubatti[142], C. Luci[75a,75b], F. L. Lucio Alves[114a], F. Luehring[68], B. S. Lunday[131], O. Lundberg[150], J. Lunde[37], N. A. Luongo[6], M. S. Lutz[37], A. B. Lux[26], D. Lynn[30], R. Lysak[134], V. Lysenko[135], E. Lytken[100], V. Lyubushkin[39], T. Lyubushkina[39], M. M. Lyukova[151], H. Ma[30], K. Ma[62], L. L. Ma[143a], W. Ma[62], Y. Ma[124], J. C. MacDonald[102], P. C. Machado De Abreu Farias[83e], D. Macina[37], R. Madar[41], T. Madula[98], J. Maeda[86], T. Maeno[30], P. T. Mafa[34c,j], H. Maguire[145], M. Maheshwari[33], V. Maiboroda[66], A. Maio[133a,133b,133d], K. Maj[87a], O. Majersky[48], S. Majewski[126], R. Makhmanazarov[38], N. Makovec[66], V. Maksimovic[16], B. Malaescu[130], J. Malamant[128], Pa. Malecki[88], V. P. Maleev[38], F. Malek[60,o], M. Mali[95], D. Malito[97], U. Mallik[80,*], A. Maloizel[5], S. Maltezos[10], A. Malvezzi Lopes[83d], S. Malyukov[39], J. Mamuzic[95], G. Mancini[53], M. N. Mancini[27], G. Manco[73a,73b], J. P. Mandalia[96], S. S. Mandarry[152], I. Mandić[95], L. Manhaes de Andrade Filho[83a], I. M. Maniatis[175], J. Manjarres Ramos[91], D. C. Mankad[175], A. Mann[111], T. Manoussos[37], M. N. Mantinan[40], S. Manzoni[37], L. Mao[144a], X. Mapekula[34c], A. Marantis[158], R. R. Marcelo Gregorio[96], G. Marchiori[5], C. Marcon[71a], E. Maricic[16], M. Marinescu[48], S. Marium[48], M. Marjanovic[123], A. Markhoos[54], M. Markovitch[66], M. K. Maroun[105], M. C. Marr[148], G. T. Marsden[103], E. J. Marshall[93], Z. Marshall[18a], S. Marti-Garcia[169], J. Martin[98], T. A. Martin[137], V. J. Martin[52], B. Martin dit Latour[17], L. Martinelli[75a,75b], M. Martinez[13,x], P. Martinez Agullo[169], V. I. Martinez Outschoorn[105], P. Martinez Suarez[37], S. Martin-Haugh[137], G. Martinovicova[136], V. S. Martoiu[28b], A. C. Martyniuk[98], A. Marzin[37], D. Mascione[78a,78b], L. Masetti[102], J. Masik[103], A. L. Maslennikov[39], S. L. Mason[42], P. Massarotti[72a,72b], P. Mastrandrea[74a,74b], A. Mastroberardino[44a,44b], T. Masubuchi[127], T. T. Mathew[126], J. Matousek[136], D. M. Mattern[49], J. Maurer[28b], T. Maurin[59], A. J. Maury[66], B. Maček[95], C. Mavungu Tsava[104], D. A. Maximov[38], A. E. May[103], E. Mayer[41], R. Mazini[34h], I. Maznas[118], S. M. Mazza[139], E. Mazzeo[37], J. P. Mc Gowan[171], S. P. Mc Kee[108], C. A. Mc Lean[6], C. C. McCracken[170],

E. F. McDonald[107], A. E. McDougall[117], L. F. Mcelhinney[93], J. A. Mcfayden[152], R. P. McGovern[131], R. P. Mckenzie[34h], T. C. Mclachlan[48], D. J. Mclaughlin[98], S. J. McMahon[137], C. M. Mcpartland[94], R. A. McPherson[171,ab], S. Mehlhase[111], A. Mehta[94], D. Melini[169], B. R. Mellado Garcia[34h], A. H. Melo[55], F. Meloni[48], A. M. Mendes Jacques Da Costa[103], L. Meng[93], S. Menke[112], M. Mentink[37], E. Meoni[44a,44b], G. Mercado[118], S. Merianos[158], C. Merlassino[69a,69c], C. Meroni[71a,71b], J. Metcalfe[6], A. S. Mete[6], E. Meuser[102], C. Meyer[68], J. -P. Meyer[138], Y. Miao[114a], R. P. Middleton[137], M. Mihovilovic[66], L. Mijović[52], G. Mikenberg[175], M. Mikestikova[134], M. Mikuž[95], H. Mildner[102], A. Milic[37], D. W. Miller[40], E. H. Miller[149], A. Milov[175], D. A. Milstead[47a,47b], T. Min[114a], A. A. Minaenko[38], I. A. Minashvili[155b], A. I. Mincer[120], B. Mindur[87a], M. Mineev[39], Y. Mino[89], L. M. Mir[13], M. Miralles Lopez[59], M. Mironova[18a], M. Missio[116], A. Mitra[173], V. A. Mitsou[169], Y. Mitsumori[113], O. Miu[161], P. S. Miyagawa[96], T. Mkrtchyan[63a], M. Mlinarevic[98], T. Mlinarevic[98], M. Mlynarikova[136], L. Mlynarska[87a], C. Mo[144a], S. Mobius[20], M. H. Mohamed Farook[115], S. Mohapatra[42], M. F. Mohd Soberi[52], S. Mohiuddin[124], G. Mokgatitswane[34h], L. Moleri[175], U. Molinatti[129], L. G. Mollier[20], B. Mondal[134], S. Mondal[135], K. Mönig[48], E. Monnier[104], L. Monsonis Romero[169], J. Montejo Berlingen[13], A. Montella[47a,47b], M. Montella[122], F. Montereali[77a,77b], F. Monticelli[92], S. Monzani[69a,69c], A. Morancho Tarda[43], N. Morange[66], A. L. Moreira De Carvalho[48], M. Moreno Llácer[169], C. Moreno Martinez[56], J. M. Moreno Perez[23b], P. Morettini[57b], S. Morgenstern[37], M. Morii[61], M. Morinaga[159], M. Moritsu[90], F. Morodei[75a,75b], P. Moschovakos[37], B. Moser[54], M. Mosidze[155b], T. Moskalets[45], P. Moskvitina[116], J. Moss[32], P. Moszkowicz[87a], A. Moussa[36d], Y. Moyal[175], H. Moyano Gomez[13], E. J. W. Moyse[105], T. G. Mroz[88], O. Mtintsilana[34h], S. Muanza[104], M. Mucha[25], J. Mueller[132], R. Müller[37], G. A. Mullier[167], A. J. Mullin[33], J. J. Mullin[51], A. C. Mullins[45], A. E. Mulski[61], D. P. Mungo[161], D. Munoz Perez[169], F. J. Munoz Sanchez[103], W. J. Murray[137,173], M. Muškinja[95], C. Mwewa[48], A. G. Myagkov[38,a], A. J. Myers[8], G. Myers[108], M. Myska[135], B. P. Nachman[149], K. Nagai[129], K. Nagano[84], R. Nagasaka[159], J. L. Nagle[30,al], E. Nagy[104], A. M. Nairz[37], Y. Nakahama[84], K. Nakamura[84], K. Nakkalil[5], A. Nandi[63b], H. Nanjo[127], E. A. Narayanan[45], Y. Narukawa[159], I. Naryshkin[38], L. Nasella[71a,71b], S. Nasri[119b], C. Nass[25], G. Navarro[23a], A. Nayaz[19], P. Y. Nechaeva[38], S. Nechaeva[24a,24b], F. Nechansky[134], L. Nedic[129], T. J. Neep[21], A. Negri[73a,73b], M. Negrini[24b], C. Nellist[117], C. Nelson[106], K. Nelson[108], S. Nemecek[134], M. Nessi[37,g], M. S. Neubauer[168], J. Newell[94], P. R. Newman[21], Y. W. Y. Ng[168], B. Ngair[119a], H. D. N. Nguyen[110], J. D. Nichols[123], R. B. Nickerson[129], R. Nicolaidou[138], J. Nielsen[139], M. Niemeyer[55], J. Niermann[37], N. Nikiforou[37], V. Nikolaenko[38,a], I. Nikolic-Audit[130], P. Nilsson[30], I. Ninca[48], G. Ninio[157], A. Nisati[75a], R. Nisius[112], N. Nitika[69a,69c], J. -E. Nitschke[50], E. K. Nkadimeng[34b], T. Nobe[159], D. Noll[18a], T. Nommensen[153], M. B. Norfolk[145], B. J. Norman[35], L. C. Nosler[18a], M. Noury[36a], J. Novak[95], T. Novak[95], R. Novotny[135], L. Nozka[125], K. Ntekas[165], D. Ntounis[149], N. M. J. Nunes De Moura Junior[83b], J. Ocariz[130], I. Ochoa[133a], S. Oerdek[48,y], J. T. Offermann[40], A. Ogrodnik[136], A. Oh[103], C. C. Ohm[150], H. Oide[84], M. L. Ojeda[37], Y. Okumura[159], L. F. Oleiro Seabra[133a], I. Oleksiyuk[56], G. Oliveira Correa[13], D. Oliveira Damazio[30], J. L. Oliver[165], R. Omar[68], Ö. O. Öncel[54], A. P. O'Neill[20], A. Onofre[133a,133e,e], P. U. E. Onyisi[11], M. J. Oreglia[40], D. Orestano[77a,77b], R. Orlandini[77a,77b], R. S. Orr[161], L. M. Osojnak[42], Y. Osumi[113], G. Otero y Garzon[31], H. Otono[90], M. Ouchrif[36d], F. Ould-Saada[128], T. Ovsiannikova[142], M. Owen[59], R. E. Owen[137], V. E. Ozcan[22a], F. Ozturk[88], N. Ozturk[8], S. Ozturk[82], H. A. Pacey[129], K. Pachal[162a], A. Pacheco Pages[13], C. Padilla Aranda[13], G. Padovano[75a,75b], S. Pagan Griso[18a], G. Palacino[68], A. Palazzo[70a,70b], J. Pampel[25], J. Pan[178], T. Pan[64a], D. K. Panchal[11], C. E. Pandini[60], J. G. Panduro Vazquez[137], H. D. Pandya[1], H. Pang[138], P. Pani[48], G. Panizzo[69a,69c], L. Panwar[130], L. Paolozzi[56], S. Parajuli[168], A. Paramonov[6], C. Paraskevopoulos[53], D. Paredes Hernandez[64b], A. Pareti[73a,73b], K. R. Park[42], T. H. Park[112], F. Parodi[57a,57b], J. A. Parsons[42], U. Parzefall[54], B. Pascual Dias[41], L. Pascual Dominguez[101], E. Pasqualucci[75a], S. Passaggio[57b], F. Pastore[97], P. Patel[88], U. M. Patel[51], J. R. Pater[103], T. Pauly[37], F. Pauwels[136], C. I. Pazos[164], M. Pedersen[128], R. Pedro[133a], S. V. Peleganchuk[38], O. Penc[134], E. A. Pender[52], S. Peng[15], G.D. Penn[178], K. E. Penski[111], M. Penzin[38], B. S. Peralva[83d], A. P. Pereira Peixoto[142], L. Pereira Sanchez[149], D. V. Perepelitsa[30,al], G. Perera[105], E. Perez Codina[37], M. Perganti[10], H. Pernegger[37], S. Perrella[75a,75b], K. Peters[48], R. F. Y. Peters[103], B. A. Petersen[37], T. C. Petersen[43], E. Petit[104], V. Petousis[135], A. R. Petri[71a,71b], C. Petridou[158,d], T. Petru[136], A. Petrukhin[147], M. Pettee[18a], A. Petukhov[82], K. Petukhova[37], R. Pezoa[140g], L. Pezzotti[24a,24b], G. Pezzullo[178], L. Pfaffenbichler[37], A. J. Pfleger[79], T. M. Pham[176], T. Pham[107], P. W. Phillips[137], G. Piacquadio[151], E. Pianori[18a], F. Piazza[126], R. Piegaia[31], D. Pietreanu[28b], A. D. Pilkington[103], M. Pinamonti[69a,69c], J. L. Pinfold[2], B. C. Pinheiro Pereira[133a],

J. Pinol Bel[13], A. E. Pinto Pinoargote[130], L. Pintucci[69a,69c], K. M. Piper[152], A. Pirttikoski[56], D. A. Pizzi[35], L. Pizzimento[64b], A. Plebani[33], M. -A. Pleier[30], V. Pleskot[136], E. Plotnikova[39], G. Poddar[96], R. Poettgen[100], L. Poggioli[130], S. Polacek[136], G. Polesello[73a], A. Poley[148], A. Polini[24b], C. S. Pollard[173], Z. B. Pollock[122], E. Pompa Pacchi[123], N. I. Pond[98], D. Ponomarenko[68], L. Pontecorvo[37], S. Popa[28a], G. A. Popeneciu[28d], A. Poreba[37], D. M. Portillo Quintero[162a], S. Pospisil[135], M. A. Postill[145], P. Postolache[28c], K. Potamianos[173], P. A. Potepa[87a], I. N. Potrap[39], C. J. Potter[33], H. Potti[153], J. Poveda[169], M. E. Pozo Astigarraga[37], R. Pozzi[37], A. Prades Ibanez[76a,76b], S. R. Pradhan[145], J. Pretel[171], D. Price[103], M. Primavera[70a], L. Primomo[69a,69c], M. A. Principe Martin[101], R. Privara[125], T. Procter[87b], M. L. Proffitt[142], N. Proklova[131], K. Prokofiev[64c], G. Proto[112], J. Proudfoot[6], M. Przybycien[87a], W. W. Przygoda[87b], A. Psallidas[46], J. E. Puddefoot[145], D. Pudzha[53], H. I. Purnell[1], D. Pyatiizbyantseva[116], J. Qian[108], R. Qian[109], D. Qichen[129], Y. Qin[13], T. Qiu[52], A. Quadt[55], M. Queitsch-Maitland[103], G. Quetant[56], R. P. Quinn[170], G. Rabanal Bolanos[61], D. Rafanoharana[112], F. Raffaeli[76a,76b], F. Ragusa[71a,71b], J. L. Rainbolt[40], S. Rajagopalan[30], E. Ramakoti[39], L. Rambelli[57a,57b], I. A. Ramirez-Berend[35], K. Ran[48,114c], D. S. Rankin[131], N. P. Rapheeha[34h], H. Rasheed[28b], D. F. Rassloff[63a], A. Rastogi[18a], S. Rave[102], S. Ravera[57a,57b], B. Ravina[37], I. Ravinovich[175], M. Raymond[37], A. L. Read[128], N. P. Readioff[145], D. M. Rebuzzi[73a,73b], A. S. Reed[59], K. Reeves[27], J. A. Reidelsturz[177], D. Reikher[37], A. Rej[49], C. Rembser[37], H. Ren[62], M. Renda[28b], F. Renner[48], A. G. Rennie[59], A. L. Rescia[57a,57b], S. Resconi[71a], M. Ressegotti[57a,57b], S. Rettie[117], W. F. Rettie[35], M. M. Revering[33], E. Reynolds[18a], O. L. Rezanova[39], P. Reznicek[136], H. Riani[36d], N. Ribaric[51], B. Ricci[69a,69c], E. Ricci[78a,78b], R. Richter[112], S. Richter[47a,47b], E. Richter-Was[87b], M. Ridel[130], S. Ridouani[36d], P. Rieck[120], P. Riedler[37], E. M. Riefel[47a,47b], J. O. Rieger[117], M. Rijssenbeek[151], M. Rimoldi[37], L. Rinaldi[24a,24b], P. Rincke[55,167], G. Ripellino[167], I. Riu[13], J. C. Rivera Vergara[171], F. Rizatdinova[124], E. Rizvi[96], B. R. Roberts[18a], S. S. Roberts[139], D. Robinson[33], M. Robles Manzano[102], A. Robson[59], A. Rocchi[76a,76b], C. Roda[74a,74b], S. Rodriguez Bosca[37], Y. Rodriguez Garcia[23a], A. M. Rodríguez Vera[118], S. Roe[37], J. T. Roemer[37], O. Røhne[128], R. A. Rojas[37], C. P. A. Roland[130], A. Romaniouk[79], E. Romano[73a,73b], M. Romano[24b], A. C. Romero Hernandez[168], N. Rompotis[94], L. Roos[130], S. Rosati[75a], B. J. Rosser[40], E. Rossi[129], E. Rossi[72a,72b], L. P. Rossi[61], L. Rossini[54], R. Rosten[122], M. Rotaru[28b], B. Rottler[54], D. Rousseau[66], D. Rousso[48], S. Roy-Garand[161], A. Rozanov[104], Z. M. A. Rozario[59], Y. Rozen[156], A. Rubio Jimenez[169], V. H. Ruelas Rivera[19], T. A. Ruggeri[1], A. Ruggiero[129], A. Ruiz-Martinez[169], A. Rummler[37], Z. Rurikova[54], N. A. Rusakovich[39], S. Ruscelli[49], H. L. Russell[171], G. Russo[75a,75b], J. P. Rutherfoord[7], S. Rutherford Colmenares[33], M. Rybar[136], P. Rybczynski[87a], A. Ryzhov[45], J. A. Sabater Iglesias[56], H. F. -W. Sadrozinski[139], F. Safai Tehrani[75a], S. Saha[1], M. Sahinsoy[82], B. Sahoo[175], A. Saibel[169], B. T. Saifuddin[123], M. Saimpert[138], G. T. Saito[83c], M. Saito[159], T. Saito[159], A. Sala[71a,71b], A. Salnikov[149], J. Salt[169], A. Salvador Salas[157], F. Salvatore[152], A. Salzburger[37], D. Sammel[54], E. Sampson[93], D. Sampsonidis[158,d], D. Sampsonidou[126], J. Sánchez[169], V. Sanchez Sebastian[169], H. Sandaker[128], C. O. Sander[48], J. A. Sandesara[176], M. Sandhoff[177], C. Sandoval[23b], L. Sanfilippo[63a], D. P. C. Sankey[137], T. Sano[89], A. Sansoni[53], M. Santana Queiroz[18b], L. Santi[37], C. Santoni[41], H. Santos[133a,133b], A. Santra[175], E. Sanzani[24a,24b], K. A. Saoucha[85b], J. G. Saraiva[133a,133d], J. Sardain[7], O. Sasaki[84], K. Sato[163], C. Sauer[37], E. Sauvan[4], P. Savard[161,ai], R. Sawada[159], C. Sawyer[137], L. Sawyer[99], C. Sbarra[24b], A. Sbrizzi[24a,24b], T. Scanlon[98], J. Schaarschmidt[142], U. Schäfer[102], A. C. Schaffer[45,66], D. Schaile[111], R. D. Schamberger[151], C. Scharf[19], M. M. Schefer[20], V. A. Schegelsky[38], D. Scheirich[136], M. Schernau[140f], C. Scheulen[56], C. Schiavi[57a,57b], M. Schioppa[44a,44b], B. Schlag[149], S. Schlenker[37], J. Schmeing[177], E. Schmidt[112], M. A. Schmidt[177], K. Schmieden[102], C. Schmitt[102], N. Schmitt[102], S. Schmitt[48], N. A. Schneider[111], L. Schoeffel[138], A. Schoening[63b], P. G. Scholer[35], E. Schopf[147], M. Schott[25], S. Schramm[56], T. Schroer[56], H. -C. Schultz-Coulon[63a], M. Schumacher[54], B. A. Schumm[139], Ph. Schune[138], H. R. Schwartz[7], A. Schwartzman[149], T. A. Schwarz[108], Ph. Schwemling[138], R. Schwienhorst[109], F. G. Sciacca[20], A. Sciandra[30], G. Sciolla[27], F. Scuri[74a], C. D. Sebastiani[37], K. Sedlaczek[118], S. C. Seidel[115], A. Seiden[139], B. D. Seidlitz[42], C. Seitz[48], J. M. Seixas[83b], G. Sekhniaidze[72a], L. Selem[60], N. Semprini-Cesari[24a,24b], A. Semushin[179], D. Sengupta[56], V. Senthilkumar[169], L. Serin[66], M. Sessa[72a,72b], H. Severini[123], F. Sforza[57a,57b], A. Sfyrla[56], Q. Sha[14], E. Shabalina[55], H. Shaddix[118], A. H. Shah[33], R. Shaheen[150], J. D. Shahinian[131], M. Shamim[37], L. Y. Shan[14], M. Shapiro[18a], A. Sharma[37], A. S. Sharma[170], P. Sharma[30], P. B. Shatalov[38], K. Shaw[152], S. M. Shaw[103], Q. Shen[14], D. J. Sheppard[148], P. Sherwood[98], L. Shi[98], X. Shi[14], S. Shimizu[84], C. O. Shimmin[178], I. P. J. Shipsey[129,*], S. Shirabe[90], M. Shiyakova[39,z], M. J. Shochet[40], D. R. Shope[128], B. Shrestha[123], S. Shrestha[122,an], I. Shreyber[39], M. J. Shroff[171],

P. Sicho[134], A. M. Sickles[168], E. Sideras Haddad[34h,166], A. C. Sidley[117], A. Sidoti[24b], F. Siegert[50], Dj. Sijacki[16], F. Sili[92], J. M. Silva[52], I. Silva Ferreira[83b], M. V. Silva Oliveira[30], S. B. Silverstein[47a], S. Simion[66], R. Simoniello[37], E. L. Simpson[103], H. Simpson[152], L. R. Simpson[6], S. Simsek[82], S. Sindhu[55], P. Sinervo[161], S. N. Singh[27], S. Singh[30], S. Sinha[48], S. Sinha[103], M. Sioli[24a,24b], K. Sioulas[9], I. Siral[37], E. Sitnikova[48], J. Sjölin[47a,47b], T. B. Sjursen[17], A. Skaf[55], E. Skorda[21], P. Skubic[123], M. Slawinska[88], I. Slazyk[17], I. Sliusar[128], V. Smakhtin[175], B. H. Smart[137], S. Yu. Smirnov[140b], Y. Smirnov[82], L. N. Smirnova[38,a], O. Smirnova[100], A. C. Smith[42], D. R. Smith[165], J. L. Smith[103], M. B. Smith[35], R. Smith[149], H. Smitmanns[102], M. Smizanska[93], K. Smolek[135], P. Smolyanskiy[135], A. A. Snesarev[39], H. L. Snoek[117], S. Snyder[30], R. Sobie[171,ab], A. Soffer[157], C. A. Solans Sanchez[37], E. Yu. Soldatov[39], U. Soldevila[169], A. A. Solodkov[34h], S. Solomon[27], A. Soloshenko[39], K. Solovieva[54], O. V. Solovyanov[41], P. Sommer[50], A. Sonay[13], A. Sopczak[135], A. L. Sopio[52], F. Sopkova[29b], J. D. Sorenson[115], I. R. Sotarriva Alvarez[141], V. Sothilingam[63a], O. J. Soto Sandoval[140b,140c], S. Sottocornola[68], R. Soualah[85a], Z. Soumaimi[36e], D. South[48], N. Soybelman[175], S. Spagnolo[70a,70b], M. Spalla[112], D. Sperlich[54], B. Spisso[72a,72b], D. P. Spiteri[59], L. Splendori[104], M. Spousta[136], E. J. Staats[35], R. Stamen[63a], E. Stanecka[88], W. Stanek-Maslouska[48], M. V. Stange[50], B. Stanislaus[18a], M. M. Stanitzki[48], B. Stapf[48], E. A. Starchenko[38], G. H. Stark[139], J. Stark[91], P. Staroba[134], P. Starovoitov[85b], R. Staszewski[88], C. Stauch[111], G. Stavropoulos[46], A. Stefl[37], A. Stein[102], P. Steinberg[30], B. Stelzer[148,162a], H. J. Stelzer[132], O. Stelzer[162a], H. Stenzel[58], T. J. Stevenson[152], G. A. Stewart[37], J. R. Stewart[124], G. Stoicea[28b], M. Stolarski[133a], S. Stonjek[112], A. Straessner[50], J. Strandberg[150], S. Strandberg[47a,47b], M. Stratmann[177], M. Strauss[123], T. Strebler[104], P. Strizenec[29b], R. Ströhmer[172], D. M. Strom[126], R. Stroynowski[45], A. Strubig[47a,47b], S. A. Stucci[30], B. Stugu[17], J. Stupak[123], N. A. Styles[48], D. Su[149], S. Su[62], X. Su[62], D. Suchy[29a], A.D. Sudhakar Ponnu[55], K. Sugizaki[131], V. V. Sulin[38], D. M. S. Sultan[129], L. Sultanaliyeva[25], S. Sultansoy[3b], S. Sun[176], W. Sun[14], O. Sunneborn Gudnadottir[167], N. Sur[100], M. R. Sutton[152], M. Svatos[134], P. N. Swallow[33], M. Swiatlowski[162a], T. Swirski[172], A. Swoboda[37], I. Sykora[29a], M. Sykora[136], T. Sykora[136], D. Ta[102], K. Tackmann[48,y], A. Taffard[165], R. Tafirout[162a], Y. Takubo[84], M. Talby[104], A. A. Talyshev[38], K. C. Tam[64b], N. M. Tamir[157], A. Tanaka[159], J. Tanaka[159], R. Tanaka[66], M. Tanasini[151], Z. Tao[170], S. Tapia Araya[140g], S. Tapprogge[102], A. Tarek Abouelfadl Mohamed[37], S. Tarem[156], K. Tariq[14], G. Tarna[37], G. F. Tartarelli[71a], M. J. Tartarin[91], P. Tas[136], M. Tasevsky[134], E. Tassi[44a,44b], A. C. Tate[168], Y. Tayalati[36e,aa], G. N. Taylor[107], W. Taylor[162b], R. J. Taylor Vara[169], A. S. Tegetmeier[91], P. Teixeira-Dias[97], J. J. Teoh[161], K. Terashi[159], J. Terron[101], S. Terzo[13], M. Testa[53], R. J. Teuscher[161,ab], A. Thaler[79], O. Theiner[56], T. Theveneaux-Pelzer[104], D. W. Thomas[97], J. P. Thomas[21], E. A. Thompson[18a], P. D. Thompson[21], E. Thomson[131], R. E. Thornberry[45], C. Tian[62], Y. Tian[56], V. Tikhomirov[82], Yu. A. Tikhonov[39], S. Timoshenko[38], D. Timoshyn[136], E. X. L. Ting[1], P. Tipton[178], A. Tishelman-Charny[30], K. Todome[141], S. Todorova-Nova[136], L. Toffolin[69a,69c], M. Togawa[84], J. Tojo[90], S. Tokár[29a], O. Toldaiev[68], G. Tolkachev[104], M. Tomoto[84], L. Tompkins[149,n], E. Torrence[126], H. Torres[91], E. Torró Pastor[169], M. Toscani[31], C. Tosciri[40], M. Tost[11], D. R. Tovey[145], T. Trefzger[172], P. M. Tricarico[13], A. Tricoli[30], I. M. Trigger[162a], S. Trincaz-Duvoid[130], D. A. Trischuk[27], A. Tropina[39], L. Truong[34c], M. Trzebinski[88], A. Trzupek[88], F. Tsai[151], M. Tsai[108], A. Tsiamis[158], P. V. Tsiareshka[39], S. Tsigaridas[162a], A. Tsirigotis[158,u], V. Tsiskaridze[155a], E. G. Tskhadadze[155a], Y. Tsujikawa[89], I. I. Tsukerman[38], V. Tsulaia[18a], S. Tsuno[84], K. Tsuri[121], D. Tsybychev[151], Y. Tu[64b], A. Tudorache[28b], V. Tudorache[28b], S. B. Tuncay[129], S. Turchikhin[57a,57b], I. Turk Cakir[3a], R. Turra[71a], T. Turtuvshin[39,ac], P. M. Tuts[42], S. Tzamarias[158,d], Y. Uematsu[84], F. Ukegawa[163], P. A. Ulloa Poblete[140b,140c], E. N. Umaka[30], G. Unal[37], A. Undrus[30], G. Unel[165], J. Urban[29b], P. Urrejola[140e], G. Usai[8], R. Ushioda[160], M. Usman[110], F. Ustuner[52], Z. Uysal[82], V. Vacek[135], B. Vachon[106], T. Vafeiadis[37], A. Vaitkus[98], C. Valderanis[111], E. Valdes Santurio[47a,47b], M. Valente[37], S. Valentinetti[24a,24b], A. Valero[169], E. Valiente Moreno[169], A. Vallier[91], J. A. Valls Ferrer[169], D. R. Van Arneman[117], A. Van Der Graaf[49], H. Z. Van Der Schyf[34h], P. Van Gemmeren[6], M. Van Rijnbach[37], S. Van Stroud[98], I. Van Vulpen[117], P. Vana[136], M. Vanadia[76a,76b], U. M. Vande Voorde[150], W. Vandelli[37], E. R. Vandewall[124], D. Vannicola[157], L. Vannoli[53], R. Vari[75a], M. Varma[178], E. W. Varnes[7], C. Varni[118], D. Varouchas[66], L. Varriale[169], K. E. Varvell[153], M. E. Vasile[28b], L. Vaslin[84], M. D. Vassilev[149], A. Vasyukov[39], L. M. Vaughan[124], R. Vavricka[136], T. Vazquez Schroeder[13], J. Veatch[32], V. Vecchio[103], M. J. Veen[105], I. Veliscek[30], I. Velkovska[95], L. M. Veloce[161], F. Veloso[133a,133c], S. Veneziano[75a], A. Ventura[70a,70b], A. Verbytskyi[112], M. Verducci[74a,74b], C. Vergis[96], M. Verissimo De Araujo[83b], W. Verkerke[117], J. C. Vermeulen[117], C. Vernieri[149], M. Vessella[165], M. C. Vetterli[148,ai], A. Vgenopoulos[102], N. Viaux Maira[140g,af], T. Vickey[145], O. E. Vickey Boeriu[145],

G. H. A. Viehhauser[129], L. Vigani[63b], M. Vigl[112], M. Villa[24a,24b], M. Villaplana Perez[169], E. M. Villhauer[40], E. Vilucchi[53], M. Vincent[169], M. G. Vincter[35], A. Visibile[117], A. Visive[117], C. Vittori[37], I. Vivarelli[24a,24b], M. I. Vivas Albornoz[48], E. Voevodina[112], F. Vogel[111], J. C. Voigt[50], P. Vokac[135], Yu. Volkotrub[87b], L. Vomberg[25], E. Von Toerne[25], B. Vormwald[37], K. Vorobev[51], M. Vos[169], K. Voss[147], M. Vozak[37], L. Vozdecky[123], N. Vranjes[16], M. Vranjes Milosavljevic[16], M. Vreeswijk[117], N. K. Vu[144a,144b], R. Vuillermet[37], O. Vujinovic[102], I. Vukotic[40], I. K. Vyas[35], J. F. Wack[33], S. Wada[163], C. Wagner[149], J. M. Wagner[18a], W. Wagner[177], S. Wahdan[177], H. Wahlberg[92], C. H. Waits[123], J. Walder[137], R. Walker[111], K. Walkingshaw Pass[59], W. Walkowiak[147], A. Wall[131], E. J. Wallin[100], T. Wamorkar[18a], K. Wandall-Christensen[169], A. Wang[62], A. Z. Wang[139], C. Wang[102], C. Wang[11], H. Wang[18a], J. Wang[64c], P. Wang[103], P. Wang[98], R. Wang[61], R. Wang[6], S. M. Wang[154], S. Wang[14], T. Wang[116], T. Wang[62], W. T. Wang[129], W. Wang[14], X. Wang[168], X. Wang[144a], X. Wang[48], Y. Wang[114a], Y. Wang[62], Z. Wang[108], Z. Wang[144b], Z. Wang[108], C. Wanotayaroj[84], A. Warburton[106], A. L. Warnerbring[147], S. Waterhouse[97], A. T. Watson[21], H. Watson[52], M. F. Watson[21], E. Watton[59], G. Watts[142], B. M. Waugh[98], J. M. Webb[54], C. Weber[30], H. A. Weber[19], M. S. Weber[20], S. M. Weber[63a], C. Wei[62], Y. Wei[54], A. R. Weidberg[129], E. J. Weik[120], J. Weingarten[49], C. Weiser[54], C. J. Wells[48], T. Wenaus[30], T. Wengler[37], N. S. Wenke[112], N. Wermes[25], M. Wessels[63a], A. M. Wharton[93], A. S. White[61], A. White[8], M. J. White[1], D. Whiteson[165], L. Wickremasinghe[127], W. Wiedenmann[176], M. Wielers[137], R. Wierda[150], C. Wiglesworth[43], H. G. Wilkens[37], J. J. H. Wilkinson[33], D. M. Williams[42], H. H. Williams[131], S. Williams[33], S. Willocq[105], B. J. Wilson[103], D. J. Wilson[103], P. J. Windischhofer[40], F. I. Winkel[31], F. Winklmeier[126], B. T. Winter[54], M. Wittgen[149], M. Wobisch[99], T. Wojtkowski[60], Z. Wolffs[117], J. Wollrath[37], M. W. Wolter[88], H. Wolters[133a,133c], M. C. Wong[139], E. L. Woodward[42], S. D. Worm[48], B. K. Wosiek[88], K. W. Woźniak[88], S. Wozniewski[55], K. Wraight[59], C. Wu[161], C. Wu[21], J. Wu[159], M. Wu[114b], M. Wu[116], S. L. Wu[176], S. Wu[14,ak], X. Wu[62], Y. Q. Wu[161], Y. Wu[62], Z. Wu[4], Z. Wu[114a], J. Wuerzinger[112], T. R. Wyatt[103], B. M. Wynne[52], S. Xella[43], L. Xia[114a], M. Xia[15], M. Xie[62], A. Xiong[126], J. Xiong[18a], D. Xu[14], H. Xu[62], L. Xu[62], R. Xu[131], T. Xu[108], Y. Xu[142], Z. Xu[52], R. Xue[132], B. Yabsley[153], S. Yacoob[34a], Y. Yamaguchi[84], E. Yamashita[159], H. Yamauchi[163], T. Yamazaki[18a], Y. Yamazaki[86], S. Yan[59], Z. Yan[105], H. J. Yang[144a,144b], H. T. Yang[62], S. Yang[62], T. Yang[64c], X. Yang[37], X. Yang[14], Y. Yang[159], Y. Yang[62], W. -M. Yao[18a], C. L. Yardley[152], J. Ye[14], S. Ye[30], X. Ye[62], Y. Yeh[98], I. Yeletskikh[39], B. Yeo[18b], M. R. Yexley[98], T. P. Yildirim[129], K. Yorita[174], C. J. S. Young[37], C. Young[149], N. D. Young[126], Y. Yu[62], J. Yuan[14,114c], M. Yuan[108], R. Yuan[144a,144b], L. Yue[98], M. Zaazoua[62], B. Zabinski[88], I. Zahir[36a], A. Zaio[57a,57b], Z. K. Zak[88], T. Zakareishvili[169], S. Zambito[56], J. A. Zamora Saa[140d], J. Zang[159], R. Zanzottera[71a,71b], O. Zaplatilek[135], C. Zeitnitz[177], H. Zeng[14], J. C. Zeng[168], D. T. Zenger Jr[27], O. Zenin[38], T. Ženiš[29a], S. Zenz[96], D. Zerwas[66], M. Zhai[14,114c], D. F. Zhang[145], G. Zhang[14,ak], J. Zhang[143a], J. Zhang[6], K. Zhang[14,114c], L. Zhang[62], L. Zhang[114a], P. Zhang[14,114c], R. Zhang[114a], S. Zhang[91], T. Zhang[159], Y. Zhang[142], Y. Zhang[98], Y. Zhang[62], Y. Zhang[114a], Z. Zhang[18a], Z. Zhang[143a], Z. Zhang[66], H. Zhao[142], T. Zhao[143a], Y. Zhao[35], Z. Zhao[62], Z. Zhao[62], A. Zhemchugov[39], J. Zheng[114a], K. Zheng[168], X. Zheng[62], Z. Zheng[149], D. Zhong[168], B. Zhou[108], H. Zhou[7], N. Zhou[144a], Y. Zhou[15], Y. Zhou[114a], Y. Zhou[7], C. G. Zhu[143a], J. Zhu[108], X. Zhu[144b], Y. Zhu[144a], Y. Zhu[62], X. Zhuang[14], K. Zhukov[68], N. I. Zimine[39], J. Zinsser[63b], M. Ziolkowski[147], L. Živković[16], A. Zoccoli[24a,24b], K. Zoch[61], A. Zografos[37], T. G. Zorbas[145], O. Zormpa[46], L. Zwalinski[37]

[1] Department of Physics, University of Adelaide, Adelaide, Australia
[2] Department of Physics, University of Alberta, Edmonton, AB, Canada
[3] [(a)]Department of Physics, Ankara University, Ankara, Türkiye; [(b)]Division of Physics, TOBB University of Economics and Technology, Ankara, Türkiye
[4] LAPP, Université Savoie Mont Blanc, CNRS/IN2P3, Annecy, France
[5] APC, Université Paris Cité, CNRS/IN2P3, Paris, France
[6] High Energy Physics Division, Argonne National Laboratory, Argonne, IL, USA
[7] Department of Physics, University of Arizona, Tucson, AZ, USA
[8] Department of Physics, University of Texas at Arlington, Arlington, TX, USA
[9] Physics Department, National and Kapodistrian University of Athens, Athens, Greece
[10] Physics Department, National Technical University of Athens, Zografou, Greece
[11] Department of Physics, University of Texas at Austin, Austin, TX, USA

[12] Institute of Physics, Azerbaijan Academy of Sciences, Baku, Azerbaijan
[13] Institut de Física d'Altes Energies (IFAE), Barcelona Institute of Science and Technology, Barcelona, Spain
[14] Institute of High Energy Physics, Chinese Academy of Sciences, Beijing, China
[15] Physics Department, Tsinghua University, Beijing, China
[16] Institute of Physics, University of Belgrade, Belgrade, Serbia
[17] Department for Physics and Technology, University of Bergen, Bergen, Norway
[18] [(a)]Physics Division, Lawrence Berkeley National Laboratory, Berkeley, CA, USA; [(b)]University of California, Berkeley, CA, USA
[19] Institut für Physik, Humboldt Universität zu Berlin, Berlin, Germany
[20] Albert Einstein Center for Fundamental Physics and Laboratory for High Energy Physics, University of Bern, Bern, Switzerland
[21] School of Physics and Astronomy, University of Birmingham, Birmingham, UK
[22] [(a)]Department of Physics, Bogazici University, Istanbul, Türkiye; [(b)]Department of Physics Engineering, Gaziantep University, Gaziantep, Türkiye; [(c)]Department of Physics, Istanbul University, Istanbul, Türkiye
[23] [(a)]Facultad de Ciencias y Centro de Investigaciónes, Universidad Antonio Nariño, Bogotá, Colombia; [(b)]Departamento de Física, Universidad Nacional de Colombia, Bogotá, Colombia
[24] [(a)]Dipartimento di Fisica e Astronomia A. Righi, Università di Bologna, Bologna, Italy; [(b)]INFN Sezione di Bologna, Bologna, Italy
[25] Physikalisches Institut, Universität Bonn, Bonn, Germany
[26] Department of Physics, Boston University, Boston, MA, USA
[27] Department of Physics, Brandeis University, Waltham, MA, USA
[28] [(a)]Transilvania University of Brasov, Brasov, Romania; [(b)]Horia Hulubei National Institute of Physics and Nuclear Engineering, Bucharest, Romania; [(c)]Department of Physics, Alexandru Ioan Cuza University of Iasi, Iasi, Romania; [(d)]National Institute for Research and Development of Isotopic and Molecular Technologies, Physics Department, Cluj-Napoca, Romania; [(e)]National University of Science and Technology Politechnica, Bucharest, Romania; [(f)]West University in Timisoara, Timisoara, Romania; [(g)]Faculty of Physics, University of Bucharest, Bucharest, Romania
[29] [(a)]Faculty of Mathematics, Physics and Informatics, Comenius University, Bratislava, Slovak Republic; [(b)]Department of Subnuclear Physics, Institute of Experimental Physics of the Slovak Academy of Sciences, Kosice, Slovak Republic
[30] Physics Department, Brookhaven National Laboratory, Upton, NY, USA
[31] Universidad de Buenos Aires, Facultad de Ciencias Exactas y Naturales, Departamento de Física, y CONICET, Instituto de Física de Buenos Aires (IFIBA), Buenos Aires, Argentina
[32] California State University, Long Beach, CA, USA
[33] Cavendish Laboratory, University of Cambridge, Cambridge, UK
[34] [(a)]Department of Physics, University of Cape Town, Cape Town, South Africa; [(b)]iThemba Labs, Western Cape, South Africa; [(c)]Department of Mechanical Engineering Science, University of Johannesburg, Johannesburg, South Africa; [(d)]National Institute of Physics, University of the Philippines Diliman (Philippines), Quezon City, Philippines; [(e)]Department of Physics, Stellenbosch University, Matieland, South Africa; [(f)]Department of Physics, University of South Africa, Pretoria, South Africa; [(g)]University of Zululand, KwaDlangezwa, South Africa; [(h)]School of Physics, University of the Witwatersrand, Johannesburg, South Africa
[35] Department of Physics, Carleton University, Ottawa, ON, Canada
[36] [(a)]Faculté des Sciences Ain Chock, Université Hassan II de Casablanca, Casablanca, Morocco; [(b)]Faculté des Sciences, Université Ibn-Tofail, Kénitra, Morocco; [(c)]Faculté des Sciences Semlalia, Université Cadi Ayyad, LPHEA-Marrakech, Marrakesh, Morocco; [(d)]LPMR, Faculté des Sciences, Université Mohamed Premier, Oujda, Morocco; [(e)]Faculté des sciences, Université Mohammed V, Rabat, Morocco; [(f)]Institute of Applied Physics, Mohammed VI Polytechnic University, Ben Guerir, Morocco
[37] CERN, Geneva, Switzerland
[38] Affiliated with an Institute Formerly Covered by a Cooperation Agreement with CERN, Geneva, Switzerland
[39] Affiliated with an International Laboratory Covered by a Cooperation Agreement with CERN, Geneva, Switzerland
[40] Enrico Fermi Institute, University of Chicago, Chicago, IL, USA
[41] LPC, Université Clermont Auvergne, CNRS/IN2P3, Clermont-Ferrand, France
[42] Nevis Laboratory, Columbia University, Irvington, NY, USA
[43] Niels Bohr Institute, University of Copenhagen, Copenhagen, Denmark

[44] [(a)]Dipartimento di Fisica, Università della Calabria, Rende, Italy; [(b)]INFN Gruppo Collegato di Cosenza, Laboratori Nazionali di Frascati, Frascati, Italy
[45] Physics Department, Southern Methodist University, Dallas, TX, USA
[46] National Centre for Scientific Research "Demokritos", Agia Paraskevi, Greece
[47] [(a)]Department of Physics, Stockholm University, Stockholm, Sweden; [(b)]Oskar Klein Centre, Stockholm, Sweden
[48] Deutsches Elektronen-Synchrotron DESY, Hamburg and Zeuthen, Germany
[49] Fakultät Physik , Technische Universität Dortmund, Dortmund, Germany
[50] Institut für Kern- und Teilchenphysik, Technische Universität Dresden, Dresden, Germany
[51] Department of Physics, Duke University, Durham, NC, USA
[52] SUPA-School of Physics and Astronomy, University of Edinburgh, Edinburgh, UK
[53] INFN e Laboratori Nazionali di Frascati, Frascati, Italy
[54] Physikalisches Institut, Albert-Ludwigs-Universität Freiburg, Freiburg, Germany
[55] II. Physikalisches Institut, Georg-August-Universität Göttingen, Göttingen, Germany
[56] Département de Physique Nucléaire et Corpusculaire, Université de Genève, Geneva, Switzerland
[57] [(a)]Dipartimento di Fisica, Università di Genova, Genoa, Italy; [(b)]INFN Sezione di Genova, Genoa, Italy
[58] II. Physikalisches Institut, Justus-Liebig-Universität Giessen, Giessen, Germany
[59] SUPA-School of Physics and Astronomy, University of Glasgow, Glasgow, UK
[60] LPSC, Université Grenoble Alpes, CNRS/IN2P3, Grenoble INP, Grenoble, France
[61] Laboratory for Particle Physics and Cosmology, Harvard University, Cambridge, MA, USA
[62] Department of Modern Physics and State Key Laboratory of Particle Detection and Electronics, University of Science and Technology of China, Hefei, China
[63] [(a)]Kirchhoff-Institut für Physik, Ruprecht-Karls-Universität Heidelberg, Heidelberg, Germany; [(b)]Physikalisches Institut, Ruprecht-Karls-Universität Heidelberg, Heidelberg, Germany
[64] [(a)]Department of Physics, Chinese University of Hong Kong, Shatin N.T., Hong Kong; [(b)]Department of Physics, University of Hong Kong, Pok Fu Lam, Hong Kong; [(c)]Department of Physics and Institute for Advanced Study, Hong Kong University of Science and Technology, Clear Water Bay, Kowloon, Hong Kong, China
[65] Department of Physics, National Tsing Hua University, Hsinchu, Taiwan
[66] IJCLab, Université Paris-Saclay, CNRS/IN2P3, 91405 Orsay, France
[67] Centro Nacional de Microelectrónica (IMB-CNM-CSIC), Barcelona, Spain
[68] Department of Physics, Indiana University, Bloomington, IN, USA
[69] [(a)]INFN Gruppo Collegato di Udine, Sezione di Trieste, Udine, Italy; [(b)]ICTP, Trieste, Italy; [(c)]Dipartimento Politecnico di Ingegneria e Architettura, Università di Udine, Udine, Italy
[70] [(a)]INFN Sezione di Lecce, Lecce, Italy; [(b)]Dipartimento di Matematica e Fisica, Università del Salento, Lecce, Italy
[71] [(a)]INFN Sezione di Milano, Milan, Italy; [(b)]Dipartimento di Fisica, Università di Milano, Milan, Italy
[72] [(a)]INFN Sezione di Napoli, Naples, Italy; [(b)]Dipartimento di Fisica, Università di Napoli, Naples, Italy
[73] [(a)]INFN Sezione di Pavia, Pavia, Italy; [(b)]Dipartimento di Fisica, Università di Pavia, Pavia, Italy
[74] [(a)]INFN Sezione di Pisa, Pisa, Italy; [(b)]Dipartimento di Fisica E. Fermi, Università di Pisa, Pisa, Italy
[75] [(a)]INFN Sezione di Roma, Rome, Italy; [(b)]Dipartimento di Fisica, Sapienza Università di Roma, Rome, Italy
[76] [(a)]INFN Sezione di Roma Tor Vergata, Rome, Italy; [(b)]Dipartimento di Fisica, Università di Roma Tor Vergata, Rome, Italy
[77] [(a)]INFN Sezione di Roma Tre, Rome, Italy; [(b)]Dipartimento di Matematica e Fisica, Università Roma Tre, Rome, Italy
[78] [(a)]INFN-TIFPA, Povo, Italy; [(b)]Università degli Studi di Trento, Trento, Italy
[79] Universität Innsbruck, Department of Astro and Particle Physics, Innsbruck, Austria
[80] University of Iowa, Iowa City, IA, USA
[81] Department of Physics and Astronomy, Iowa State University, Ames, IA, USA
[82] Istinye University, Sariyer, Istanbul, Türkiye
[83] [(a)]Departamento de Engenharia Elétrica, Universidade Federal de Juiz de Fora (UFJF), Juiz de Fora, Brazil; [(b)]Universidade Federal do Rio De Janeiro COPPE/EE/IF, Rio de Janeiro, Brazil; [(c)]Instituto de Física, Universidade de São Paulo, São Paulo, Brazil; [(d)]Rio de Janeiro State University, Rio de Janeiro, Brazil; [(e)]Federal University of Bahia, Bahia, Brazil
[84] KEK, High Energy Accelerator Research Organization, Tsukuba, Japan
[85] [(a)]Khalifa University of Science and Technology, Abu Dhabi, United Arab Emirates; [(b)]University of Sharjah, Sharjah, United Arab Emirates

[86] Graduate School of Science, Kobe University, Kobe, Japan
[87] [(a)]Faculty of Physics and Applied Computer Science, AGH University of Krakow, Krakow, Poland; [(b)]Marian Smoluchowski Institute of Physics, Jagiellonian University, Krakow, Poland
[88] Institute of Nuclear Physics Polish Academy of Sciences, Krakow, Poland
[89] Faculty of Science, Kyoto University, Kyoto, Japan
[90] Research Center for Advanced Particle Physics and Department of Physics, Kyushu University, Fukuoka , Japan
[91] L2IT, Université de Toulouse, CNRS/IN2P3, UPS, Toulouse, France
[92] Instituto de Física La Plata, Universidad Nacional de La Plata and CONICET, La Plata, Argentina
[93] Physics Department, Lancaster University, Lancaster, UK
[94] Oliver Lodge Laboratory, University of Liverpool, Liverpool, UK
[95] Department of Experimental Particle Physics, Jožef Stefan Institute and Department of Physics, University of Ljubljana, Ljubljana, Slovenia
[96] Department of Physics and Astronomy, Queen Mary University of London, London, UK
[97] Department of Physics, Royal Holloway University of London, Egham, UK
[98] Department of Physics and Astronomy, University College London, London, UK
[99] Louisiana Tech University, Ruston, LA, USA
[100] Fysiska institutionen, Lunds universitet, Lund, Sweden
[101] Departamento de Física Teorica C-15 and CIAFF, Universidad Autónoma de Madrid, Madrid, Spain
[102] Institut für Physik, Universität Mainz, Mainz, Germany
[103] School of Physics and Astronomy, University of Manchester, Manchester, UK
[104] CPPM, Aix-Marseille Université, CNRS/IN2P3, Marseille, France
[105] Department of Physics, University of Massachusetts, Amherst, MA, USA
[106] Department of Physics, McGill University, Montreal, QC, Canada
[107] School of Physics, University of Melbourne, Melbourne, VIC, Australia
[108] Department of Physics, University of Michigan, Ann Arbor, MI, USA
[109] Department of Physics and Astronomy, Michigan State University, East Lansing, MI, USA
[110] Group of Particle Physics, University of Montreal, Montreal, QC, Canada
[111] Fakultät für Physik, Ludwig-Maximilians-Universität München, Munich, Germany
[112] Max-Planck-Institut für Physik (Werner-Heisenberg-Institut), Munich, Germany
[113] Graduate School of Science and Kobayashi-Maskawa Institute, Nagoya University, Nagoya, Japan
[114] [(a)]Department of Physics, Nanjing University, Nanjing, China; [(b)]School of Science, Shenzhen Campus of Sun Yat-sen University, Guangzhou, China; [(c)]University of Chinese Academy of Science (UCAS), Beijing, China
[115] Department of Physics and Astronomy, University of New Mexico, Albuquerque, NM, USA
[116] Institute for Mathematics, Astrophysics and Particle Physics, Radboud University/Nikhef, Nijmegen, The Netherlands
[117] Nikhef National Institute for Subatomic Physics and University of Amsterdam, Amsterdam, The Netherlands
[118] Department of Physics, Northern Illinois University, DeKalb, IL, USA
[119] [(a)]New York University Abu Dhabi, Abu Dhabi, United Arab Emirates; [(b)]United Arab Emirates University, Al Ain, United Arab Emirates
[120] Department of Physics, New York University, New York, NY, USA
[121] Ochanomizu University, Otsuka, Bunkyo-ku, Tokyo, Japan
[122] Ohio State University, Columbus, OH, USA
[123] Homer L. Dodge Department of Physics and Astronomy, University of Oklahoma, Norman, OK, USA
[124] Department of Physics, Oklahoma State University, Stillwater, OK, USA
[125] Palacký University, Joint Laboratory of Optics, Olomouc, Czech Republic
[126] Institute for Fundamental Science, University of Oregon, Eugene, OR, USA
[127] Graduate School of Science, University of Osaka, Osaka, Japan
[128] Department of Physics, University of Oslo, Oslo, Norway
[129] Department of Physics, Oxford University, Oxford, UK
[130] LPNHE, Sorbonne Université, Université Paris Cité, CNRS/IN2P3, Paris, France
[131] Department of Physics, University of Pennsylvania, Philadelphia, PA, USA
[132] Department of Physics and Astronomy, University of Pittsburgh, Pittsburgh, PA, USA
[133] [(a)]Laboratório de Instrumentação e Física Experimental de Partículas - LIP, Lisbon, Portugal; [(b)]Departamento de Física, Faculdade de Ciências, Universidade de Lisboa, Lisbon, Portugal; [(c)]Departamento de Física, Universidade de Coimbra,

Coimbra, Portugal; [d]Centro de Física Nuclear da Universidade de Lisboa, Lisbon, Portugal; [e]Departamento de Física, Escola de Ciências, Universidade do Minho, Braga, Portugal; [f]Departamento de Física Teórica y del Cosmos, Universidad de Granada, Granada, Spain; [g]Departamento de Física, Instituto Superior Técnico, Universidade de Lisboa, Lisbon, Portugal
[134] Institute of Physics of the Czech Academy of Sciences, Prague, Czech Republic
[135] Czech Technical University in Prague, Prague, Czech Republic
[136] Faculty of Mathematics and Physics, Charles University, Prague, Czech Republic
[137] Particle Physics Department, Rutherford Appleton Laboratory, Didcot, UK
[138] IRFU, CEA, Université Paris-Saclay, Gif-sur-Yvette, France
[139] Santa Cruz Institute for Particle Physics, University of California Santa Cruz, Santa Cruz, CA, USA
[140] [a]Departamento de Física, Pontificia Universidad Católica de Chile, Santiago, Chile; [b]Millennium Institute for Subatomic Physics at High Energy Frontier (SAPHIR), Santiago, Chile; [c]Instituto de Investigación Multidisciplinario en Ciencia y Tecnología y Departamento de Física, Universidad de La Serena, La Serena, Chile; [d]Department of Physics, Universidad Andres Bello, Santiago, Chile; [e]Universidad San Sebastian, Recoleta, Chile; [f]Instituto de Alta Investigación, Universidad de Tarapacá, Arica, Chile; [g]Departamento de Física, Universidad Técnica Federico Santa María, Valparaíso, Chile
[141] Department of Physics, Institute of Science, Tokyo, Japan
[142] Department of Physics, University of Washington, Seattle, WA, USA
[143] [a]Institute of Frontier and Interdisciplinary Science and Key Laboratory of Particle Physics and Particle Irradiation (MOE), Shandong University, Qingdao, China; [b]School of Physics, Zhengzhou University, Zhengzhou, China
[144] [a]State Key Laboratory of Dark Matter Physics, School of Physics and Astronomy, Shanghai Jiao Tong University, Key Laboratory for Particle Astrophysics and Cosmology (MOE), SKLPPC, Shanghai, China; [b]State Key Laboratory of Dark Matter Physics, Tsung-Dao Lee Institute, Shanghai Jiao Tong University, Shanghai, China
[145] Department of Physics and Astronomy, University of Sheffield, Sheffield, UK
[146] Department of Physics, Shinshu University, Nagano, Japan
[147] Department Physik, Universität Siegen, Siegen, Germany
[148] Department of Physics, Simon Fraser University, Burnaby, BC, Canada
[149] SLAC National Accelerator Laboratory, Stanford, CA, USA
[150] Department of Physics, Royal Institute of Technology, Stockholm, Sweden
[151] Departments of Physics and Astronomy, Stony Brook University, Stony Brook, NY, USA
[152] Department of Physics and Astronomy, University of Sussex, Brighton, UK
[153] School of Physics, University of Sydney, Sydney, Australia
[154] Institute of Physics, Academia Sinica, Taipei, Taiwan
[155] [a]E. Andronikashvili Institute of Physics, Iv. Javakhishvili Tbilisi State University, Tbilisi, Georgia; [b]High Energy Physics Institute, Tbilisi State University, Tbilisi, Georgia; [c]University of Georgia, Tbilisi, Georgia
[156] Department of Physics, Technion, Israel Institute of Technology, Haifa, Israel
[157] Raymond and Beverly Sackler School of Physics and Astronomy, Tel Aviv University, Tel Aviv, Israel
[158] Department of Physics, Aristotle University of Thessaloniki, Thessaloniki, Greece
[159] International Center for Elementary Particle Physics and Department of Physics, University of Tokyo, Tokyo, Japan
[160] Graduate School of Science and Technology, Tokyo Metropolitan University, Tokyo, Japan
[161] Department of Physics, University of Toronto, Toronto, ON, Canada
[162] [a]TRIUMF, Vancouver, BC, Canada; [b]Department of Physics and Astronomy, York University, Toronto, ON, Canada
[163] Division of Physics and Tomonaga Center for the History of the Universe, Faculty of Pure and Applied Sciences, University of Tsukuba, Tsukuba, Japan
[164] Department of Physics and Astronomy, Tufts University, Medford, MA, USA
[165] Department of Physics and Astronomy, University of California Irvine, Irvine, CA, USA
[166] University of West Attica, Athens, Greece
[167] Department of Physics and Astronomy, University of Uppsala, Uppsala, Sweden
[168] Department of Physics, University of Illinois, Urbana, IL, USA
[169] Instituto de Física Corpuscular (IFIC), Centro Mixto Universidad de Valencia - CSIC, Valencia, Spain
[170] Department of Physics, University of British Columbia, Vancouver, BC, Canada
[171] Department of Physics and Astronomy, University of Victoria, Victoria, BC, Canada

[172] Fakultät für Physik und Astronomie, Julius-Maximilians-Universität Würzburg, Würzburg, Germany
[173] Department of Physics, University of Warwick, Coventry, UK
[174] Waseda University, Tokyo, Japan
[175] Department of Particle Physics and Astrophysics, Weizmann Institute of Science, Rehovot, Israel
[176] Department of Physics, University of Wisconsin, Madison, WI, USA
[177] Fakultät für Mathematik und Naturwissenschaften, Fachgruppe Physik, Bergische Universität Wuppertal, Wuppertal, Germany
[178] Department of Physics, Yale University, New Haven, CT, USA
[179] Yerevan Physics Institute, Yerevan, Armenia

[a] Also at Affiliated with an Institute Formerly Covered by a Cooperation Agreement with CERN, Geneva, Switzerland
[b] Also at An-Najah National University, Nablus, Palestine
[c] Also at Borough of Manhattan Community College, City University of New York, New York, NY, USA
[d] Also at Center for Interdisciplinary Research and Innovation (CIRI-AUTH), Thessaloniki, Greece
[e] Also at Centre of Physics of the Universities of Minho and Porto (CF-UM-UP), Braga, Portugal
[f] Also at CERN, Geneva, Switzerland
[g] Also at Département de Physique Nucléaire et Corpusculaire, Université de Genève, Geneva, Switzerland
[h] Also at Departament de Fisica de la Universitat Autonoma de Barcelona, Barcelona, Spain
[i] Also at Department of Financial and Management Engineering, University of the Aegean, Chios, Greece
[j] Also at Department of Mathematical Sciences, University of South Africa, Johannesburg, South Africa
[k] Also at Department of Modern Physics and State Key Laboratory of Particle Detection and Electronics, University of Science and Technology of China, Hefei, China
[l] Also at Department of Physics, Bolu Abant Izzet Baysal University, Bolu, Türkiye
[m] Also at Department of Physics, King's College London, London, UK
[n] Also at Department of Physics, Stanford University, Stanford, CA, USA
[o] Also at Department of Physics, Stellenbosch University, Stellenbosch, South Africa
[p] Also at Department of Physics, University of Fribourg, Fribourg, Switzerland
[q] Also at Department of Physics, University of Thessaly, Greece
[r] Also at Department of Physics, Westmont College, Santa Barbara, USA
[s] Also at Faculty of Physics, Sofia University, 'St. Kliment Ohridski', Sofia, Bulgaria
[t] Also at Faculty of Physics, University of Bucharest , Romania
[u] Also at Hellenic Open University, Patras, Greece
[v] Also at Henan University, Kaifeng, China
[w] Also at Imam Mohammad Ibn Saud Islamic University, Riyadh, Saudi Arabia
[x] Also at Institucio Catalana de Recerca i Estudis Avancats, ICREA, Barcelona, Spain
[y] Also at Institut für Experimentalphysik, Universität Hamburg, Hamburg, Germany
[z] Also at Institute for Nuclear Research and Nuclear Energy (INRNE) of the Bulgarian Academy of Sciences, Sofia, Bulgaria
[aa] Also at Institute of Applied Physics, Mohammed VI Polytechnic University, Ben Guerir, Morocco
[ab] Also at Institute of Particle Physics (IPP), Toronto, Canada
[ac] Also at Institute of Physics and Technology, Mongolian Academy of Sciences, Ulaanbaatar, Mongolia
[ad] Also at Institute of Physics, Azerbaijan Academy of Sciences, Baku, Azerbaijan
[ae] Also at Institute of Theoretical Physics, Ilia State University, Tbilisi, Georgia
[af] Also at Millennium Institute for Subatomic physics at high energy frontier (SAPHIR), Santiago, Chile
[ag] Also at National Institute of Physics, University of the Philippines Diliman (Philippines), Quezon City, Philippines
[ah] Also at The Collaborative Innovation Center of Quantum Matter (CICQM), Beijing, China
[ai] Also at TRIUMF, Vancouver, BC, Canada
[aj] Also at Università di Napoli Parthenope, Naples, Italy
[ak] Also at University of Chinese Academy of Sciences (UCAS), Beijing, China
[al] Also at University of Colorado Boulder, Department of Physics, Colorado, USA
[am] Also at University of Sienna, Siena, Italy

[an] Also at Washington College, Chestertown, MD, USA
[ao] Also at Yeditepe University, Physics Department, Istanbul, Türkiye
* Deceased